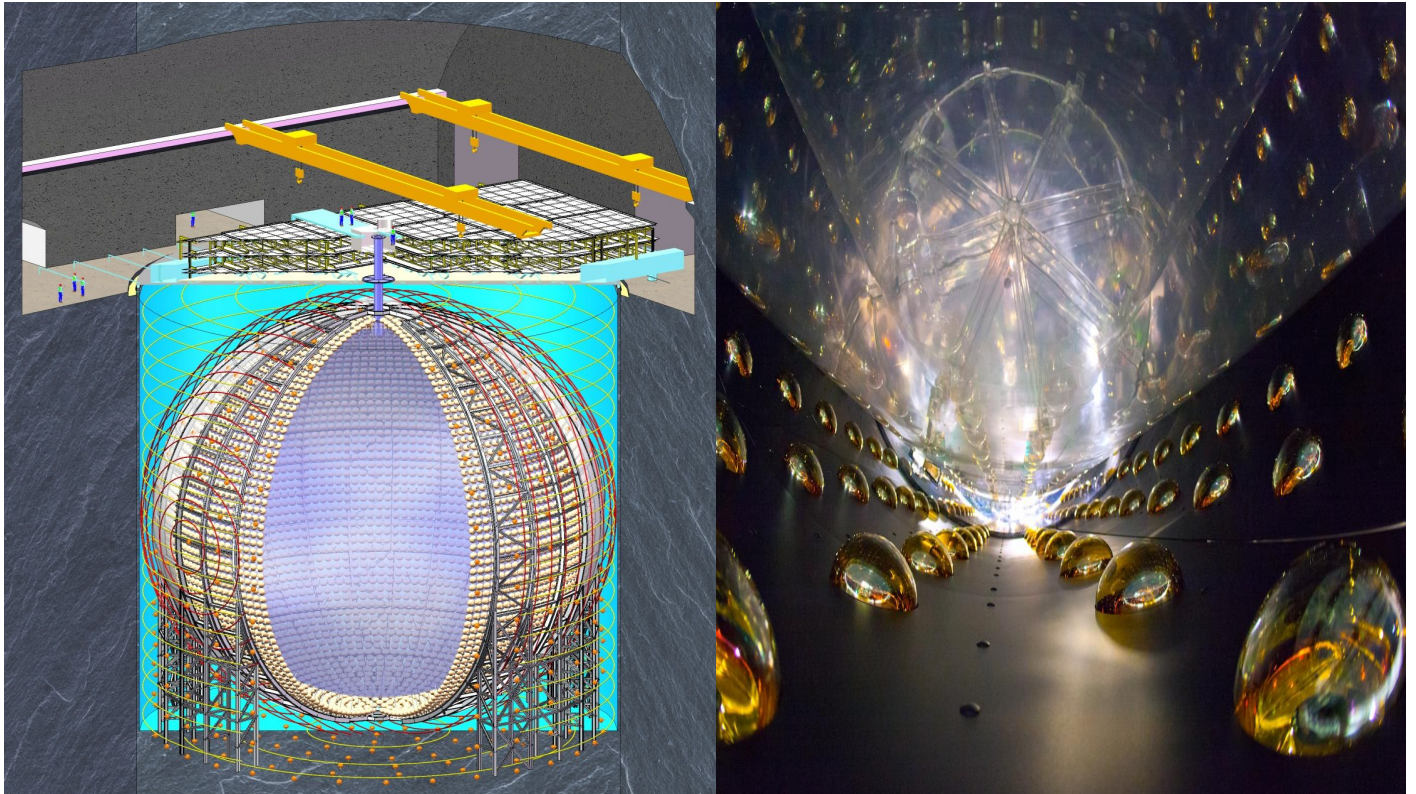# Study of Neutrino Oscillations in JUNO and Daya Bay Experiments



# JINR Participation
# 2018-2020

**Изучение осцилляций нейтрино в экспериментах JUNO/Daya Bay**

**(Участие ОИЯИ)**

**Продление проекта на период 2018-2020 гг**

**Study of Neutrino Oscillations in JUNO/Daya Bay experiments**

**(JINR Participation)**

**Project extension for the period 2018-2020**

**Шифр темы**: 02-2-1099-2010/2018  Study of Neutrino Oscillations (Project JUNO/Daya Bay)

**Направление**:      Физика частиц и релятивистская ядерная физика

**Авторы от ОИЯИ:**

N. Anfimov[1], T. Antoshkina[1], D. Biaré[1], S. Biktemerova[1], I. Butorov[1], A. Chukanov[1], A. Chuvashova[1], S. Dmitrievsky[1], D. Fedoseev[1], K. Fomenko[1], A. Formozov[1], M. Gonchar[1], O. Gorchakov[1], Yu. Gornushkin[1], V. Gromov[1], N. Kolganov[1], D. Korablyev[1], A.Krasnoperov[1], N. Morozov[1], D. Naumov[1], E. Naumova[1], I. Nemchenok[1], A. Olshevskiy[1], T. Rezinko[1], A. Rybnikov[1], A. Sadovsky[1], A. Selyunin[1], O. Smirnov[1], S. Sokolov[1], A. Sotnikov[1], M. Strizh[1], K. Treskov[1]

[1] Dzhelepov Laboratory of Nuclear Problems (DLNP)

Руководитель проекта:      Д.В.Наумов

Зам.руководителя:      М.О.Гончар

Дата представления проекта в НОО _____

Дата НТС Лаборатории  *20/04/2017 (ЛЯП)*      Номер документа _____

Дата представления физического обоснования на семинаре Лаборатории: *19/04/2017(ЛЯП)*

Дата первого утверждения проекта _____ *(ЛЯП)*

ЛИСТ СОГЛАСОВАНИЙ ПРОЕКТА

**Изучение осцилляций нейтрино в экспериментах JUNO и Daya Bay
(Участие ОИЯИ)
Продление проекта на период 2018-2020 гг**

**Study of Neutrino Oscillations in JUNO and Daya Bay experiments
(JINR Participation)
Project extension for the period 2018-2020**

**Шифр темы: 02-2-1099-2010/2018**

**Наумов Дмитрий Вадимович**

Утвержден директором ОИЯИ          _____          _____

                                                              подпись                                    дата

СОГЛАСОВАНО

ВИЦЕ-ДИРЕКТОР ОИЯИ          _____          _____

ГЛАВНЫЙ УЧЕНЫЙ СЕКРЕТАРЬ          _____          _____

ГЛАВНЫЙ ИНЖЕНЕР          _____          _____

НАЧАЛЬНИК НОО          _____          _____

ДИРЕКТОР ЛАБОРАТОРИИ          _____          _____

ГЛАВНЫЙ ИНЖЕНЕР ЛАБОРАТОРИИ          _____          _____

РУКОВОДИТЕЛЬ ПРОЕКТА          _____          _____

ЗАМ. РУКОВОДИТЕЛЯ ПРОЕКТА          _____          _____

О Д О Б Р Е Н

ПКК ПО НАПРАВЛЕНИЮ          _____          _____

4

**Предлагаемый план-график и необходимые ресурсы для осуществления проекта JUNO/Daya Bay**

| Наименование затрат, ресурсов, источников финансирования | | | Стоимость (тыс.долл.). Потребности в ресурсах | Предложения лаборатории по распределению финансирования и ресурсов | | |
|---|---|---|---|---|---|---|
| | | | | 1 год | 2 год | 3 год |
| Основные узлы и оборудование | Изготовление системы высоковольтного питания ФЭУ JUNO | | 2000 | 1000 | 1000 | - |
| | Поставка детекторов ТТ вето системы JUNO (in-kind contribution) | | 750 | 250 | 250 | 250 |
| | Изготовление и поставка рам ТТ вето системы | | 180 | 90 | 90 | - |
| | Оборудование для тестов ФЭУ и хранилища данных результатов | | 100 | 40 | 30 | 30 |
| | Разработка прототипов защиты ФЭУ от Магнитного Поля Земли | | 30 | 10 | 10 | 10 |
| Необходимые ресурсы | *нормо-часы* | ОП ОИЯИ<br>ООЭП ЛЯП<br>КО ЛЯП | *2100*<br>*2400*<br>*2400* | *700*<br>*800*<br>*800* | *700*<br>*800*<br>*800* | *700*<br>*800*<br>*800* |
| | тыс. долл. | Командировки сотрудников | 500 | 153 | 151 | 196 |
| | | Эксплуатационный взнос Daya Bay | 180 | 60 | 60 | 60 |
| Источники финансирования | Бюджет | | 2990 | 1353 | 1341 | 296 |
| | Внебюджетные средства | Вклад "in-kind" в детекторы ТТ вето | 750 | 250 | 250 | 250 |
| | | | | | | |

Руководитель проекта

**Смета затрат по проекту JUNO/Daya Bay**

| № № пп | Наименование статей затрат | Полная Стоимость Нормочасы Тыс. долл. | 1 год | 2 год | 3 год |
|---|---|---|---|---|---|
| 1. | Ускоритель | - | - | - | - |
| 2. | ЭВМ | - | - | - | - |
| 3. | Комп. Связь | - | - | - | - |
| 4. | *ООЭП ЛЯП (нормочасы)* | *2100* | *700* | *700* | *700* |
| 5. | *ОП ОИЯИ (нормочасы)* | *2400* | *800* | *800* | *800* |
| 6. | *КО ЛЯП (нормочасы)* | *2400* | *800* | *800* | *800* |
| 6. | Материалы | 120 | 60 | 50 | 10 |
| 7. | Оборудование | 2160 | 1070 | 1070 | 20 |
| 8. | Оплата НИР | 30 | 10 | 10 | 10 |
| 9. | Эксплуатационный взнос | 180 | 60 | 60 | 60 |
|  | Командировочные расходы | 500 | 153 | 151 | 196 |
|  | **Итого по прямым расходам (тыс. долл.)** | **2990** | **1353** | **1341** | **296** |

**Руководитель Проекта**

**Директор Лаборатории**

**Ведущий инженер-экономист Лаборатории**

6

# 1. Executive Summary

With a discovery of a non-zero value of $\theta_{13}$ by Daya Bay experiment in 2012, all angles of the lepton mixing matrix are now measured. The neutrino mass hierarchy appears currently as one of the hottest topics in neutrino physics. Many researchers all over the world focus their attention on determination of neutrino mass hierarchy using various experimental techniques.

JUNO, a reactor antineutrino experiment under construction in China, aims to determine the neutrino mass hierarchy with median sensitivity corresponding to 3-4 standard deviations by 2026. The expected result will be the most accurate by that time and could be superseded by next generation of accelerator experiments, DUNE [1] only a decade later.

JUNO is an international Collaboration bringing scientists from Asia, Europe, Northern and Southern America to work together. Overall, there are more than 440 scientists and engineers from about 50 institutions in JUNO Collaboration. JINR plays a major role in JUNO Collaboration.

JINR team is responsible for design and production of high voltage units for JUNO large (20 inches) and small (3 inches) photomultipliers (PMTs). A JINR proposal to develop the HV unit situated at the PMT itself was accepted by the Collaboration and contributed to the motivation of the attached to the PMT overall design of the whole JUNO electronics.

JINR team is also participating in the construction of the Top Tracker detector aiming to precisely identify cosmic muons passing through the JUNO central detector and producing in their deep inelastic interactions a serious background due to $^9$Li/$^8$He unstable isotopes. The JUNO Top Tracker (TT) is based on OPERA target tracker plastic scintillator planes constructed with a large contribution of JINR in the past. Major part of this detector will be reused for JUNO and accounted as an in-kind contribution of JINR. The JINR team develops a mechanical support system, hardware and software for monitoring of Top Tracker scintillators, tracks reconstruction and data acquisition system (DAQ).

JINR designed and produced a brand new equipment for precise tests and characterization of large PMTs - a scanning station. Four of these instruments will be produced and delivered to JUNO site for precise characterization of about 1000 PMTs.

The mass testing of PMTs will be realized using special containers with 36 boxes each hosting a single PMT. The JINR team is responsible for supplying the light sources used in these containers. The JINR team is also responsible for the corresponding software development, including DAQ and data analysis. Given a great experience of JINR team in PMT tests and characterization, members of our team plan to participate in the development, delivery and commissioning of PMT testing devices, their maintenance and data taking and analyses.

JINR team performed calculations of required design of Helmholtz coils needed to achieve the required shielding of the central detector against the Earth magnetic field. The Collaboration having cross-checked these calculations follows now this design in the construction of shielding equipment.

Large PMTs of the water pool veto system should be shielded individually and JINR group is currently the major force which performs the corresponding shielding design. There are several design options which are currently under investigations.

Another important task which is under active consideration of JINR scientists is related to research and development (R&D) of liquid scintillator (LS) to be used in the central detector of JUNO.

JINR team is also involved in the software development. A study of JUNO sensitivity to neutrino mass hierarchy determination and expected performance of measurement of $\theta_{12}$, $\theta_{13}$, $\Delta m^2_{12}$, $\Delta m^2_{32}$ parameters was performed. We investigated also an impact of $^9$Li/$^8$He and $^{14}$C background contamination on JUNO sensitivity to neutrino mass hierarchy determination and formulated the scientific requirements for the corresponding contributions. These studies are performed within the framework of Global Neutrino Analysis (GNA) package which is under development by the JINR team.

A model for the optics response of a PMT immersed in a medium was developed by JINR scientists and is now implemented in the official JUNO simulation software. The corresponding calculations are being used also for the formulation of requirements to the PMT mass testing technique of JUNO experiment.

A wide front of activities of JINR group in JUNO makes its participation highly visible also in terms of financial  contribution and intellectual impact. Several members of JINR team take leading positions in the organizational structure of JUNO. D.Naumov is a member of Institutional Board and Executive Board. A.Olshevsky is Level 2 Manager in the PMT Instrumentation group. N.Anfimov, Yu.Gornushkin, A.Sadovski and O.Smirnov are Level 3 managers, responsible for PMT testing, TT mechanics, HV system development and Earth Magnetic Field (EMF) shielding, respectively.

In 2018-2020 major weight of JINR team activity is going to be shifted towards JUNO project. This explains the change in the name of our proposal from Daya Bay/JUNO to JUNO/Daya Bay.

Within the Daya Bay Collaboration JINR team performed the following activities during the previous period.

We developed a Dubna selection algorithm which identifies candidates for antineutrino inverse beta decay (IBD) interactions with free proton.

We performed also studies estimating the background to IBD candidates. A study of optimal selection criteria minimizing the expected uncertainty of estimates of oscillation parameters was performed.

We performed an oscillation analysis of Daya Bay data based on 1230 days of collected statistics. This analysis was selected as an official analysis of Daya Bay Collaboration. The most accurate results of Daya Bay Collaboration are based on JINR team analysis. JINR team members were among the editors of a detailed Daya Bay paper.

For the first time we performed a study of wave packet impact on neutrino oscillations using the Daya Bay data. The corresponding collaboration paper was based on JINR team analysis and written by JINR team members.

The reactor antineutrino flux measurement was cross-checked by JINR team. We also participated in the review of the Daya Bay paper.

We conducted a research on measurement of reactor antineutrino energy spectra due to different isotopes. This work is not yet finalized. We also participated in a review of reactor antineutrino spectrum evolution paper by Daya Bay Collaboration.

Last but not least we conducted a search for sterile neutrino, reviewed analyses of other groups and were among the editors of Daya Bay papers.

Within the Daya Bay Collaboration we plan to continue data analyses to release the most precise determination of $\theta_{13}$ and $\Delta m^2_{32}$;  more precise measurement of reactor antineutrino energy spectra and possibly its isotope decomposition; continue data taking and its calibrations.

In summary,
- the JINR team showed a strong involvement in analyses of Daya Bay data and plans to continue this work
- the JINR team plays a leading role in many of the subjects of JUNO detector construction and analyses preparation. There are very well defined plans for the next three years which should be critical for the success of the experiment startup planned for 2020.

We request 2930 K$ for three years of the project extension 2018-2020 for a successful participation in JUNO and Daya Bay experiments. The details of this request are presented in relevant parts of the project below.

# 2. Introduction

## 2.1. Physics Motivation

In the Standard Model (SM) charged leptons and neutrinos are mixed in their interactions with charged W bosons. The mixing is governed by the corresponding Pontecorvo-Maki-Nakagawa-Sakata mixing matrix. To date, all the elements of the mixing matrix, except for Dirac and Majorana possible phases of CP violation, are measured. The last unknown till 2012 mixing angle $\theta_{13}$ was precisely measured by Daya Bay experiment [2] and confirmed by reactor (RENO, Double Chooz) and accelerator (T2K, NOvA) experiments.

Observation of neutrino oscillations proved that at least two of the three neutrino masses are nonzero. The matter effect in the Sun allowed to determine that $m_2 > m_1$. The neutrino mass hierarchy ($m_3 > m_1$ or $m_1 > m_3$) today is an open question and it is one of the key issues of neutrino physics.

### 2.1.1. Open questions in neutrino physics

While last two decades are remarkable in significant progress in understanding of neutrino properties, there are still open questions in neutrino physics intriguing the researchers. Let us briefly mention some of these topics.

1. Neutrino mass nature. We still do not know if neutrino is Dirac or Majorana particle.
    - A number of experiments like GERDA, CUORE, KamLand-Zen, EXO, SuperNEMO are pushing forward to address this issue.
2. Neutrino mass hierarchy.
    - There are several proposals to determine the neutrino mass hierarchy using accelerator (NOVA, T2HK, DUNE), atmospheric (PINGU/ORCA, INO) and reactor neutrinos (JUNO, RENO-50).
3. CP violation. The CP-violation phase is currently not known while there are experimental indications that its value is close two $3\pi/2$.
    - Accelerator experiments T2HK, NOVA and DUNE should shed a light on this parameter.
4. Mixing matrix unitarity. Currently all oscillation analyses assumed the unitarity of the mixing matrix. However, in presence of a hypothetical sterile neutrino state, the 3x3 mixing matrix is not unitary anymore. Therefore, a thorough verification of lepton mixing unitarity is highly relevant.
    - A joint analysis of data from accelerator, reactor including highly accurate JUNO data will address this issue.
5. Neutrino mass.
    - The KATRIN experiment using tritium decays will probe the mass scale down to 0.2 eV.
    - The next generation of cosmological experiments, like CMB-S4 will probe the scale down to 0.05 eV.
6. Origin of astrophysical neutrinos detected by IceCube.

### 2.1.2. Neutrino mass hierarchy

Let us briefly discuss possible prospects of determining the hierarchy of the neutrino masses in different approaches. Sometimes in the literature can be found the assertion that the hierarchy of neutrino masses is just a sign of $\Delta m^2_{31}$, which is only partly correct, as it is more

correct to say that the various hierarchies of neutrino mass and changing the sign and the absolute value of $\Delta m_{31}^2$ .

The probability of vacuum oscillations depends on the ordering of the neutrino masses. Different orderings of neutrino masses result in a different value of the neutrino oscillation probability. This observation is a key in determining the hierarchy in experiments with reactor antineutrinos. The optimum detector distance from the reactor to increase the sensitivity to the determination of the mass base of the hierarchy is about 52-53 km.

Two experiments JUNO [3] and RENO-50 [4] plan to measure the neutrino mass hierarchy using reactor antineutrinos. JUNO experiment with an active participation of JINR physicists will use the liquid scintillation detector weighing 20 kilotons, viewed from the inside with two tens of thousands of PMT. The energy spectrum of antineutrinos from reactors is modulated by neutrino oscillations with frequencies driven by $\Delta m_{21}^2$ and $\Delta m_{31}^2$ , and will depend on the neutrino mass hierarchy. Measurement of the mass of the hierarchy is only possible with good energy resolution of the detector, better than 3% at 1 MeV of released energy.

Experiments with accelerator neutrinos NOvA [5] (gathering data) and the DUNE [1] (in preparation) used the oscillations of neutrinos and antineutrinos in the matter to determine the neutrino mass hierarchy. In these experiments, observing the appearance of electron (anti)neutrinos in the beam of muon (anti)neutrino at a great distance from the source. Since the main way of neutrinos passes through the Earth, the neutrino oscillation probability is modified by matter. Qualitatively, the effect of matter can be represented as follows. Electronic neutrino in matter becomes heavier and exiting the Earth most probably would appear as $v_\tau$ for the normal mass hierarchy and as $v_\mu$ for the inverted one.

As a result, due to the effect of matter, the probability of neutrino oscillations $P_{\mu e}$ is amplified for normal hierarchy and suppressed for the inverted, leading to different numbers of observed $v_\mu$ and $v_e$.

Modification of neutrino oscillations in the matter to be used in experiments with atmospheric neutrinos, such as PINGU [6] and ORCA [7], HyperKamiokaNDE [8], INO [9]. Since both muon and electron neutrino and antineutrino are produced in the atmosphere, such experiments are sensitive to four channels of the oscillations at once: $v_\mu \rightarrow v_\mu$, $v_\mu \rightarrow v_e$, $v_e \rightarrow v_e$, $v_e \rightarrow v_\mu$ for neutrino and antineutrino. Furthermore, these experiments are sensitive to neutrinos coming from different angles, which corresponds to a different path traveled in the Earth.

In the case of normal hierarchy the survival probability of atmospheric muon neutrinos passing through the Earth, has a resonance at an energy of 5 GeV and zenith angle determined by cosθ = -0.95. The other three channels have a more pronounced oscillations of neutrinos with respect to the antineutrino.

In the case of the inverse hierarchy behavior changes: antineutrinos would have a more pronounced transition probability than neutrinos. Despite the fact that the experiments with atmospheric neutrinos, as a rule, can not distinguish between neutrinos from antineutrinos, the definition of the hierarchy with their help it is possible, taking into account the differences in the flux, cross-section and kinematics of (anti) neutrino.

Cosmological measurements also have a sensitivity to the neutrino mass hierarchy. In the case of the normal mass hierarchy sum $\sum m_i$ is primarily determined by the greatest mass $m_3$, as $\Delta m_{31}^2 >> \Delta m_{21}^2$ and $\sum m_i \cong m_3 \gtrsim 0.05$ eV. The inverted hierarchy implies that $m_3 << m_{1,2}$ and now the sum $\sum m_i \cong m_1 + m_2 \gtrsim 0.1$ eV. In order to achieve sensitivity to the neutrino mass hierarchy it is required to increase the accuracy of cosmological measurements by 2-4 times in comparison with the present day. The next generation of catalogs of clusters and superclusters of galaxies will have sufficient sensitivity to neutrino mass scale, which will explore both hierarchies of neutrino masses.

The value of the effective mass of the neutrino obtained from the probability neutrinoless double beta decay $m_{\beta\beta}$ depends on the neutrino mass hierarchy. Thus, the search $m_{\beta\beta}$ decay is an additional source of information about the hierarchy of neutrino masses.

In we provide for a reader convenience a comparison of expected median sensitivities to neutrino mass hierarchy determination of various accelerator, atmospheric, reactor and cosmological experiments. JUNO has a good perspective to be the first experiment to determine the mass hierarchy statistical significance exceeding three standard deviations.

| Project | v source | Detector | Goal | Challenges |
|---------|----------|----------|------|------------|
| NOVA | LBL (810 km) | 14 kt tracking calorimeter | 2σ (2020) | Parameter degeneracy |
| JUNO | Reactor (53 km) | 20 kt LS | (3-4)σ (2026) | Energy resolution |
| PINGU/ORCA | Atmosphere | (1-10) Mt of ice | (3-5)σ (unknown) | Energy resolution, systematics |
| INO | Atmosphere | 50 kt magnetized calorimeter | 3σ (2030) | Low statistics (10 years) |
| T2HK | LBL (295 km) | 1Mt of water | 3σ (2030) | Parameter degeneracy |
| DUNE | LBL (1300 km) | 1kt of liquid argon | (3-5)σ (2030) | Parameter degeneracy |
| Cosmology | Early Universe | CMB-S4 bolometers | 4σ (>2023) | Dependence on cosmological models |
| Tab.2.1.1 Comparison of expected median sensitivities to neutrino mass hierarchy determination of various accelerator, atmospheric, reactor and cosmological experiments. | | | | |

## 2.2. JUNO Experiment

JUNO is an experiment with reactor antineutrinos of the next generation. It will be located in southern China and is under preparation by a large international team, comprising staff members of JINR. The main objectives of the experiment are to determine the mass hierarchy and precise measurement of the neutrino mixing parameters.

JUNO is a multi-purpose experiment with rich physics program, including:

- neutrino mass hierarchy determination with expected sensitivity corresponding to 3-4 standard deviations,
- precision measurement of $\sin^2 2\theta_{13}$, $\Delta m^2_{32}$, $\sin^2 \theta_{12}$ with accuracy better than 1%,
- possible observation of SuperNova neutrinos,
- detection of geo-neutrinos with a factor ten larger statistics than currently available,

- detection of diffuse SuperNova neutrinos,
- detection of solar neutrinos,
- detection of atmospheric neutrinos,
- study of sterile neutrino,
- indirect dark matter search,
- non-standard interaction study and other probes of new physics.

The detector of JUNO will be located in the Kaiping country of the Guangzhou province in China (to the west from the Hong Kong) on average distance of 53 km from the reactors (see Fig. 2.1.). Experiment will observe the antineutrino flux mainly from two nuclear power plants of total expected thermal power 35.8 GW: NPP Taishan, 2 cores under construction; and NPP Yang Jiang, 4 cores running, 2 cores under construction.

JUNO will use spherical scintillator detector with diameter of 35 meters. The schematic view of it is presented on figure 2.2. It will contain 20 kt of liquid scintillator and will be equipped with 18k of 20″ PMTs and with 25k of 3″ PMTs. In order to observe the neutrino mass hierarchy JUNO detector should be able to discriminate fine oscillations in the observed inverse beta-decay spectrum. In order to do this it is necessary to achieve the remarkable energy resolution[1] of σ=3% at 1 MeV.

The energy uncertainty in case of JUNO is dominated by the uncertainty of the collected photon statistics. Therefore, the resolution may be maximized by the maximization of the photon collection. In order to achieve σ=3% at 1 MeV the photon collection should be 1200 p.e./MeV. The steps made in order to achieve such a resolution include:



Figure 2.1. JUNO experiment will be located in the Kaiping country and will observe electron antineutrino flux from the nuclear power plants Yangjiang and Taishan. Second mark represents the secondary experiment location option at Huizhou. The location of the Daya Bay experiment is also marked.

1. Maximizing the PMT geometrical coverage;
2. Maximizing the PMT quantum efficiency;

---

[1]In what follows we refer to gaussian σ (square root of variance) when talking about energy resolution

3. Optimization of the fluor concentration, operational temperature and scintillator light yield;
4. Disregarding the gadolinium doping option which is commonly used in reactor neutrino experiments. Adding the gadolinium to the scintillator greatly increases signal to background ratio, but lowers the scintillator transparency and makes it less stable in time. The expected experiment lifetime of 6-10 years is not compatible with usage of the gadolinium doped liquid scintillator;

The required numbers are summarized in table 2.1. For the comparison we show also the characteristics of the KamLAND detector, the largest scintillator detector so far.

The overburden is 700 m of rock, which is equivalent to 2000 m.w.(e.). The detector is located within water pool which is used as active muon veto. In addition there is precision muon Top Tracker, covering about ⅓ of the top surface.

The detector will see about 83 antineutrino events per day. The main source of the background events are the events of the $^{8}He/^{9}Li$, produced by cosmogenic muons. We expect to have 84 of $^{8}He/^{9}Li$ events per days before cuts and 1.6 after applying cuts. Other sources of the background events include accidental events due to natural radioactivity, muon induced fast neutrons, $^{13}C(\alpha,n)^{16}O$ reaction and geoneutrinos. After applying the cuts we expect to detect 60 antineutrino events per day and 3.8 of the background events per day. More details can be found in table 3.3.2 on page 24.
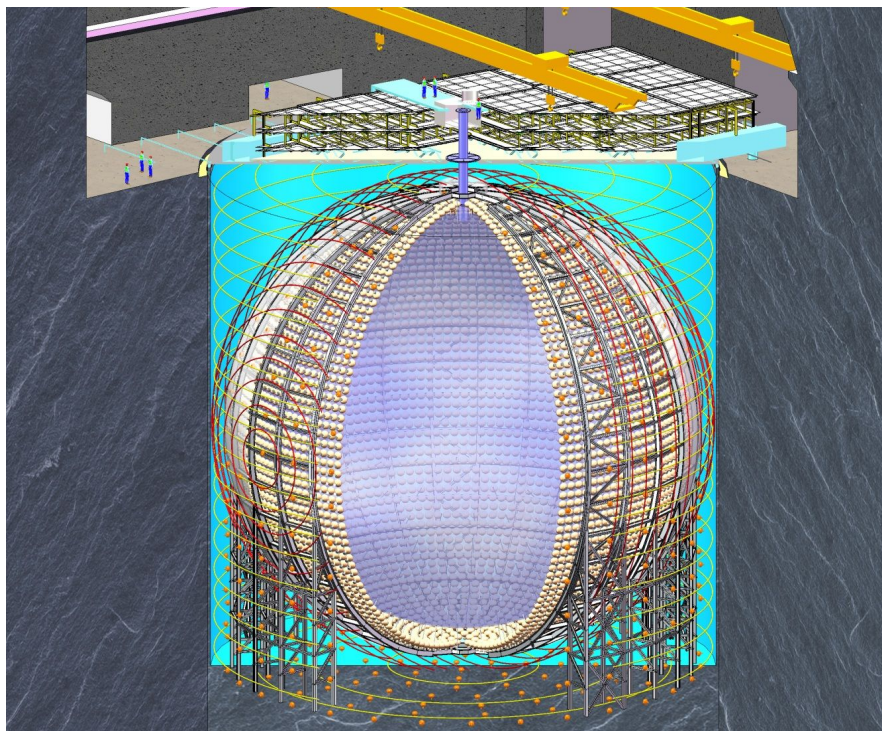


Figure 2.2. Schematic view of the JUNO detector.

In Fig.2.2.1 we display expected prompt energy spectrum of JUNO experiment for the hypothesis of no oscillations, and for 3 neutrino oscillation models assuming normal and inverted hierarchies. The statistics corresponds to six years of data taking. The difference in shapes of the latters is a key in determination of neutrino mass hierarchy. The expectations in Fig.2.2.1 account for matter effects on neutrino oscillations (up to 3%), geo-neutrino signal and actual configuration of JUNO reactors.

In Fig.2.2.2 we display $\Delta\chi^2$ corresponding to the test of neutrino mass hierarchy as a function of the mass splitting parameter. Assumptions about accuracy of $\Delta m^2_{\mu\mu}$ are also used as

penalty terms in $\chi^2$. $\Delta\chi^2$ is above 10 when no information about $\Delta m^2_{\mu\mu}$ is used and is above 16 if $\Delta m^2_{\mu\mu}$ is known with 1% accuracy.

|  | KamLAND | JUNO | Factor |
|---|---|---|---|
| Target mass, kt | 1 | 20 | 20 |
| Energy resolution, %/ $\sqrt{E}$ | 6 | <3 | >0.5 |
| Photon collection, p. e./MeV | 250 | 1200 | 5 |
| PMT coverage, % | 34 | 75 | 2.3 |
| PMT QE, % | 11 | 35 | 3.2 |
| Position reconstruction, cm/ $\sqrt{E}$ | ~12 | 12 | 1 |

Table 2.1. Main requirements to the characteristics of the JUNO detector and comparison to that of KamLAND experiment.

Final resolution of reconstructed prompt energy partially washes out the difference in energy spectra due to mass hierarchy as illustrated in Figs. 2.2.3-2.2.4 which correspond to 3%/√E and 4%/√E energy resolution accuracy.



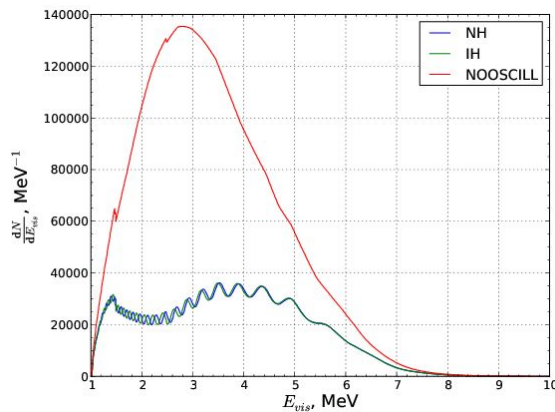Fig.2.2.1 Expected prompt energy spectrum of JUNO experiment for the hypothesis of no oscillations (NOOSCILL), and for 3 neutrino oscillation models assuming normal (NH) and inverted (IH) hierarchies.
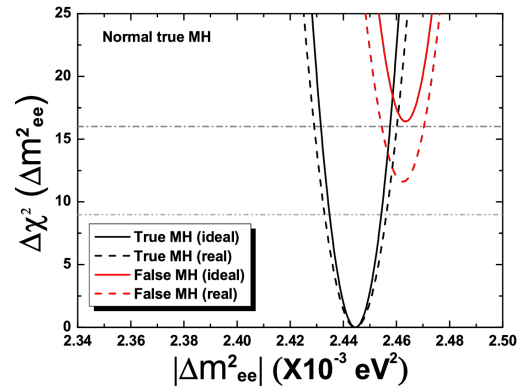
Fig.2.2.2 $\Delta\chi^2$ corresponding to the test of neutrino mass hierarchy as a function of the mass splitting parameter. Assumptions about accuracy of $\Delta m^2_{\mu\mu}$ are also used as penalty terms in $\chi^2$.
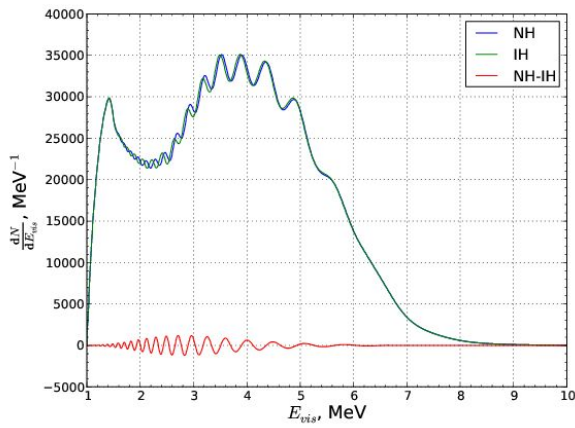
Fig.2.2.3 Reconstructed JUNO prompt energy spectra for normal (NH) and inverted (IH) neutrino mass hierarchies assuming 3%/√E energy resolution.
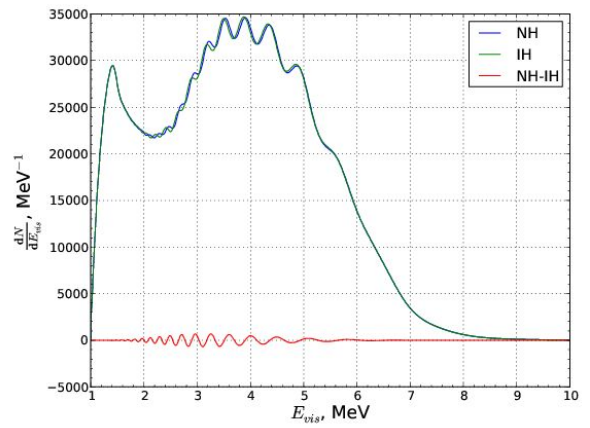
Fig.2.2.4 Reconstructed JUNO prompt energy spectra for normal (NH) and inverted (IH) neutrino mass hierarchies assuming 4%/√E energy resolution.

## 2.3. Daya Bay Experiment

The Daya Bay experiment is an experiment with reactor antineutrinos currently ongoing in China. In Fig.2.3.1 we show the location of reactor complexes Daya Bay, Ling Ao and Ling-Ao II. Antineutrino detectors of Daya Bay experiment are located in three experimental halls: two near and one far. Two near halls contain a pair of antineutrino detectors each. The far hall contains four antineutrino detectors. The far hall is shielded by 350 m of rock from cosmics.

Fig.2.3.1 Reactor complexes Daya Bay, Ling Ao and Ling-Ao-II. Antineutrino detectors of Daya Bay experiment are located in three experimental halls: two near and one far. Two near halls contain a pair of antineutrino detectors each. The far hall contains four antineutrino detectors. The far hall is shielded by 350 m of rock from cosmics.

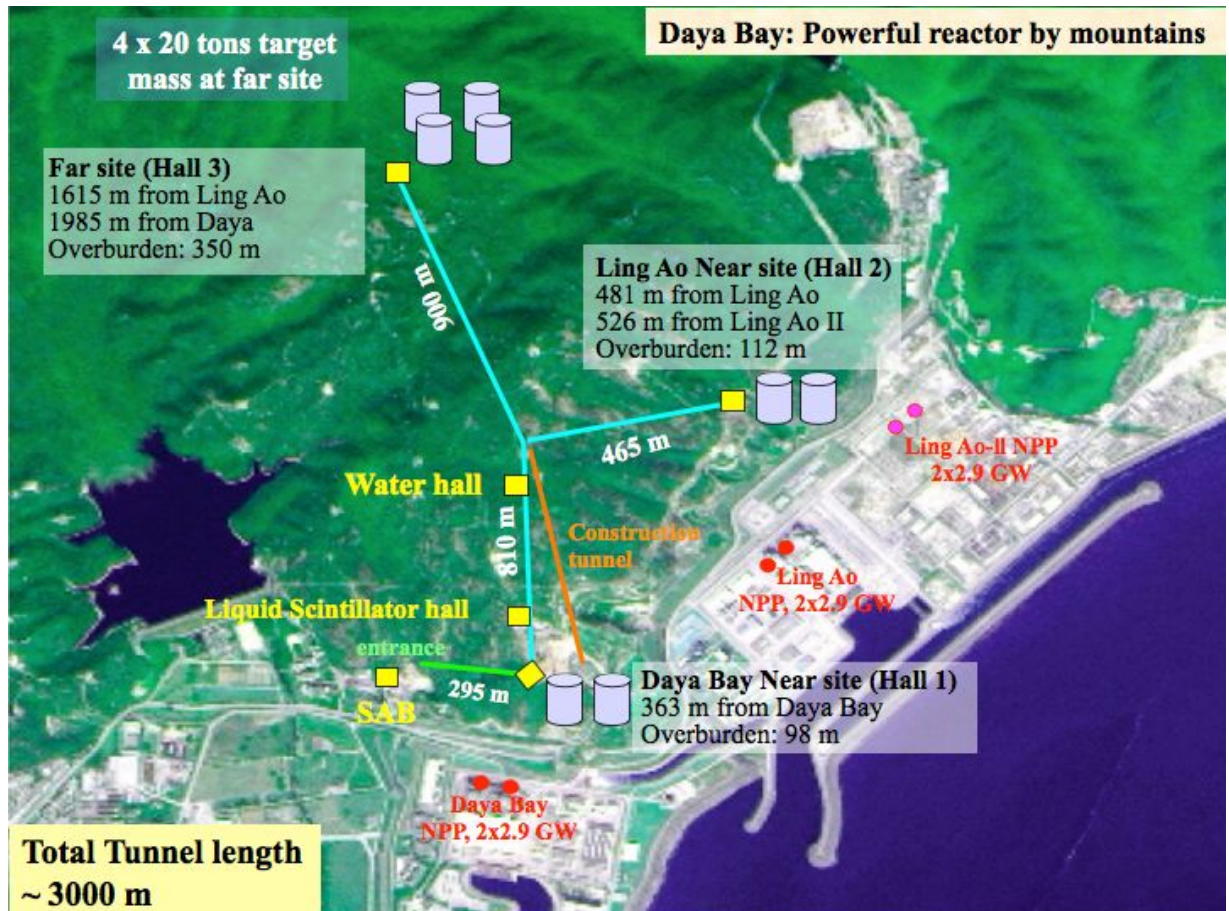The antineutrino detectors of Daya Bay experiment are identically designed. A sketch of the antineutrino detector is shown in Fig.2.3.2. It is a three zone detector. The inner zone containing 20 tons of LS doped with gadolinium is used as a main target of antineutrino interactions. The middle zone containing 20 tons LS without gadolinium is used primarily as gamma catcher which ensures good energy resolution and uniformity of the detector. The outer zone containing 40 tons of mineral oil suppresses the background due to radioactivity.

Each antineutrino is served with three automatic calibration systems to ensure stable time and energy response of the detector.

The main objective of the Daya Bay experiment was a measurement of $\theta_{13}$. A non-zero value of $\theta_{13}$ was discovered in 2012 by the Daya Bay Collaboration. This discovery was awarded by a number of prizes, for example, a prestigious Breakthrough Prize was awarded to members of the Daya Bay Collaboration[2] in 2016.

Now Daya Bay experiment provides the most accurate measurement of $\theta_{13}$ and $\Delta m^2_{32}$. There are several other important analyses of Daya Bay data performed so far which yielded important results. We discuss these results in the corresponding section 6.
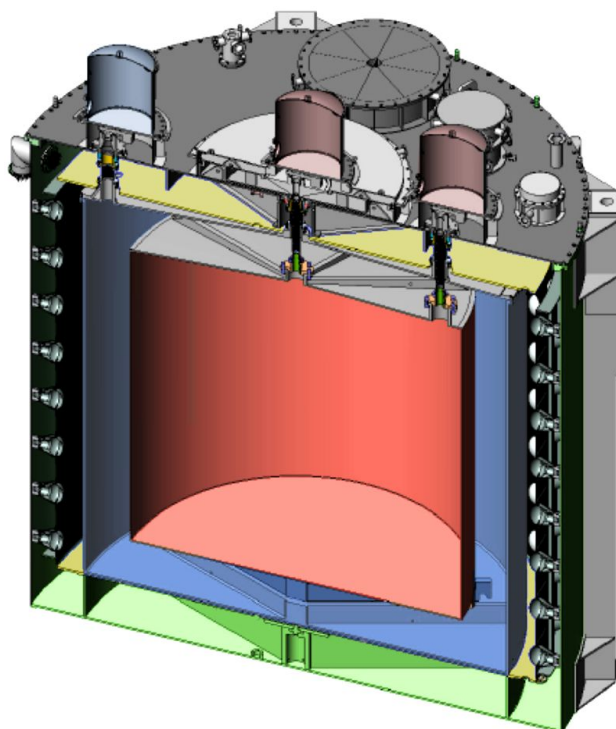


Fig.2.3.3 Daya Bay antineutrino detector.

The main objectives of proposed prolongation of Daya Bay project in JINR are related to
- most precise determination of $\theta_{13}$ and $\Delta m^2_{32}$;
- measure more precisely reactor antineutrino energy spectra and possibly its isotope decomposition;
- more sensitive search for a light sterile neutrino;
- search for supernova neutrinos;
- search for non-standard neutrino interactions;

---

[2] including members of JINR team

● perform R&D for JUNO related to LS.

## 2.4. JUNO/Daya Bay project in the context of JINR Neutrino Program

JINR Neutrino program is a wide experimental and theoretical neutrino research program encompassing essentially all most relevant aspects of neutrino physics [10].

In what follows we give a brief summary of the program. Next we discuss the place of the proposed project extension in the program.

JINR Neutrino Program deals with most of existing sources of neutrinos: accelerator (NOVA and OPERA; will be extended by DUNE in the future); short (DANSS, GEMMA-2, vGEN), medium (Daya Bay) and long (JUNO) baseline reactor; solar and geo (BOREXINO, JUNO); astrophysical and atmospheric (BAIKAL GVD); radioactive source (SOX); and neutrinoless double beta decay (GERDA, SuperNEMO) experiments.

In terms of physical topics studied in the JINR Neutrino Program let us mention the following:

- Neutrino mass hierarchy determination:
  - NOVA, JUNO and DUNE address this issue. Different systematics and sensitivity should provide the most robust result.
- Precise determination of lepton mixing angles $\theta_{12}$, $\theta_{13}$, $\theta_{23}$ and neutrino mass splittings $\Delta m^2_{32}$, $\Delta m^2_{21}$:
  - NOVA, DUNE, OPERA, BOREXINO, Daya Bay and JUNO provide a complementary picture.
- Detection of geo-neutrino:
  - BOREXINO is one of the two experiments (including KamLAND) which unambiguously observed geo-neutrino signal, creating a new field in physics.
  - JUNO will collect a factor of ten more events than the current record.
- Nature of neutrino mass or whether neutrino is a Dirac or Majorana particle:
  - GERDA and SuperNEMO experiments.
- Observation of astrophysical neutrino of ultra high energies is a primary goal of
  - BAIKAL GVD detector which is currently under construction with up to about cubic kilometer volume. BAIKAL GVD is already taking data and has detected some promising events.
- Atmospheric neutrinos are detected by
  - BAIKAL GVD experiment.
  - Also JUNO would be able to detect and study atmospheric neutrinos in great details.
- Solar neutrinos are studied in great details by
  - BOREXINO experiment.
  - JUNO will also provide a unique study of solar neutrinos given it large detector and unprecedented energy resolution.
- Search for sterile neutrino is performed by
  - Experiments with reactor antineutrinos: Daya Bay, DANSS and JUNO.
  - An experiment with a radioactive source: SOX.
- Search for Supernova neutrinos is performed by
  - Daya Bay, NOVA and JUNO experiments.
- Studies of electromagnetic properties of neutrinos are performed by
  - GEMMA-II reactor antineutrino experiment performed at Kalinin NPP.
  - BOREXINO solar neutrino experiment.
- Coherent Neutrino Germanium Nucleus Elastic Scattering
  - is planned to be observed for the first time by vGEN experiment performed at Kalinin NPP.

JINR has acquired a wide and deep expertise in all fields of neutrino physics, including theoretical studies not mentioned here. JINR plays a leading role in JUNO and Daya Bay experiments. The proposed extension of JUNO/Daya Bay project aims to further increase JINR visibility in these experiments and consolidate efforts of JINR physicists and engineers  in first class worldwide research programs.

JUNO/Daya Bay project is considered by JINR scientists as one of the fundamental pillars of JINR Neutrino Program including BAIKAL GVD, Kalinin NPP and NOVA (DUNE). The budget associated to these projects exceeds 85% of the total funding of JINR Neutrino Program.

# 3. JUNO at JINR

## 3.1. Brief summary

JINR plays a key role in the JUNO project addressing a wide range of topics. The list of tasks harmoniously contains development of manufacture of hardware, methodological problems, the solution of which will allow to overcome the main technological difficulty of the experiment - a record accuracy in recovering of released energy in the liquid scintillator; development of software for the energy reconstruction, position of events of antineutrino interactions, their selection, calibration, background suppression, statistical data analysis using modern approaches; development of methods and software for the measurement of boron solar neutrinos. These items are briefly summarized below.

1. JINR contribution to the JUNO experiment comprises the development and manufacture of high-voltage power supply for about 20 000 Photoelectron multipliers (PMT) with a diameter of 20" and 36 000 PMT with a diameter of 3"

2. JINR contributes in a development and construction of a precision part of the JUNO muon veto system - Top Tracker. The latter is based on OPERA Target Tracker detector which was constructed with a large contribution of JINR in the past. This detector, is now refurbished and will be reused again. JINR group will provide its maintenance, installation, DAQ, design, production and delivery of mechanical support, and simulation and reconstruction software.

3. JINR continue a development of measurement techniques evaluating PMT performance, including scanning over its surface; develop criteria for acceptance of PMT based on the experimental requirements for the energy resolution. Develop fast PMT testing procedures that can be used for mass testing of all 20,000 photomultipliers of JUNO experiment. This procedure should effectively identify possible deviations in the characteristics of the PMT and, at the same time be simple enough to enable automation and implementation within a reasonable time (2 days).

4. JINR team develops methods of the PMT protection against the EMF. This is particularly relevant for large photomultipliers with a diameter of 20", essentially losing the detection efficiency of photons in the Earth's magnetic field.

5. JINR works on software development for the simulation of the detector response accounting for results of calibrations. Software development for the reconstruction of a energy deposited in liquid scintillator, position of antineutrino interaction and tracks of muons.

6. Development of software for selection of events of antineutrino interactions in the LS detector. Study of background contamination, development of criteria for background suppression.

7. Software development for the statistical analysis of the data, including the evaluation of sensitivity to the JUNO mass hierarchy and measurement of mixing according to different sources of systematic uncertainty. Software will serve as an useful tool for the JUNO collaboration in the development of requirements for the allowable level of background, the accuracy of calibrations and systematic uncertainties.

8. Development of the method of measurement and the corresponding software for the precise measurement of the flux of boron neutrinos from the Sun in the energy range from 3 to 15 MeV. The relevance of such a measurement is related to the possibility of solving the problem of solar metallicity.

## 3.2. Research and Development of High Voltage Unit

An important functional part of the JUNO electronics is the High Voltage (HV) supply of PMT. Given the experience of many other experiments this part represents one of the most delicate ones, driving, to the large extent, the reliability and stable operation of the whole electronic channel. Different electronics layouts were considered in the JUNO experiment from the very beginning, but practically all of them were requiring underwater layout of the HV Unit (HVU). Finally, the layout presented in Figure 3.2.1 was chosen as a baseline.
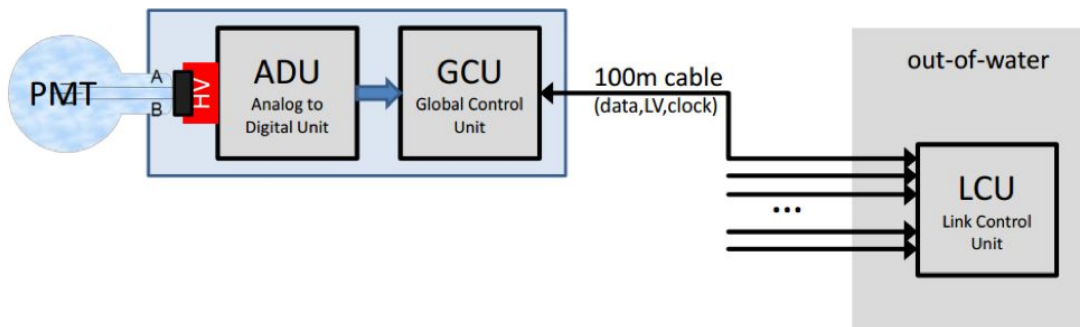


Figure 3.2.1. Layout of the baseline option of JUNO electronics.

It contains the full electronics chain, including digitisation of the signal, potted with the PMT itself and operating in the underwater conditions. While such a scheme has clear advantages in the low noise level during signal processing, it poses additional stringent requirements to the reliability and stable operation of the whole electronics, in particular, the HVU, because the exchange of the failed part becomes impossible. The general requirement to the JUNO PMT+Electronics channel was formulated as <1% failures during 6 years of operation and <10% failures during 20 years of operation. Such level of reliability is very difficult to achieve, in particular, because for the reliability proof at that level numerous elements long time tests are required, even in temperature accelerated conditions.

The JINR group from the very beginning took the responsibility of designing the necessary PMT HV power supply and formulated the requirements to the HVU parameters. These requirements are matched to the PMT performance and physics goals of the experiment, which should be achieved, in particular, stable operation providing an ultimate energy resolution of 3% at 1 MeV of the deposited antineutrino energy. After taking into account an experience of different experimental solutions the following general principles were applied: the HVU was proposed to be designed as a separate intellectual unit powered by the low voltage (+24V) and producing HV up to 3KV with the maximum current of 300 mkA and as lower power dissipation as possible. The latter requirement suggests the use of a Cocroft-Walton scheme, which can provide up to 90% efficient DC-DC conversion. Operation and a cross check of the HV parameters should be controlled internally by the micro-controller, which sets the necessary parameters and monitors the operation by measurements of the actual HV and some other parameters. The HVU micro-controller communicates to the Global Control Unit (GCU) by means of a hardware interface and a set of commands implemented in the HVU firmware. The proposed set of basic requirements to the HVU is presented in Table 3.2.2.

| Parameter | Requested value |
|-----------|-----------------|

| | |
|---|---|
| HV Polarity | Positive, PMT Cathode grounded scheme |
| Output voltage regulation range | 1500-3000 V |
| Step of the output voltage regulation | ~ 0.5 V |
| Output voltage ripple (peak to peak) | 10 mV at maximum output |
| Systematic error of the output voltage setting | 3% |
| Stability of the output voltage | 0.05% |
| Output voltage temperature coefficient | 100 ppm/degree C |
| Maximum anode current | 300 mkA |
| Input voltage | +24 V |
| Control interface | RS485 |
| Dimensions | Reasonably small, to be checked later |

Table 3.2.2. Set of basic requirements to the HV unit.

On the basis of these requirements the design of HVU first prototype was requested from two companies: HVSYS and MARATHON. The HVSYS company was known to have an experience of constructing the HV systems for some of the detectors of large experiments, like ATLAS, COMPASS and some others. It uses the outsource production and performs final tuning and operation cross checks at its own facilities. Contrary to that, the MARATHON company has full design and production chain but can also use the larger scale partners for mass production. The first prototypes of HVU from both companies were produced under the contracts with JINR and were tested for functionality and reliability. The pictures of the HVSYS and MARATHON units are presented in Figure 3.2.3 left and right, respectively.
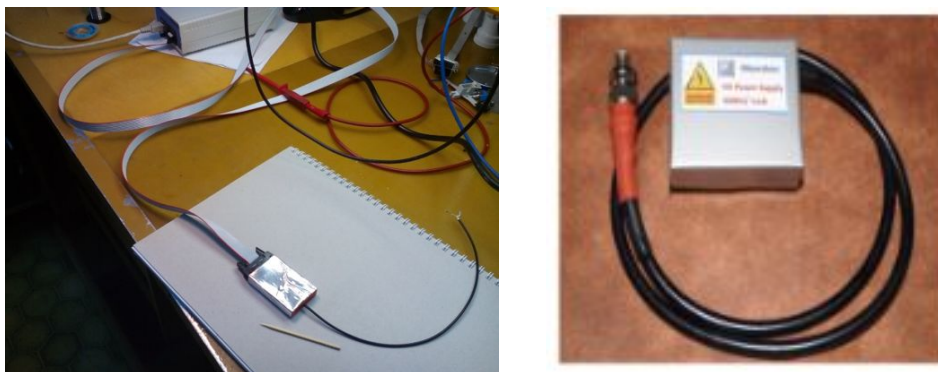


Figure 3.2.3. First prototype from HVSYS (left) and MARATHON (right).

In below, we refer to the design of the HVSYS, which was proven to fully match the expected requested parameters. In addition to the simple functionality and stability tests 38 HVU were exposed to the temperature accelerated test of reliability. The layout of this test and results are shown in Figure 3.2.4.

# HV Units Acceleration Life Test
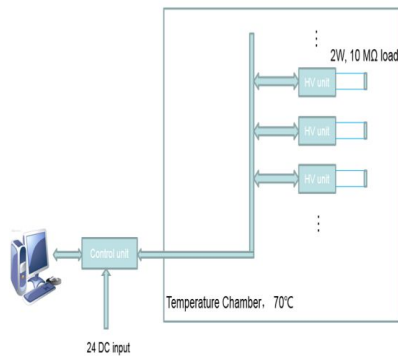


The structure          The inner          The outer

# HV Units Drift observed
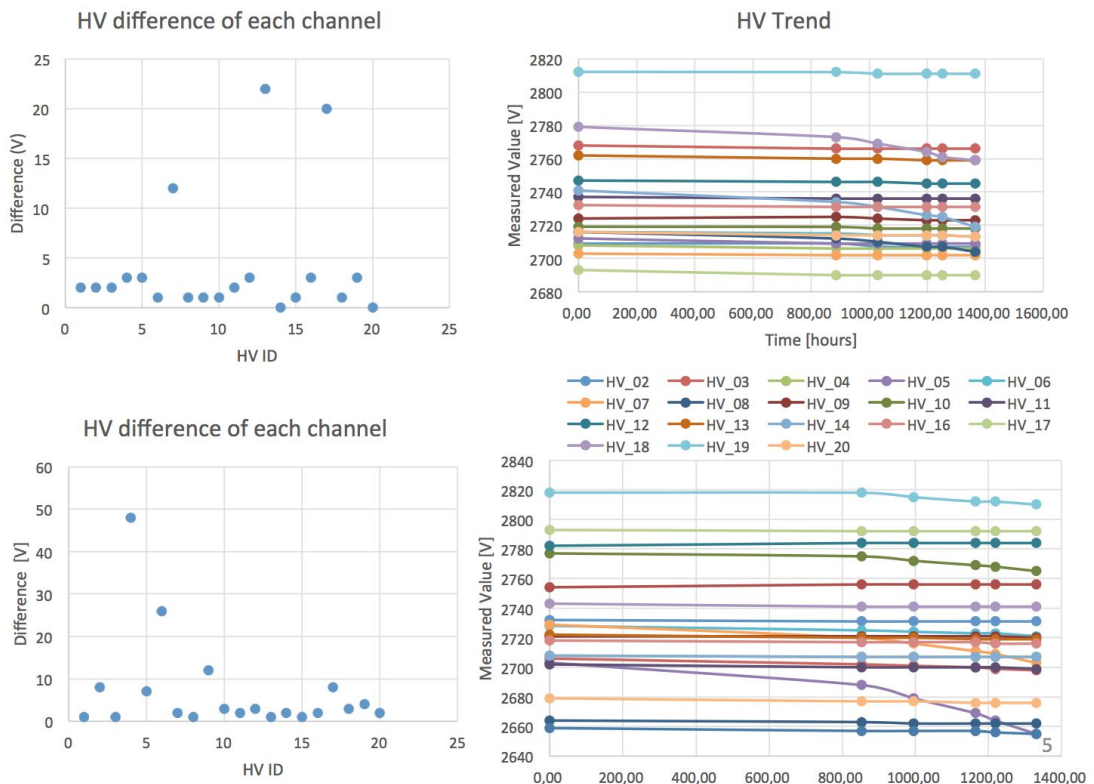


Figure 3.2.4. Layout of temperature accelerated test and results.

The test was performed at the temperature of 70 degrees C, which is close to the maximum allowed for several components inside the HVU. The test was running for nearly one year, integrating about 7000 hours of useful test time. During the test the HV was set up and down and HV measurements were logged. All of the units remained alive and operational after this test, although 5 of them have shown the drift of HV, the exact reason for which should be further understood.

The first prototype design, production and test was actually pioneering the general

design of the JUNO electronics. After the design of the other parts became available the modifications were necessary to be introduced in the HVU to match the design of the PMT base, GCU and Power Board. These modifications were implemented in the design of a second prototype, which we requested from HVSYS only. However, as it was mentioned above, the advantage of the MARATHON company is that it is more suitable for implementing and supervising the internal production tests, which will become an important issue during the HVU mass production and especially quality assurance. Therefore, we initiated a collaboration between those companies, where the HVSYS responsibility stands for the design and MARATHON implements this design in the production and test chain.

The second prototype design at HVSYS was finished by the fall of 2016 and transferred for the production to MARATHON. First samples of this prototype were produced in February 2017 just in time for the test of JUNO electronics assembly. The new schematic and picture of printed circuit board (PCB) are shown in Figure 3.2.5.



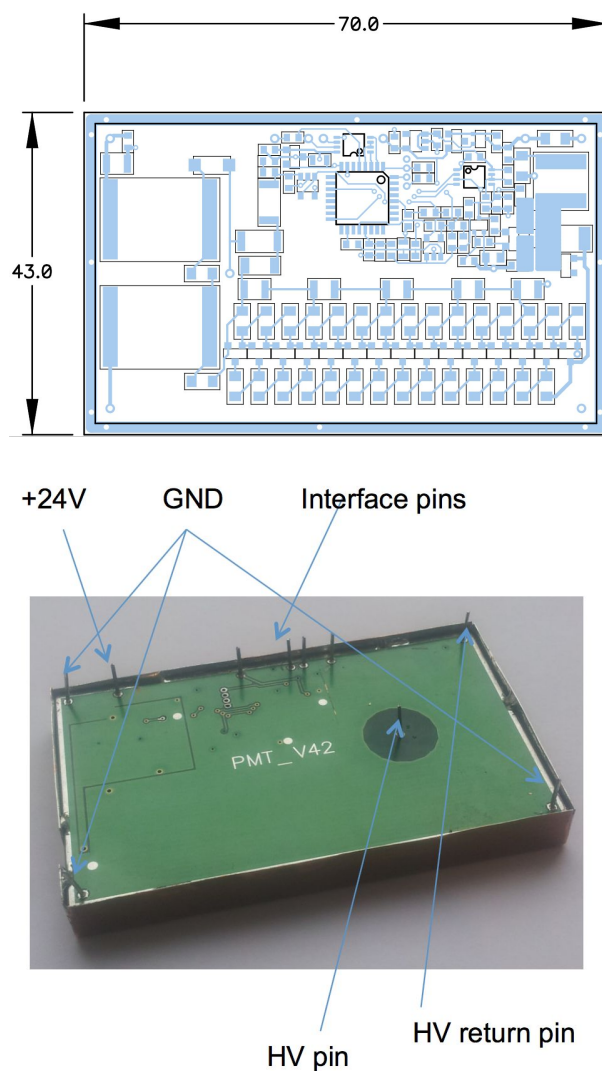Figure 3.2.5. The new schematic and picture of the second HVU prototype.

The test of JUNO electronics assembly went well and, according to our schedule, about 200 HV units will be produced now for the new temperature accelerated reliability tests.

In addition to the work on the design and production of HVU itself we have provided an information about HVU components to the collaborating groups for reliability calculations. First

estimations are showing that the HVU reliability values are reasonably close to the expected ones. However, we are planning to identify by these calculations the least reliable components and try to exchange them for more reliable ones available on the market.

Another important work is the ongoing test of components for radiopurity. The measurements are done by the  collaborating groups with the help of high precision spectrometers. Samples of PCB, metal case and sealant, provided for measurements so far, have shown acceptable level of radioactivity in these materials.

The HVU design and production preparation work is planned to be finished by the end of 2017. The HVU mass production should start at the beginning of 2018 and is planned to take 14 months, in line with the schedule of the JUNO electronics production and potting. By the end of 2017 we should also specify in more details factory tests and quality assurance parameters. The tests are planned to be performed at the MARATHON and special test equipment is being designed now on our request. The JINR team will also have the responsibility to supervise the HVU mass production and quality assurance tests.

The present cost estimate of HVU is ~150$/unit. It is based on the existing experience of contracts with small scale production and take into account some costs of the preparatory work and test equipment design. Our target is to get the single HVU cost down to less than ~100$/unit, less than the cost of industrial general purpose systems, which are, moreover, not directly applicable in the case of JUNO.

Taking into account the total number of ~20'000 HV units, required for the JUNO experiment, the total cost of the HVU production will be about 2'000K$. It can be distributed over 2018-2019 budget according to the production schedule mentioned above. For the HVU mass test production we are planning to perform the bidding procedure, required by the JINR and JUNO collaboration rules.

# 3.3. Top Tracker

The performance of the JUNO experiment is related to its capability to suppress or at least to control the background processes which may have the same signature as the antineutrino signal.

Cut selections on the event time and space correlation will strongly suppress the accidental background. The major concern is the cosmic muon induced backgrounds, because they are hard to remove. They are mainly $^9$Li/ $^8$He isotopes from muon spallation and muon shower particles, and fast neutron background in the detector from muon induced high energy neutrons. The muon rate is estimated at about 0.003 Hz/m$^2$ with the average energy of about 214 GeV. The high energy cosmic muons produce a large number of neutrons in the rocks and other materials surrounding the CD those can produce a background in the CD which mimics the inverse beta decay signal.    The beta-n decay of $^9$Li/$^8$He would mimic the inverse beta decay events even more as the signature is indistinguishable of  IBD events. The number of $^9$Li/$^8$He background events is estimated to be ~ 80/day. Without proper muon veto, their existence would greatly reduce JUNO's capability to determine the neutrino mass hierarchy.
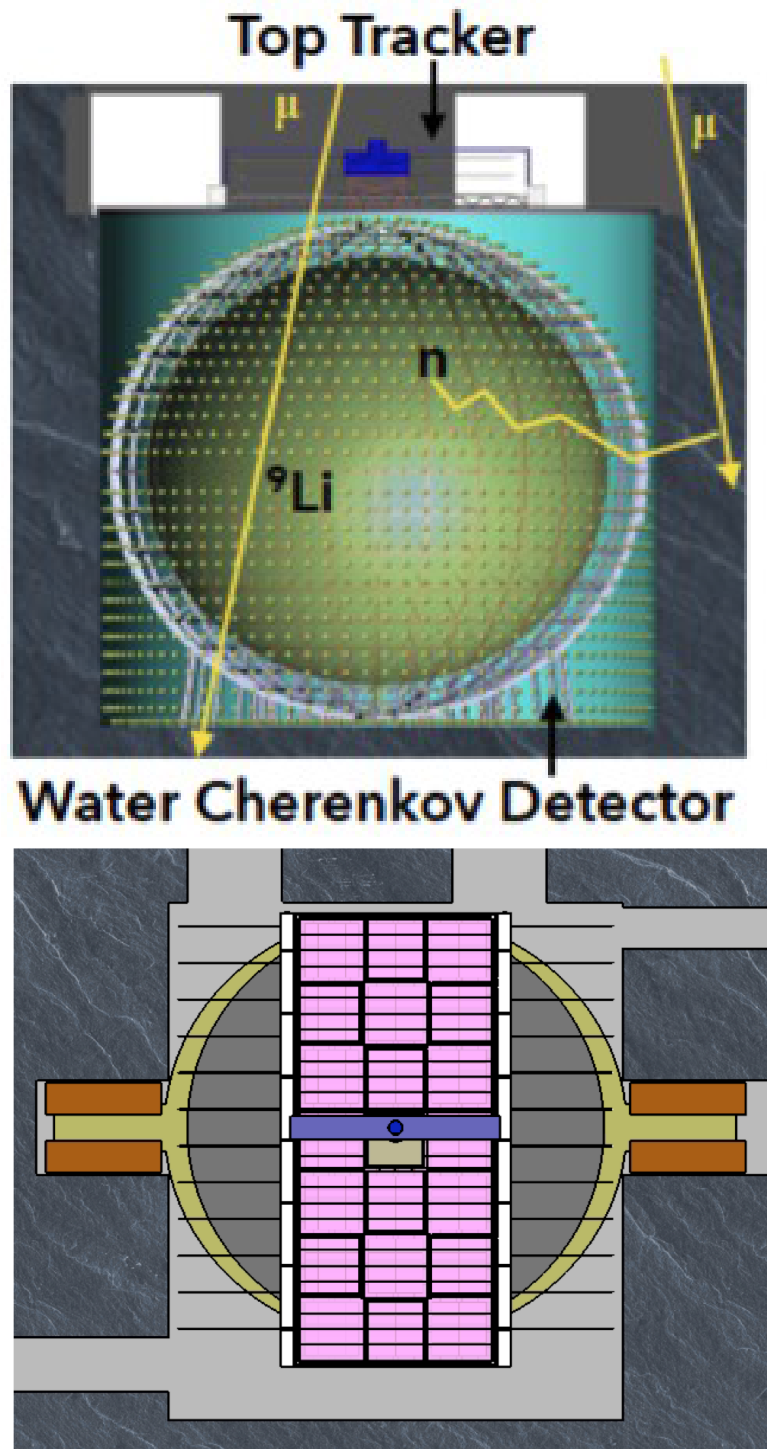
Fig.3.3.1  A general scheme of the Veto system of JUNO from aside (top) and from the top (bottom). The TT detector is shown in rose.

The Veto system of  JUNO  is designed  for muon detection and tagging, muon induced background study and its reduction. It consists of the Top Tracker system and the Water Cherenkov detector. The Water Cherenkov detector is a pool filled  with 20-30 kt purified water, instrumented with PMTs and surrounding the Central Antineutrino Detector  in order to protect the CD against  neutrons and the natural radioactivity in the surrounding rocks.  The cosmic muons passing through the detector are registered in WC by their Cherenkov light with high efficiency (95%) though with a limited spatial resolution (~1 m)  .

The Top Tracker, made of scintillating strips, covers about 1/3 of the top area with 3

layers and capable to reconstruct the cosmic muons direction with much better precision compare to WP. This independent muon information will help in muon tagging, track reconstruction and efficiency study necessary for understanding and reduction of the cosmogenic backgrounds. The $^9$Li/$^8$He background will be reduced by excluding a cylindrical region (about 3 m radius) along the muon track within a period of time (about 1.2 s) after the muon had passed through the detector. Therefore, the background reduction depends on precision of the muon track reconstruction.

With present design, TT has 3 layers of about 20 x 47 m$^2$ made of plastic scintillator strips (26 mm wide) providing X-Y coordinates of muons with about 1 cm accuracy. The tracks measured in TT can be extrapolated to the Central Detector providing spatial resolution of about 20 cm at the bottom of CD. Therefore, TT can provide an independent measurement of the $^9$Li/$^8$He background events distribution with respect to the muon track, which can improve the accuracy of the residual background estimation after applying the veto zone. Table 3.3.2 presents the expected contribution of main sources of the background events and the scheme of their reduction down to acceptable level.

| Selection | IBD efficiency | IBD | Geo-$\nu$s | Accidental | $^9$Li/$^8$He | Fast $n$ | $(\alpha, n)$ |
|---|---|---|---|---|---|---|---|
| - | - | 83 | 1.5 | $\sim 5.7 \times 10^4$ | 84 | - | - |
| Fiducial volume | 91.8% | 76 | 1.4 | | 77 | 0.1 | 0.05 |
| Energy cut | 97.8% | | | 410 | | | |
| Time cut | 99.1% | 73 | 1.3 | | 71 | | |
| Vertex cut | 98.7% | | | 1.1 | | | |
| Muon veto | 83% | 60 | 1.1 | 0.9 | 1.6 | | |
| Combined | 73% | 60 | 3.8 | | | | |

Table 3.3.2 Main background processes (number of events per day) and their suppression after application of the cut selections. The influence on the efficiency of the antineutrino events (IBD) registration is shown.

The JUNO Top Tracker detector will be built of the modules previously used in the OPERA experiment as the Target Tracker detector. JINR took an active part in the construction of the TT detector for the OPERA experiment and the data analysis during the experiment. Now JINR is taking active role in the creation of the Top Tracker detector of the Veto system of JUNO. The significant contribution of JINR in the construction of the detectors will be accounted in JUNO as the in-kind contribution into the project.

The JINR group:
- is responsible for the design, fabrication and construction of the mechanical support of the TT detector;
- is responsible for monitoring of performance of the TT modules during the period of their storage;
- takes part in development of the data acquisition system software;
- takes part in the offline software development for the analysis of the TT data.

Assembly, installation and commissioning of the Top Tracker detector will take place in 2020 and will take 3-4 months. The participation of 4-5 JINR specialists is required for this period.

## 3.3.1. Mechanical Support

The TT detector will be placed on top of JUNO, over pool. The TT modules (there are 496 modules in total, each of about 7 x 1.7 m$^2$) are divided into three layers, and each layer has 21 units, called «walls» which are composed of 8 TT modules, 4 by 4 in X and Y direction and have the dimension of 7 by 7 m$^2$. Thus one layer is of about 1000 m$^2$. The layers are supported by a dedicated mechanical structure (see in Fig. 3.3.3). While the main supporting bridge over

the water pool (of 48 m long) is provided by Chinese institutes (blue elements), the support structure of the TT detector is under responsibility of the JINR group (gray elements of the structure) . The  first version of the design was developed along with french group from IPHC (Strasbourg). At JINR, the prototypes of the constructive elements were fabricated and tested. Several serious drawbacks were discovered. The design was further developed at JINR and the new prototype has been  built.  The procedure of the walls assembly was also developed and validated. The necessary auxiliary tools were designed and fabricated (see Fig.3.3.4).  Although the design of the support structure is close to its final version, the procedure of the TT detector assembly, including the  support, is not finally elaborated yet. Recently, the new approach was proposed by the JINR  engineers. The new ideas need to be proven with the prototype test. Then the design drawings will be finalized at JINR. This work will be conducted during 2017-2018. The fabrication of the whole mechanical structure (about 140 ton)  is supposed to be  done by an industrial company. The bidding will start in 2018.  The cost of the support (about 140 ton) including shipment to JUNO by sea is preliminary estimated as $180k.
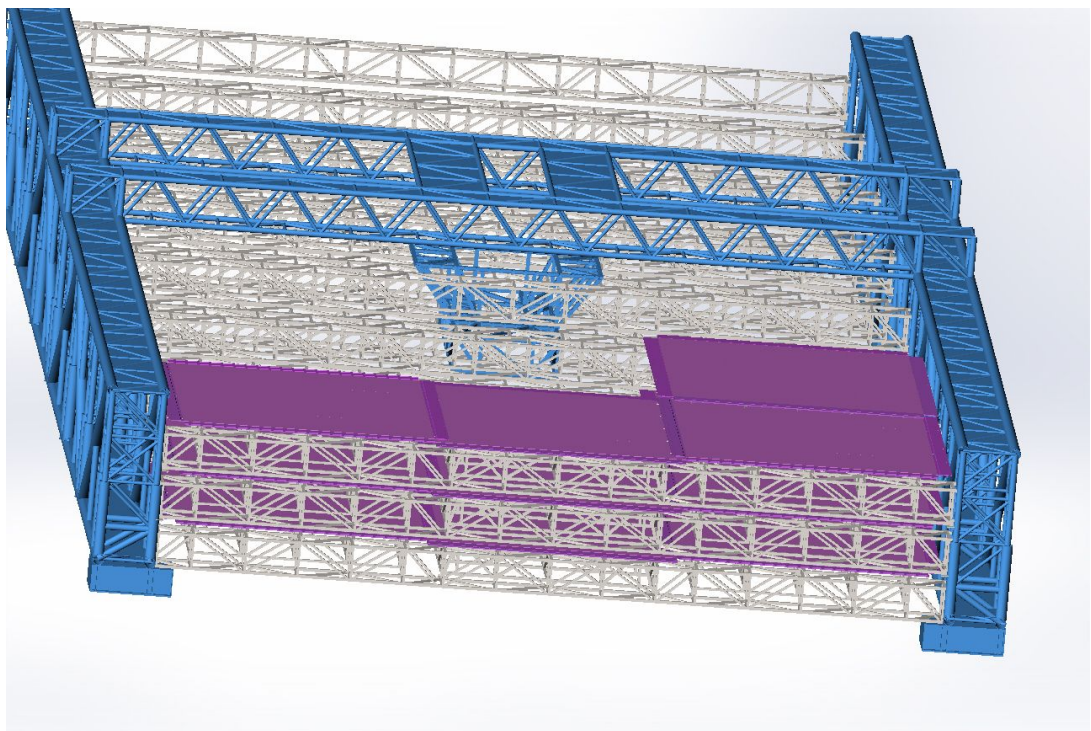
Fig.3.3.3 A general view of the assembled TT mechanical support with  partially installed TT walls.

27

Fig.3.3.4 The TT wall prototype at JINR for mechanical tests and elaboration of the assembly procedure. Auxiliary tools designed for the TT assembly are also shown.

## 3.3.2. Monitoring of the TT scintillators performance

The TT modules are assembled of the plastic scintillator (PS) strips produced in 2003-2005. Plastic scintillator performance can degrade with time due to a loss of the light output and a transparency. In the OPERA experiment the performance of PS was monitored with help of muons registered by the detector. It was found that an amplitude of the registered signal slowly decreases by 1.7% a year. After dismantling of the OPERA Target Tracker detector, the TT modules were placed in 7 containers for their shipment to China where they will be stored until the Top Tracker assembly 2020. The transportation from Italy to China by sea as well as storage for 3 years in South China can accelerate the aging, so its control is an important issue.

To control the performance of the TT modules directly in the storage containers, some of the modules are equipped with the DAQ electronics and can detect cosmic muons. So via registration of the cosmic muons, the changes in the detector response can be followed. A special mobile DAQ and dedicated software have been developed at JINR. As soon as the TT modules will arrive to the storage place in China, the data taking with cosmic muons will start.

The measurement of response of the TT modules in Gran Sasso underground laboratory was performed after their placing into the containers, thus providing a control point for further measurements.
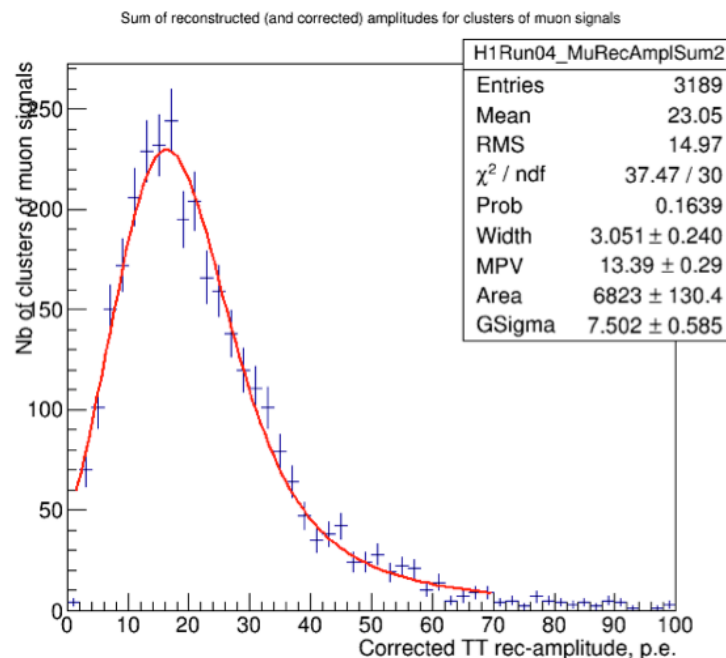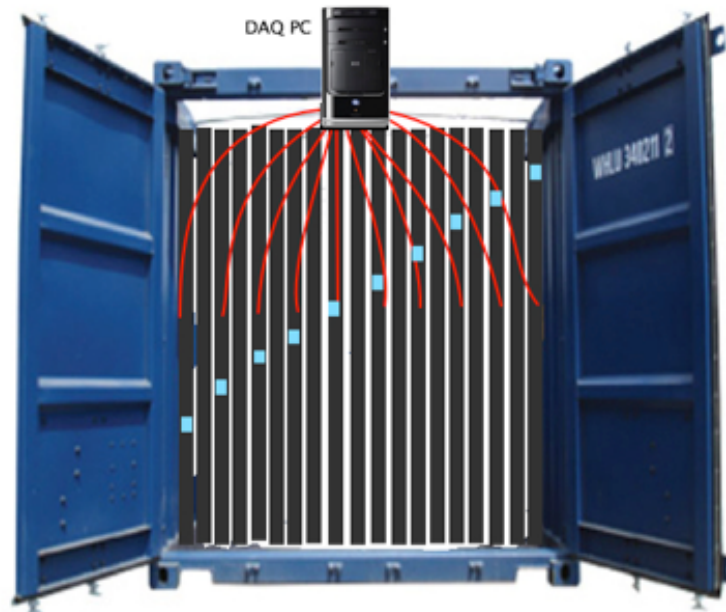
Fig. 3.3.5. A general view of the containers with the TT modules registering cosmic muons (top). The normalized amplitude of the strips response to muons to be followed with time (bottom).

### 3.3.3. Electronics, DAQ

The data taking conditions for the TT in JUNO will be different of those in the OPERA experiment. First of all, the hit rate due to the radioactivity in the experimental hall is much higher (up to 7 kHz/m²). It was decided to upgrade the DAQ electronics, replacing both the Front End (FE) cards and the Readout Boards with more modern ones to comply with the new conditions. The new FE cards based on MAROC3 chip (designed by LAL, France) are being developed at IPHC in Strasbourg, while the new Readout board – are under design at CAEN (Italy) company. The pilot prototypes of both electronics card are expected in June, 2017.

JINR is going to participate in the data acquisition software development. This work should start in 2017 and continue until the detector commissioning in 2020. For this purpose, the cosmic ray prototype was built at JINR. The prototype consists of 4 overlapping half-modules of the TT, thus providing a measurement of X-Y coordinates in two points. When the new electronics will be available, the prototype will be equipped with new electronics and

the DAQ software development will start at JINR in a close collaboration with IPHC (Strasbourg, France) and  LNF INFN (Italy).
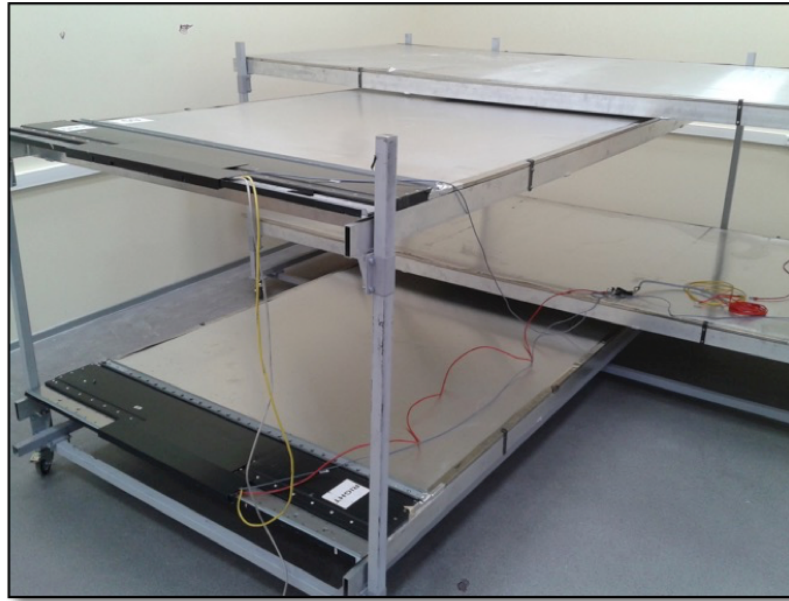


Fig.3.3.6 The cosmic ray telescope made of the TT modules at JINR for the DAQ software development.

## 3.3.4. Software

The TT detector providing the precise  reconstruction of the muon tracks in the CD,  can help to study the production of the cosmogenic isotopes like $^9$Li/$^8$He  in the interactions of the cosmic muons with the scintillator of CD.  The layout of the TT detector (there are only 3 layers) and the presence of the random signals from the radioactivity , however, make this task not easy.

The algorithms for the muon track recognition  in the TT and its parameters reconstruction are under development at JINR. The algorithms use information from the WP and CD about a rough position of the muon track to suppress the fake tracks due to an accidental noise in the TT.  Also,  the properly designed 1$^{st}$ level trigger (for example,  based on coincidence of the signals from the detectors registering  the track in X and Y projection) is expected to help to suppress the radioactivity noise and increase the efficiency of the tracks reconstruction.

The development of the algorithms of the muon track reconstruction goes on  making use the Monte Carlo simulation of the detector.


# 3.4. PMT tests and characterization

## 3.4.1. Scanning stations

The JUNO setup will use ~20'000 of 20" PhotoMultiplier Tubes (PMT), which read out a sphere filled with 20 kton of a liquid scintillator. One of the experiment's largest challenges is to achieve the unique energy resolution of ~3% at 1 MeV and to provide very stable and reliable operation during the whole life of the experiment which dictates very crucial requirements for the PMTs. Hamamatsu (Japan) R12860 20'' PMT and NNVT (China) 20'' MCP-PMT were chosen for the JUNO experiment. The JUNO collaboration has approved list of requirements for the PMT acceptance. These are: PDE  (Photon Detection Efficiency)>24% (@425 nm), Gain ~ 10^7, Dark rate<50 kHz, Peak-to-Valley ratio >2.5 etc. An important parameter is the inhomogeneity of the PDE over photocathode, which should be less than 15%. The latter

measurement needs a scanning device to obtain parameters of the PMT differentially.

The group at JINR has recently constructed a new and sophisticated laboratory for PMT testing with dark room, where a scanning station is placed (see in Fig.3.4.1). The differential and integral characteristics of a large PMT strongly depend on the direction and magnitude of the Earth's magnetic field. The JINR lab allows measurements in different orientations in the EMF. The dark room with Helmholtz coils (magnetic field compensation) is available for these tests.
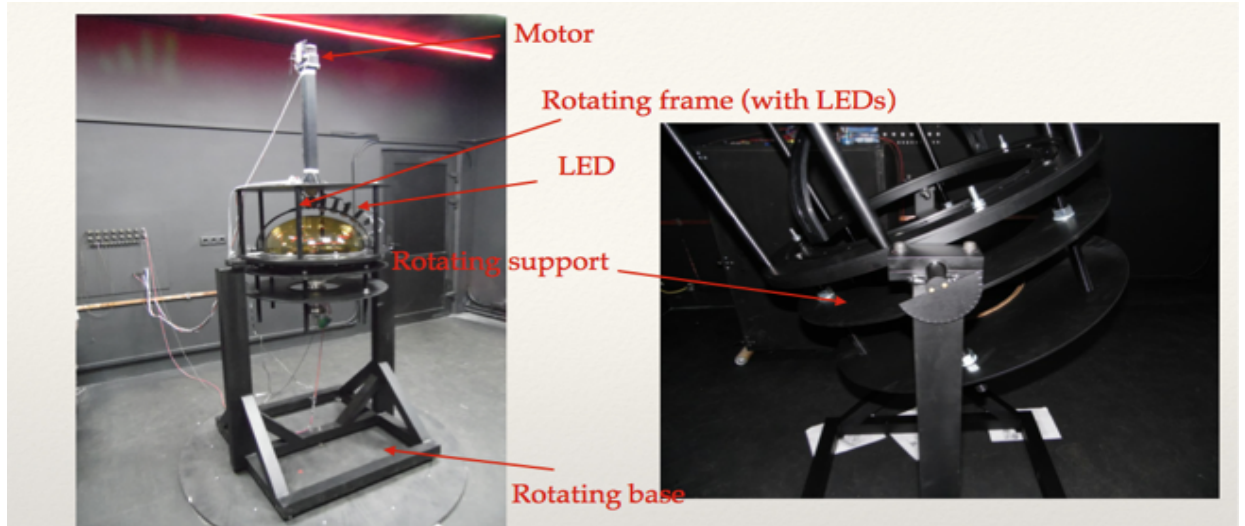


Fig.3.4.1. Scanning station in the dark room at JINR

The core of the scanning station is a rotating frame with 7 stabilized compact pulsed light generators that are placed with different zenith angles. Frame is rotated by the step motor and covers all 360-deg azimuth angles. A support system that holds PMT allows rotations in different space positions in order to put the PMT in different orientations with respect to the magnetic field provided by the dark room. It allows to test individual PMTs in all relevant aspects by scanning the photocathode and to understand the performance of a PMT in depth and to identify any potential problem.

A testing method is based on very low-intensity light flashes (~ 1 ph.e) to obtain gain, average number of photoelectrons and other parameters. By using calibrated light source we can characterize photon detection efficiency of the tested PMT.

The source of light is a know-how of the HVSYS company. It is an LED stabilized pulse source compact device of 80x22x11 mm in size, implemented in a single package. The stabilization is provided by a PIN-photodiode that monitors the LED light. The PIN feedback is made up of ADC digitizing PIN signal and DAC controlling the LED amplitude. Both of them are embedded in a small chip of the microcontroller. A calibration of the light source is done by the certified photosensor (small PMT with known PDE).
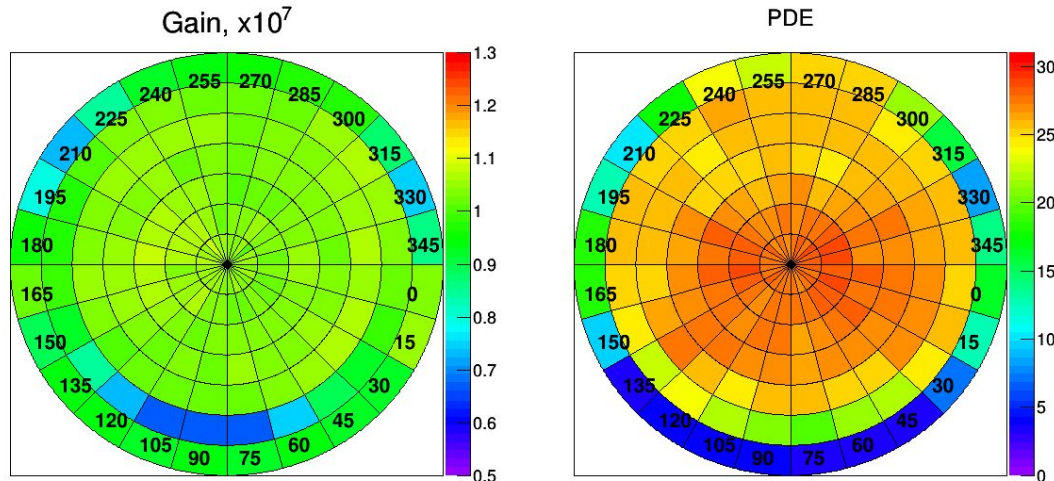
Show 25 entries        Search: [ ]

| | Scan ID | Date | PMT Type | PMT SN | HV set | EMF | Valid |
|---|---|---|---|---|---|---|---|
| ⊕ | 51 | 2017-01-24 | HAMAMATSU | 0418 | 1740 | 0 | y |
| ⊖ | 50 | 2017-01-23 | HAMAMATSU | 0406 | 1730 | 0 | y |

Leds calib coefficients: 29.27,30.0,29.06,29.81,28.92,28.95,29.52
Comment: wirst time led was set in extreme position
charge histograms root file
maps data txt file
Viewer



Gain, x10$^7$          PDE

| | Scan ID | Date | PMT Type | PMT SN | HV set | EMF | Valid |
|---|---|---|---|---|---|---|---|
| ⊕ | 49 | 2017-01-10 | HAMAMATSU | 0006 | 1720 | 0 | y |
| ⊕ | 48 | 2016-11-03 | MCP | 160513-03 | 1610 | 0 | y |
| ⊕ | 47 | 2016-11-02 | MCP | 160419-03 | 1650 | 0 | y |
| ⊕ | 46 | 2016-11-01 | HAMAMATSU | 0008 | 1680 | 0 | y |
| ⊕ | 45 | 2016-10-27 | HAMAMATSU | 0006 | 1720 | 0 | y |
| ⊕ | 44 | 2016-10-26 | MCP | 160513-03 | 1800 | 0 | y |
| ⊕ | 43 | 2016-10-25 | MCP | 160419-03 | 1650 | 0 | n |
| ⊕ | 42 | 2016-10-25 | MCP | 160513-03 | 1700 | 0 | y |
| ⊕ | 41 | 2016-10-25 | MCP | 160513-03 | 1770 | 0 | y |
| ⊕ | 40 | 2016-10-24 | MCP | 160513-03 | 1770 | 0 | y |
| ⊕ | 39 | 2016-10-14 | MCP | 160419-03 | 1580 | 0 | y |

Fig.3.4.2.Web interface of the PMT scanning station's Database with unwrapped single PMT-scanning results.

The JINR group has been developing the software based on modern IT-technologies for controlling the scanning station, acquiring, processing and storing the data (see in Fig.3.4.2) coming from the station.

User or operator can easily access the data and visually check out consistency of the measurements. In the framework of this project we are requiring funding for purchasing servers and data storage disk space.

Four scanning stations have to be prepared for on-site installation in China to provide about a thousand of PMTs testing. Each of scanning stations has to be equipped with its own dark room. So far, we have built 3 scanning stations. Two stations have been equipped with the LEDs. One of those stations will stay at JINR to carry out methodical studies with the PMTs.
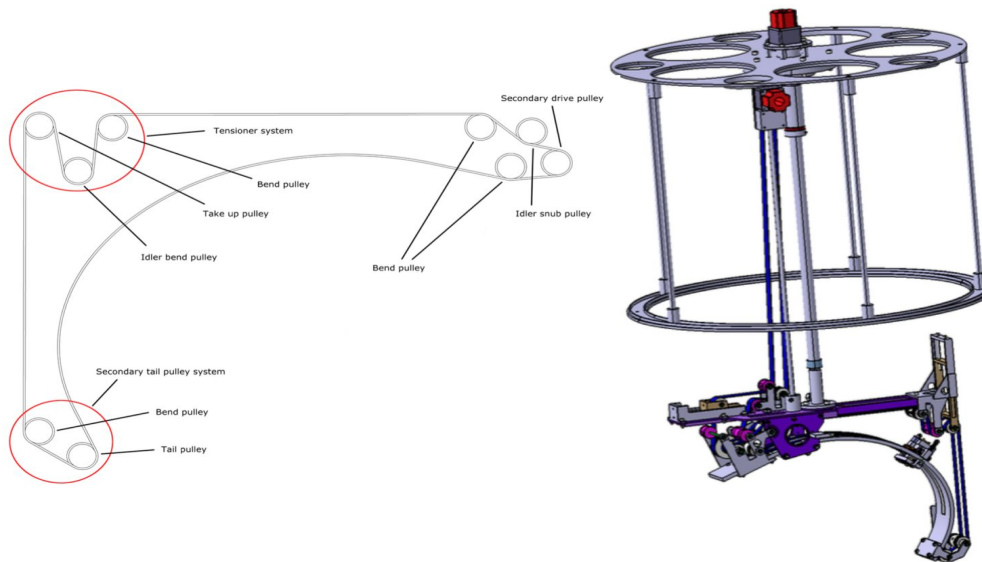
32

Fig.3.4.3 Model of the automatic scanning station: General view of the automatic scanner (right), path of the belt that drives LED source (left).

The end-product scanning station has to be all-sufficient equipment. To satisfy the requirement we are developing a system based on FPGA that provides multi trigger signals for LEDs, ADC board (DRS-4) and can be used as a scaler to change expensive commercial electronics. Our team designs and produces fast amplifier with gain of 10 for more reliable PMT's signal measurement.

Additionally to the existing scanning station an automatic scanning station with a single light source is under construction (see in Fig. 3.4.3). A single light source is used to make measurements more consistent by avoiding systematics of miscalibration of a few light sources.

The scanning station is also planning to be a precise instrument that is complementary to the mass testing (container) system. It provides a cross-checking of suspicious PMTs that failed the simple tests.

## 3.4.2. Container and mass testing

The JUNO Collaboration is preparing equipment (German group) for the mass tests of all PMTs using 4 dedicated containers (Fig.3.4.4). Each container consists of 36 drawers. Each drawer will test a single PMT. This approach allows us to test 144 PMTs in parallel. The basic measurement in the container will be the PMT response during illumination of its photocathode by the uniform light of a small intensity. All of the 20000 PMTs will undergo the container test.
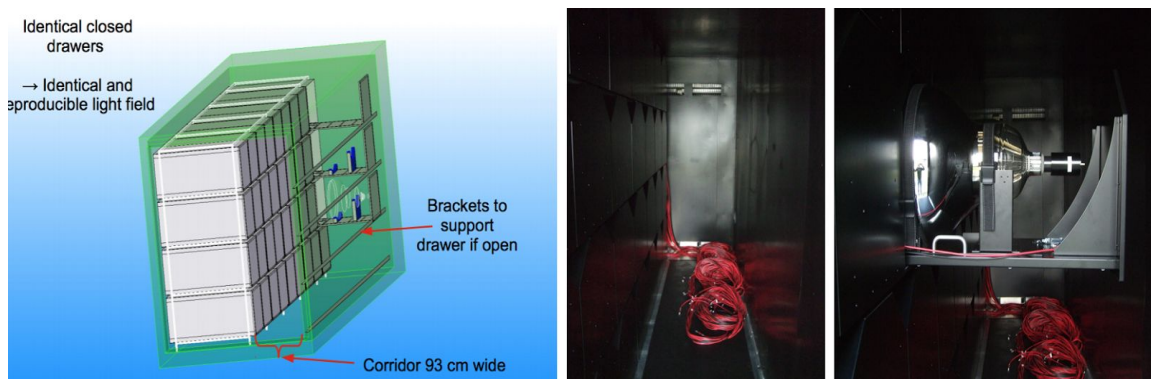


Fig.3.4.4. The Container. General view (left), corridor (middle), PMT layout in the drawer (right).

The light field inside the drawer is provided by the HVSYS  LED light source. Four

containers require about 150 of light sources. One of the JINR responsibilities is to supply collaboration with all the light sources used in the containers. Light source is placed in a special holder and light is spread by a PTFE-diffuser plate. We got the real part of the system from Germany to check light field distribution inside the drawer. Having a 3D-printer in our lab we printed out an arc that mimic large PMT shape. The arc has holes to attach small PMT. By moving small PMT for different positions we can evaluate light field on real PMT surface in the drawer.

Another important task is to match integral and differential results together. For that reason the dark room has been equipped with optical fiber that guided light from a picosecond LASER. The fiber is placed far from large PMT in order to spill the light homogeneously to the PMT surface. Another option is to apply fiber to the drawer light diffuser to check the consistency with the LED light. The PMT itself is securely held in the scanning station support without cap that driving the arc with LED. The technique allows to measure all the main PMT parameters as: gain, PDE, P/V, TTS by illuminating whole PMT surface.

We require 30 man-months of visits to provide all mass-testing measurements including installation, commissioning, maintenance and shifts. Additionally, 10 man-months are required for PMTs installations to the detector.

# 3.5. PMT protection against Earth Magnetic Field

## 3.5.1. Compensation of EMF in the central detector

The new type of PMT is rather sensitive to the Earth magnetic field (EMF). The limiting value of the EMF is about 0.06 G. It means that the possible maximal value of EMF 0.6 G should be shielded with the factor 10. Four possible strategies for EMF shielding are proposed:
- Compensation of EMF by a set of current coils on the pool walls.
- Shielding of EMF by the μ-metal sheets on the pool walls.
- Complete detector shielding by μ-metal mesh screen.
- Both coils and μ-metal shielding.

The screening effects were simulated by using the 2D POISSON code [11] and 3D TOSCA [12]. The 2D code was used for the preliminary simulations for estimation of the principal effect. Final effects were simulated using 3D TOSCA. In some simulations, when the number of mesh elements was too high for the TOSCA assumption, only the POISSON code was used.
- The cheapest strategy for EMF compensation is the utilization of compensation coils.
- Some effects may lead to uncompensated values of EMF at more than 0.06 G:
  - Uncompensated values of the transverse component of the magnetic field from the compensation coils.
  - Time variation of EMF.
  - Spatial variation of the magnetic field inside the pool due to design iron elements in the pool walls, design and technical equipment of the building and pool.
- The system of compensation coils should be added to the μ-metal shielding of each PMT.

Preliminary estimation of the EMF compensation by current coils wound at the walls was provided by 2D modeling. It has been clear from this simulation that:
- for compensation of 0.6 G EMF it needs 3900 A×turns for each direction,
- the compensation coil is generating (due to its geometry factor) the transverse magnetic field component, which can't be compensated by the coil of the transverse direction due to this component non symmetry,
- for providing the constant value of the compensated magnetic field it is required to use a

set of coils, this will also be useful for decreasing of the voltage value at each coil.

Taking into account the 100 V limitation on the single coil a set of 16 compensation coils for one direction was assumed in the 3D model. Using the coils' magnetic field responses by means of dedicated simulation code the constant value of the magnetic field was shaped. The coils' distribution on the wall surface is collected in table 3.5.1.1. In the table the unit for the current is equal 250 A×turns.

| Nc | Icoil (units) |
|----|---------------|
| $C_1$ | 0 |
| $C_2$ | 1.65 |
| $C_3$ | 0 |
| $C_4$ | 0 |
| $C_5$ | 0 |
| $C_6$ | 1.78 |
| $C_7$ | 2.5 |
| $C_8$ | 2.5 |

Table 3.5.1.1. Compensation coils currents (1 unit=250 A×turns).

Parameters of the coils and cost is collected in table 3.5.1.2. For compensation EMF at three directions it is required about 450-500 k$.

| | | |
|---|---|---|
| Number of coils | | 16 |
| Number of turns in one coil | | 25 |
| Excitation current max (A) | | 10 |
| Conductor | | Cu 3×3 mm$^2$ |
| Weight (kg) | — 1 coil<br>— 16 coils | 400<br>6500 |
| Voltage max (V) | — 1 coil | 100 |
| Power max (kW) | — 16 coils | 15 |
| Power supply | — 1 coil | 10A/100V<br>HY-10010E |
| Copper cost ($) | | 13$×6500 kg=85 000 |
| 16 power supplies cost ($) | | 420$×16=6700 |
| Copper+power supplies+design, manufacturing ($) | | 150 000 |

Table 3.5.1.2. Coils parameters per one component of EMF.

## 3.5.2. Protection of individual PMTs against EMF

Screening of the PMTs from EMF is needed as a result of the sensitivity of PMTs to the

weak magnetic fields. The deviation of photoelectrons from the optimum trajectory (calculated for zero initial energy of photoelectron) is leading to the deviation of photoelectron from the central position on its way to the first dynode. Such a deviation could be caused either by the presence of the initial component of the velocity perpendicular to the projection on the field direction, or by the influence of the magnetic field inside the PMT's volume. Photoelectron could then arrive at the first dynode under the non-favorable angle or finish in the zone of the dynode with non-efficient multiplication/electron collection. The effects lead to the decrease of the probability of the photoelectrons collection at the first dynode, decreasing the photons detection efficiency.

In frames of the project we are planning to provide a solution for the screening of PMTs from the EMF. We are not planning the mass production of the PMT screens at JINR, the developed solution, including the choice of materials and tests of their radioactivity, will be passed to collaboration.

As described in the previous section, the JUNO collaboration is considering a compensation of the EMF inside the detector using Helmholtz coils, but this solution has some flaws as the presence of the magnetic materials in the detector's construction makes precision computation of the compensation coils very difficult, so the presence of the residual magnetic fields is possible. PMTs of the muon detector (external with respect to the central detector) will be anyway located in the non-compensated magnetic field, possibly multiplied by compensation coils, thus their screening should be thought more carefully.

In respect of the EMF screening we are planning to use new generation materials (amorphous soft magnetic materials) together with more common mu-metal wires for mesh production. The use of such materials produced in Russia looks promising with respect to the quality and the price.

The structure of amorphous alloys (called also metal glasses) is characterized by the absence of the far order in the atoms alignment. Soft magnetic properties of metal glasses turns out to be better than that of permalloys, moreover these properties are more stable. Another important advantage of metglasses is their exceptional corrosion resistance. In many quite aggressive media metglasses do not corrode at all. The main reason for such a high corrosion resistance is the absence of the crystallic structure, which guarantees the absence of its characteristic defects - dislocations and boundaries between the grains. It is important that defects- free structure of amorphous alloy is passed to the thin oxide layer on its surface formed at the very initial stages of the corrosion process and guaranties its protection from the aggressive environment later. The technology of production allows to manufacture metglasses with thickness below 40 μm.

Amorphous material doesn't need annealing, this makes the manufacturing of the protective screens easier. Another important factor is their relatively low cost.

We already prepared and tested a screen in the form of a wire mesh with 50 mm cell size, the mu-metal wire has 1 mm in diameter. This geometry provide the acceptable "geometric shadow" at the level of 4%. The protective screen was produced using template shown in the Fig.3.5.1., the holes in the template on the crossing guide-lines allow the use of the point-welding technique.

The cone done from amorphous metal was prepared, providing the coverage of the PMT from the base to the glass bulb "equator". Two prototypes with 2x and 4x layers of АМАГ-170 alloy has been tested. The АМАГ-170 material type is commercially available and relatively cheap alloy, for the tests we used the tape 30 mm wide and 30 μm thick. The reported

magnetic permeability of the АМАГ-170 foil is μmax=1.2x10$^6$ compared to the ~10$^4$ of the best available permalloys.
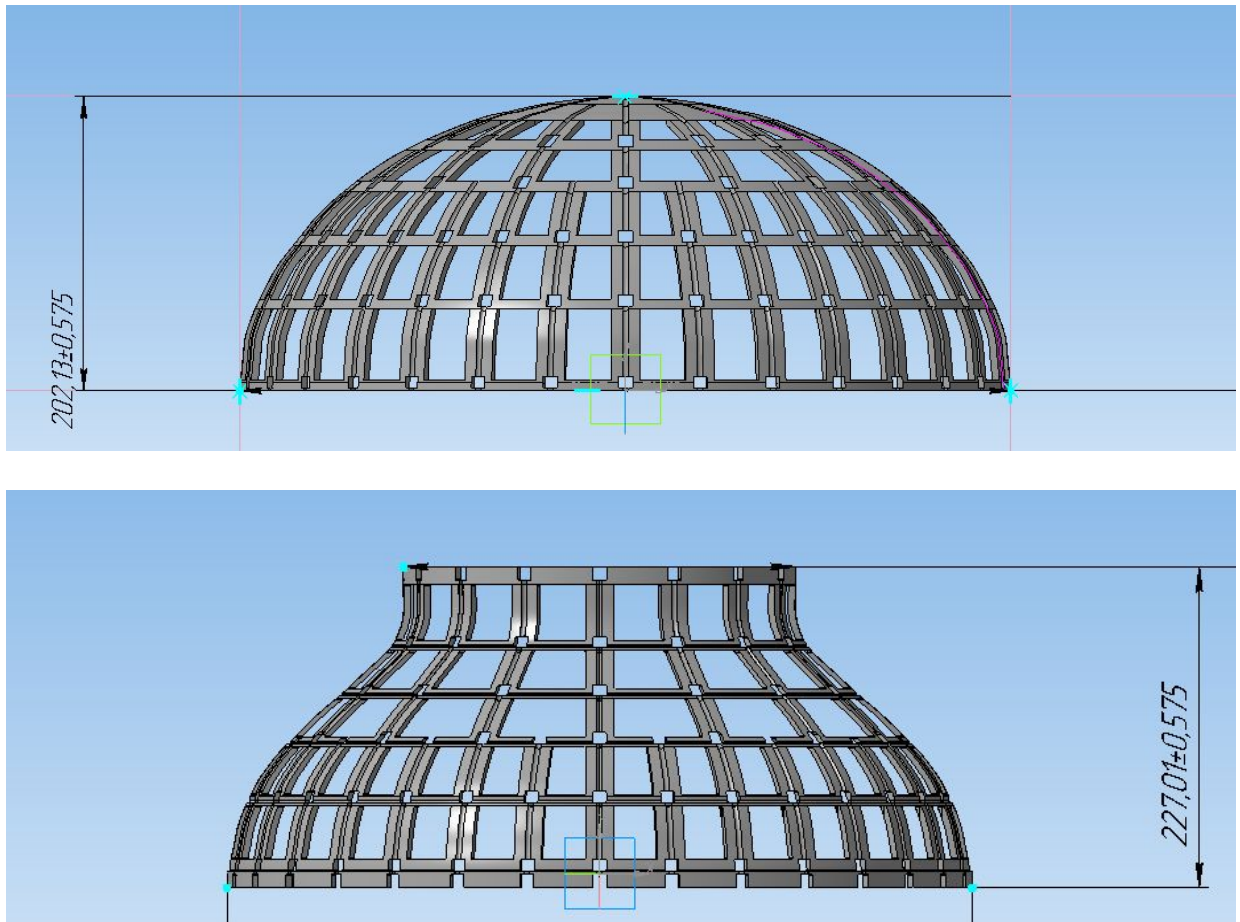


Fig.3.5.1. Design of the template used to produce wire protective screen. The template was printed using 3d printer. Plastic template turns out to be very light and convenient in use. One of the screens produced using this template is shown in foto Fig.3.5.3.

The results of the preliminary tests are shown in Table.3.5.2. For the moment only the relative sensitivity of PMTs in various conditions was measured (see in Table 3.5.2), the reference measurement was acquired in the fully compensated magnetic field. The statistical precision of measurements is about 1%, with comparable systematic error. Magnetic field was oriented perpendicular to the PMT axis (axis Y in the commonly used coordinates system is passing parallel to the dynodes, in the case of the MCP PMT, the Y axis is arbitrary). The effect of the magnetic field is practically fully compensated at the 20 μT field (corresponding to ~50% of the absolute value of the EMF), the compensation is worse in the 40 μT field. The field parallel to Z- axis (axis of symmetry) is not compensated so well. The last row corresponds to the natural direction of the EMF in the laboratory in Dubna, in this case the field along Z-axis is not maximal yet. The complete mesh and the metglass cone with upper part of the mesh demonstrates very close results, what is conforming the possibility of the magnetic field shielding made from metglass cone and upper mesh from mu-metal wire. In order to improve the screening effect we are planning to decrease the step of the mesh.

37

| Field | Nude PMT | Mesh, lower part | Cone | Mesh, complete | Cone + upper mesh |
|---|---|---|---|---|---|
| compensated | 1.00 | 0.99 | 0.99 | 0.94 | 0.94 |
| y:20 µ T | 0.87 | 0.98 | 0.94 | 0.95 | 0.96 |
| y:40 µ T | 0.22 | 0.68 | 0.63 | 0.90 | 0.87 |
| EMF | 0.44 | 0.55 | 0.49 | 0.87 | 0.84 |

Table 3.5.2: Preliminary results of the test of the magnetic shield with 20" PMT (model with MCP).



Fig.3.5.3. The prototype of the EMF screen produced by DLNP workshop.

The results of the preliminary tests look optimistic. The second prototype (consisting of the amorphous metal cone and mesh covering the photocathode) provided reasonable EMF protection.

The planned work for the near future includes:
1. The tests of the efficiency of screening with respect to the magnetic fields exceeding EMF (as it could be in induced fields inside the detector);
2. Tests of the screening efficiency for the MF orientation along Z axis;
3. Improving the annealing. Weak point of using the µ-wire cage is annealing. We are studying the possibilities to increase annealing quality. In particular we would like to try annealing in gas (He or H, either noble gas). We also have preliminary agreement with Baikal group on using their oven, they claim much better screening factor compared to our best result (5-6 against 2.5-3). Amorphous and nanocrystalline materials doesn't

need annealing, the lower part of the screen can be made of any of these materials.

4.  Development of a new template for the top cage production with more uniform spacing at the top and more dense wiring at the borders. Cone with 3-4 layers depending on material and the top cage looks to be the best choice from the point of view of simplicity of the design (no annealing of the lower part is needed) and cost (material of the cone is cheap).
5.  Providing the solution for corrosion protection. Corrosion protection is an issue for further investigation. Protection with organic film is promising. The top cage could be protected with protective lacquer.
6.  Tests of the radioactivity of the materials.

# 3.6. Software development

## 3.6.1. Global Neutrino Analysis Framework

The vast physical potential of the JUNO experiment: neutrino mass hierarchy determination, precision measurements of oscillation parameters, measurement of solar and geological neutrinos and many others; together with number of systematic uncertainties and detector effects makes it advantageous to build an analysis framework that will allow to implement all those analyzes in one tool. The current name for that framework is Global Neutrino Analysis.

The central concept in the design of the framework is the computational graph model that heavily used in the modern high-performance machine learning frameworks such as Theano and TensorFlow. The nodes of the graph are actual computational blocks: theoretical models of reactor fluxes, cross sections, oscillation probabilities, integration routines and etc. To provide an actual computation one needs to connect appropriate nodes into the directed acyclic(loopless) graph. Such a design makes it possible to avoid tight dependencies between implementation of blocks and allow easy configuration and reusing individual nodes. Such model also allows to easily incorporate lazy evaluation and caching of the intermediate results saving CPU time for recomputations.

In order to achieve high computational performance all individual nodes are implemented in C++ with heavy use of Eigen library for vectorized, cached-friendly linear algebra operations with data-parallel CPU instructions such as SSE and AVX. The configuration of the computational graph are done on Python side due its' flexible syntax and big scientific ecosystem. To share state of common parameters between computational nodes that may depend on them, the binding system has been implemented. It allows to bind the external parameters stored in the special environment object to computational nodes and it triggers recomputation of nodes when parameters they depend have changed.

Such architecture allows unified way to propagation propagate parameters into fits and with elementary blocks decoupled by design would provide tool for efficient data analysis.

By now the general building blocks: binding system, cross sections, oscillation probabilities, reactor flux model are implemented. The preliminary model of JUNO is constructed. Our next step is to refine that model by adding the following systematics: energy scale nonlinearity, energy loss in acrylic vessel based on the experience from Daya Bay, background models for $^9$Li/$^8$He, fast neutrons and geoneutrinos.

Such modular software design would provide analyzers the easy platform from sharing parts of computational graphs with each other for easier cross checks.

That framework is not tightly coupled to reactor neutrino experiments. Other types of oscillation experiments such as accelerator, solar and atmospheric experiments can be also implemented in the Global Neutrino Analysis framework. We plan to implement experiments like NOvA, T2K and other to explore the benefits JUNO can get from combined analyzes with them.

## 3.6.2. Study of impact of $^9$Li/$^8$He background on mass hierarchy determination

One of the backgrounds to the IBD sample in JUNO experiment is produced from $^9$Li/$^8$He resulting from muon spallation in the scintillator and muon shower particles. The beta-n decay of $^9$Li/$^8$He would mimic inverse beta events.

The $^9$Li/$^8$He background is reduced by excluding a certain cylindrical region along the muon track or ellipsoid around shower center induced by muons within a certain period of time after the muon had passed through the detector.

We have simulated muons in the JUNO detector and get the parameters of cylindrical and ellipsoid regions to have a compromise between survived fiducial volume and rejected isotopes number. The further optimizations will be achieved by the maximization of the sensitivity to neutrino mass hierarchy with respect to those parameters in the framework of the Global Neutrino Analysis software described above.

Different ellipsoid parameters and dependence of the excluded $^9$Li/$^8$He from excluded volume can be seen in Fig. 3.6.1.



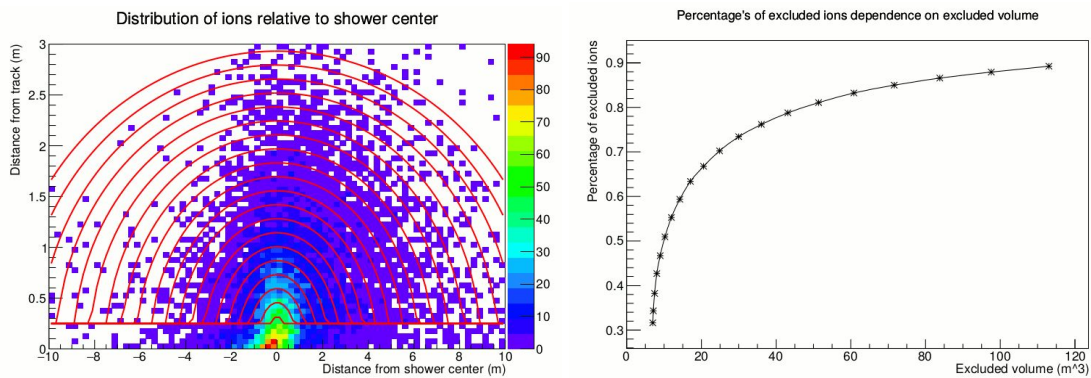Fig. 3.6.1. Excluded regions around shower center (left) and dependence of the $^9$Li/$^8$He from excluded volume (right).

## 3.6.3. Study of impact of $^{14}$C contamination in liquid scintillator on mass hierarchy determination

The JUNO sensitivity to neutrino mass hierarchy relies on the observation of fast oscillation cycles driven by mass splitting $\Delta m^2_{31}$, so called wiggles. The positions of wiggles is the cornerstone that allows to distinguish between mass hierarchies. Any distortion or smearing of antineutrino observed spectrum would lead to the weakening of the ability to find the correct hierarchy. The radiochemical purity of liquid scintillator (LS) is important to minimize such risks.

Among with other possible radioactive contaminations of LS there is one that can not be chemically extracted from LS. It is $^{14}$C - natural beta-decaying isotope with the half-life of 5730 years. It is present in the fossil fuels, e.g in the petroleum that is the starting point for producing liquid scintillator. The end-point of kinetic energy spectra of beta-electrons from $^{14}$C decays is 156 keV. If such decay happens concurrently with antineutrino interaction in the LS it will lead to the overestimation of antineutrino energy that will cause the distortion of antineutrino spectrum.

Given large mass of JUNO (20 ktons) even small fraction of $^{14}$C can affect the ability to

find out the correct hierarchy.

Currently the lowest level of $^{14}$C in LS achieved is in the LS used by Borexino experiment: the relative concentration achieved is $\frac{^{14}C}{^{12}C} \sim 10^{-18}$.

The measurements of $^{14}$C concentration in the proposed LS materials are being performed by the collaboration currently.

We plan to estimate the impact of such contamination on the sensitivity to the mass hierarchy to supplement those studies using the Global Neutrino Analysis software described in previous section. The impact of that effect on other physical analyses such as precision measurement of oscillation parameters and other mentioned in chapter 2.2 will also be studied.

Such a study will allow the collaboration to formulate the requirements for choosing the petroleum for LS production.

## 3.6.4. Simulation of optical properties of photomultiplier in various media

The required accuracy of the energy reconstruction in the JUNO experiment corresponds to 3% at 1 MeV of released energy. We want to formulate the requirements for methods of measuring the PMT's zonal photodetection efficiency as well as for mass testing techniques. The formulated requirements, based on the simulation of PMT response accounting for its optical properties and light-field distribution of the scanning device, are intended to achieve the required energy reconstruction accuracy. Obviously, the integral characteristics, which are made faster and easier, are less sensitive to variations in the zonal characteristics of the photocathode. As it was mentioned in section 3.4.2. there is an important task to match integral and differential results together. This requires to know how the quantum efficiency at each PMT's point influence on overall quantum efficiency of the PMT.

Photon Detection Efficiency (PDE) that we can measure includes both optics of all PMT inner layers and Electron Detection Efficiency (EDE), which describes photocathode properties. High efficiency of PMT requires high EDE.

PMT is a complex system consisting of three media, one of which is a thin photocathode layer with tiny thickness, where the interference of light is possible.
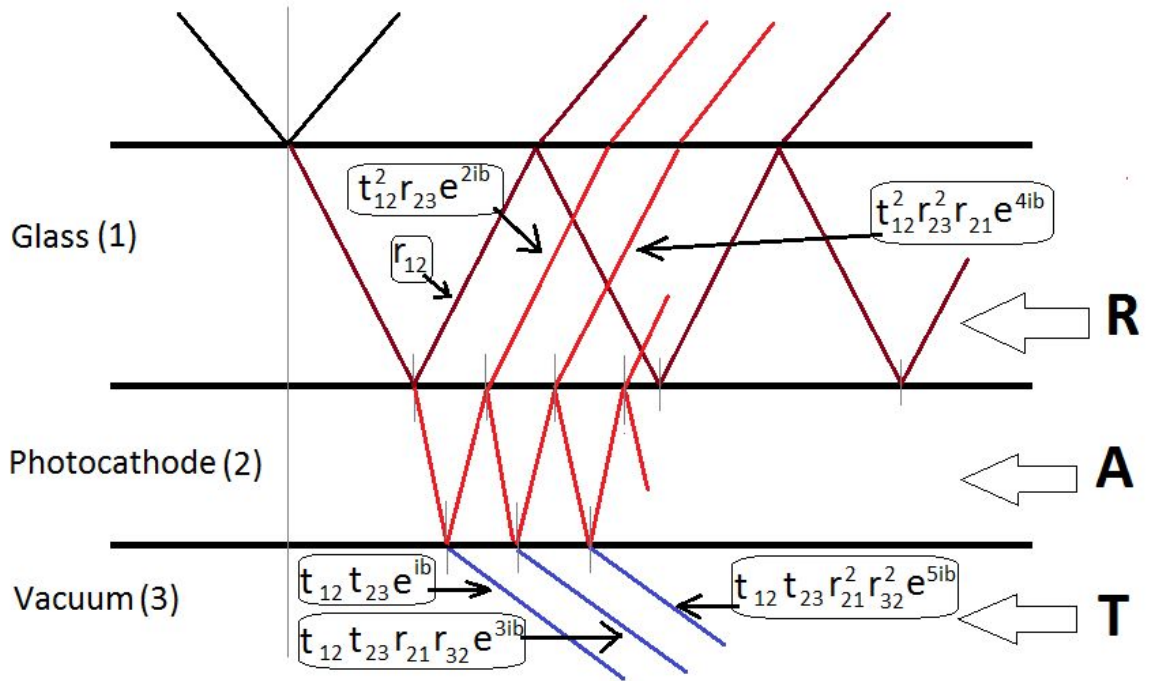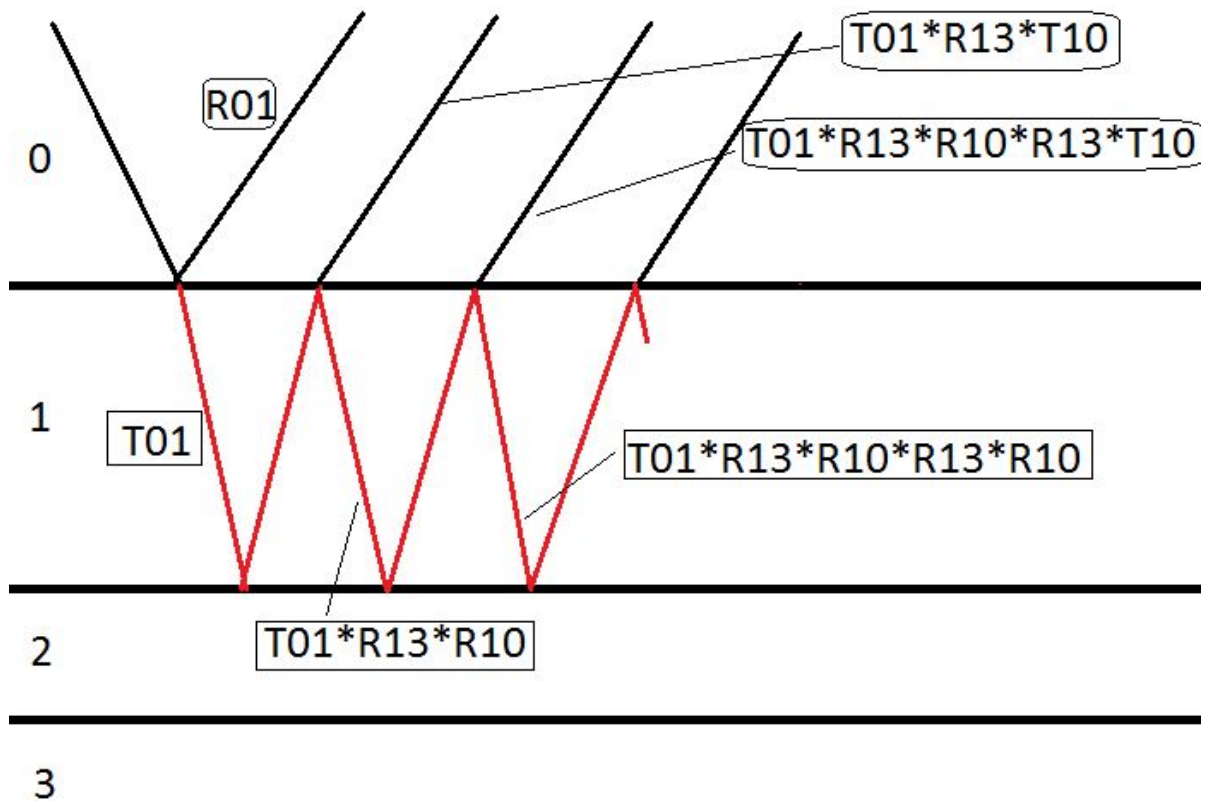
Fig. 3.6.2. Amplitude calculation scheme



Fig. 3.6.3. Coefficient calculation scheme

We can count reflection and transmission amplitudes using a scheme (see Fig. 3.6.2.)as

$$r = \frac{r_{12}+r_{23}e^{2i\beta}}{1+r_{12}r_{23}e^{2i\beta}}, \qquad t = \frac{t_{12}t_{23}e^{i\beta}}{1+r_{12}r_{23}e^{2i\beta}}, \qquad \beta = \frac{2\pi}{\lambda}d_2 n_2 cos\theta_2 = \eta \cdot n_2 cos\theta_2 \,,$$

where $r_{12}, r_{23}, t_{12}, t_{23}$ are given by Fresnel equations for different polarizations and angle $\theta_2$ is known from the Snell's law as a function of incidence angle.

If we parameterize the amplitudes $r = \rho\, exp(i\varphi)$, $t = \tau exp(i\chi)$ and take into account the fact that a thin layer in PMT (photocathode) is absorbing $n_2 \to n_2(1+ik_2)$ and following such parameterization $n_2(1+ik_2)cos\theta_2 = u_2 + iv_2$ we can obtain formulas for reflection and transmission coefficients

$$R = \frac{\rho_{12}^2 e^{-2Im(\varphi_{12})}+\rho_{23}^2 e^{-2Im(\varphi_{23})}e^{-4v_2\eta}+2Re(\rho_{12}\rho_{23}^* \cdot e^{i(\varphi_{12}-\varphi_{23}^*-2u_2\eta)}\cdot e^{-2v_2\eta})}{1+\rho_{12}^2\rho_{23}^2 e^{-2Im(\varphi_{12}+\varphi_{23})}e^{-4v_2\eta}+2Re(\rho_{12}\rho_{23}\cdot e^{i(\varphi_{12}+\varphi_{23}+2u_2\eta)}\cdot e^{-2v_2\eta})}$$

$$T = C_t \frac{\tau_{12}^2\tau_{23}^2 \cdot e^{-2Im(\chi_{12}+\chi_{23})}\cdot e^{-2v_2\eta}}{1+\rho_{12}^2\rho_{23}^2 e^{-2Im(\varphi_{12}+\varphi_{23})}e^{-4v_2\eta}+2Re(\rho_{12}\rho_{23}\cdot e^{i(\varphi_{12}+\varphi_{23}+2u_2\eta)}\cdot e^{-2v_2\eta})}$$

$$C_t = \frac{n_3 cos\theta_3}{n_1 cos\theta_1} \quad \text{for s-wave and} \quad C_t = \frac{n_1 cos\theta_3}{n_3 cos\theta_1} \quad \text{for p-wave}$$

If we consider PMT in some outer media, we also can calculate reflection and transmission coefficients using a simple scheme (see Fig. 3.6.3.)

$$R_{03} = R_{01} + \frac{R_{13}T_{01}^2}{1-R_{01}R_{13}}, \quad T_{03} = \frac{T_{01}T_{13}}{1-R_{012}R_{13}}, \quad A_{03} = 1 - R_{03} - T_{03}$$

Optical coefficients - refraction, transmission, absorption - depend on the incident angle, outer medium (see Fig. 3.6.4.) and type of light wave (s- or p-wave) (see Fig. 3.6.5.). So the number of photoelectrons depends on a way the PMT is illuminated.

Light-field distribution (LFD) of the scanning station is optimal. But the container used for PMT acceptance can not have a 100% uniform LFD. This can lead to a potential overlooking of PMTs in which a part of its photocathode surface can be less efficient than assumed. For example, a certain fraction of area could have a deficiency in quantum efficiency but the container method could mark this PMT as satisfying the quality requirements. In Fig.3.6.6 we display a hypothetical case of overlooking inefficient parts of the PMT's photocathode in cases due to LFD non-uniformity (assuming same light yield on average but linearly rising or falling with cosine of the incidence angle).

PMTs accepted by the container method with potentially less sensitive area may lead to a worsening in the resolution of released energy in the antineutrino interaction. Requirements to guarantee 3% at 1 MeV of released energy would lead to requirements of PMT zonal quantum efficiency and respectively to the uniformity of LFD and other technical aspects of the container method.

The next step is to improve the modeling of photon scattering on PMT considering the light absorption with photocathode's depth and the angular distribution of the photoelectron emission. Simulating PMT response we also must pay respect to the polarization of the scintillation and Cerenkov light generated and rescattered in a LS.

The final result of this work is to formulate the requirements for:
1. the uniformity of the PMT's photocollection, based on the results of the improved PMT simulation and the energy reconstruction in the JUNO experiment,
2. the procedure of the PMT's quantum efficiency uniformity experimental determination.
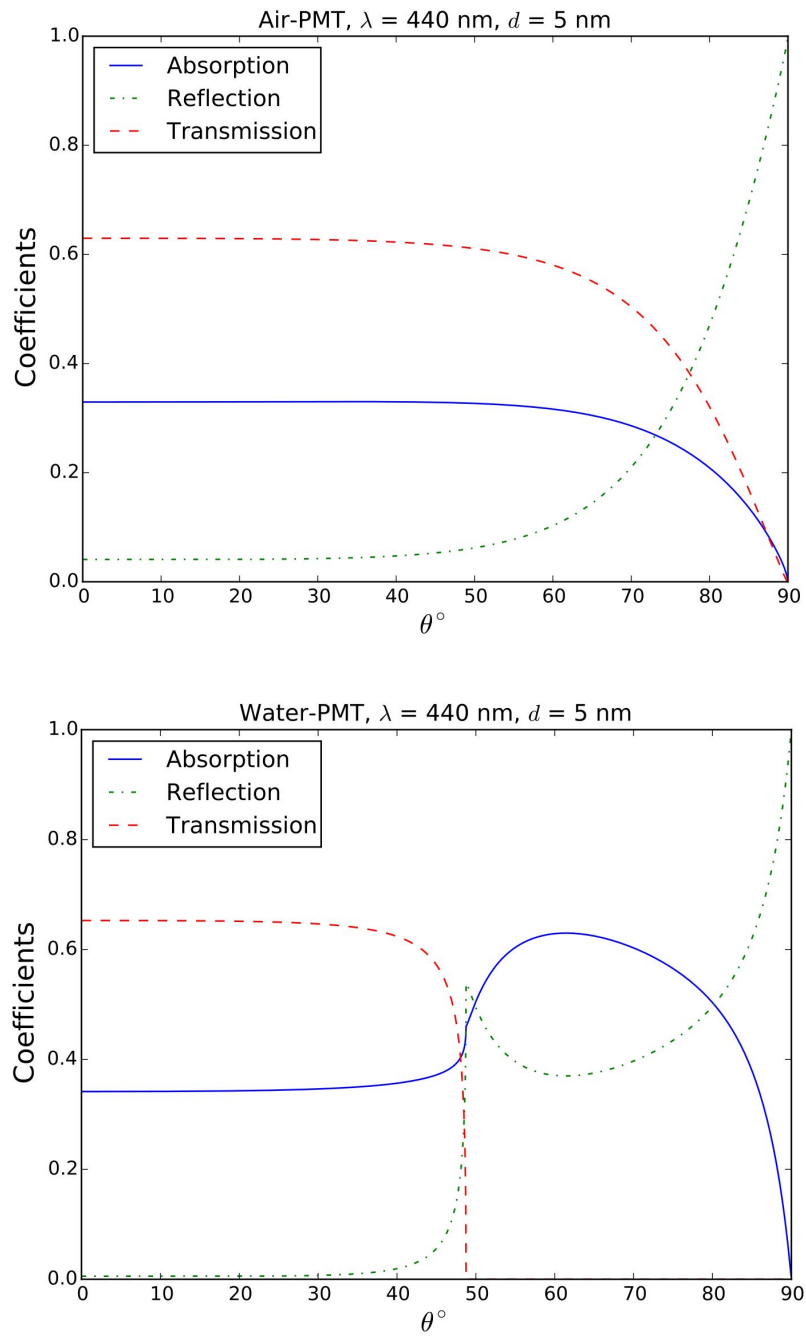
Fig. 3.6.4. Optical coefficients for different incident angles for air (top) and water (bottom) as an outer medium.
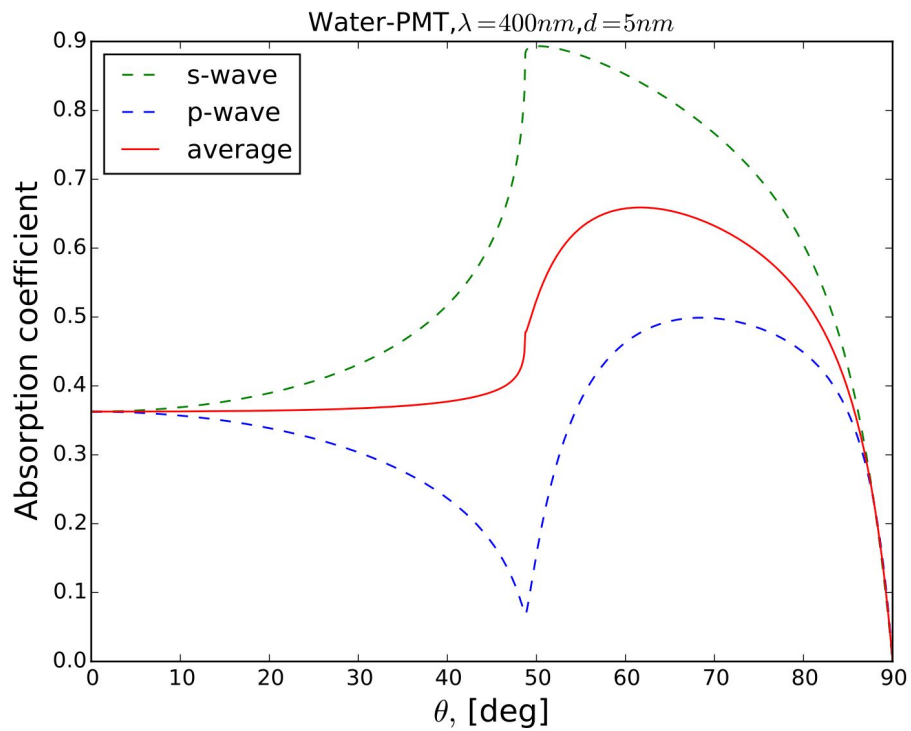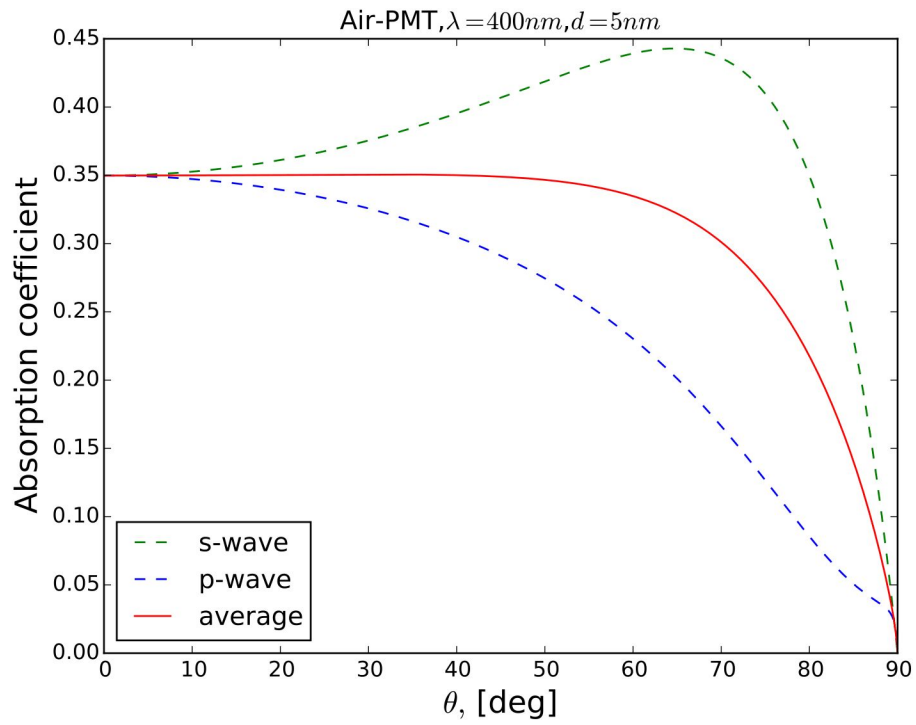
Fig. 3.6.5. Absorption coefficients for different light polarization for air (top) and water (bottom) as outer medium.
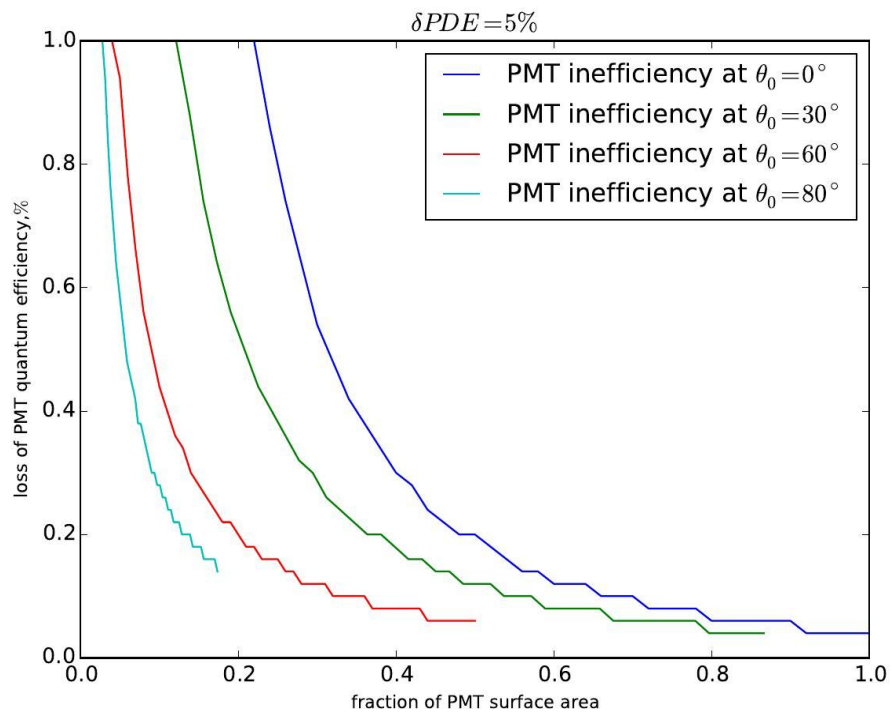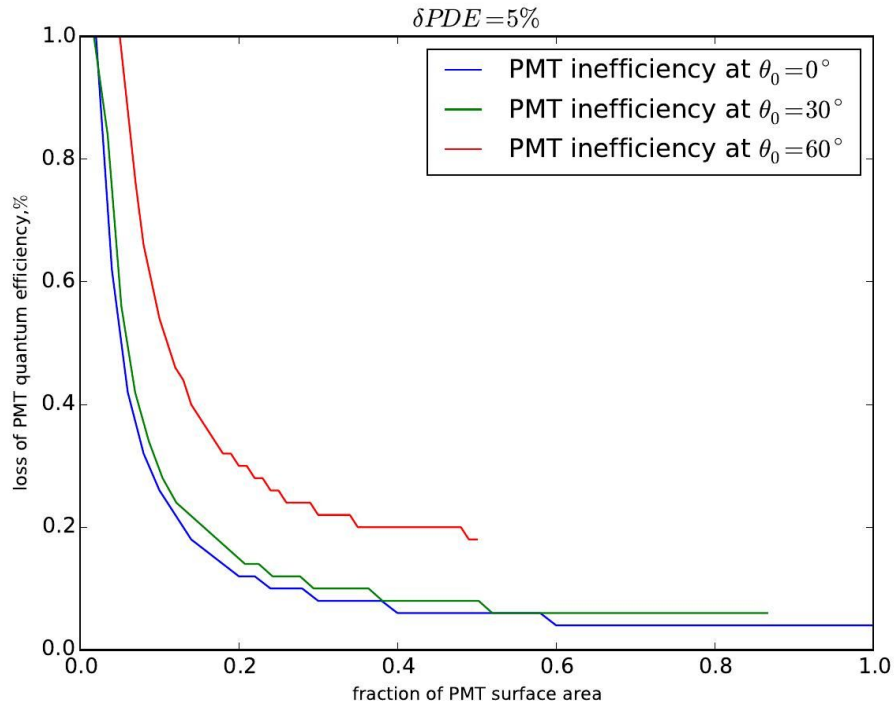
Fig. 3.6.6. A fraction of PMT surface area (x axis) with a relative depletion of quantum efficiency from its nominal value (y axis) which pass a quality requirement of the integral measurement of PDE by container. In this example, a PMT is accepted if the integral PDE is within 5% from the nominal value. The position of possible quantum efficiency depletion is marked by zenith angle theta (zero corresponds to the top of a PMT). We considered two examples of LFD non uniformity. LFD was a linearly increasing (decreasing) function of cosine of incident angle.

# 3.7. R&D of liquid scintillator

An important part of the JUNO project is to develop a liquid scintillator in accordance with requirements to large-scale detectors:

- high transparency;
- high light output;
- availability and low cost of the scintillator;
- safety of use.

## 3.7.1. Linear alkylbenzene purification

Firstly, the realization of all these requirements is related to the properties of the main compound of the scintillator. In the opinion of the JUNO collaboration, the linear alkylbenzene is most suitable for this aim. Linear alkylbenzene (LAB) is cheap and available because it is a by-product for the production of biodegradable synthetic detergents and is, therefore, large-scale product of a number of large petrochemical companies. This liquid is safe in use due to its high flash point (140 $^0$C).

The main problem that limits the linear alkylbenzene using in large-scale detectors is its insufficient transparency that limits the transparency of the LS generally. Three intensive bands are observed at the LAB optical absorption spectrum at the 350-400 nm range. This absorption is not characteristic of alkylbenzene derivatives and, therefore, is related to LAB impurities.

The possibility of LAB using for the preparation of high transparency LS connects with the search for a method of its purification that should be:

- highly effective:
- productive;
- simple;
- relatively cheap.

In the course of performing research, the composition of the impurities affecting the linear alkylbenzene transparency was studied in cooperation with Chinese colleagues. It was shown that LAB samples contain insignificant amounts of carbonyl compounds (aldehydes, ketones), alcohols, phthalic acid esters (phthalates) and other (see in Tab. 3.7.1). It may be assumed with the high probability that these substances have a negative influence both on the LAB adsorption and on light output of the LAB based LS.

| Impurities | Mass fraction, ppm | |
|---|---|---|
| | **Original LAB** | **Purified LAB** |
| Diphenylalkanes | 19 | 88 |
| Ketones | 2037 | 24 |
| Alcohols, aldehydes | 1464 | 13 |
| Phthalates | 152 | 10 |
| Other compounds | 2491 | 57 |

Table 3.7.1. Impurities concentration in LAB before and after its purification by charcoal.

We investigated few methods of LAB purification. It was shown that the most effective is the LAB treatment by charcoal. It gives possibility to reduce the impurities concentration up to two orders. This method is highly productive, effective, simple and cheap in realization.

The proposed method of the linear alkylbenzene purification leads to a significant decrease of its absorption in the near ultraviolet and in the visible regions of the spectrum (see in Fig. 3.7.2).

Simultaneously, the light output of scintillator samples based on purified linear alkylbenzene is 60% higher than the light yield of samples based on the raw solvent. The light output measurements were carried out in cylindrical Teflon cell (height 45 mm, diameter 45 mm, $V_{LS}$= 40 ml) with $^{207}$Bi as a source. Original e + γ spectra are placed at the figure 3.7.3.
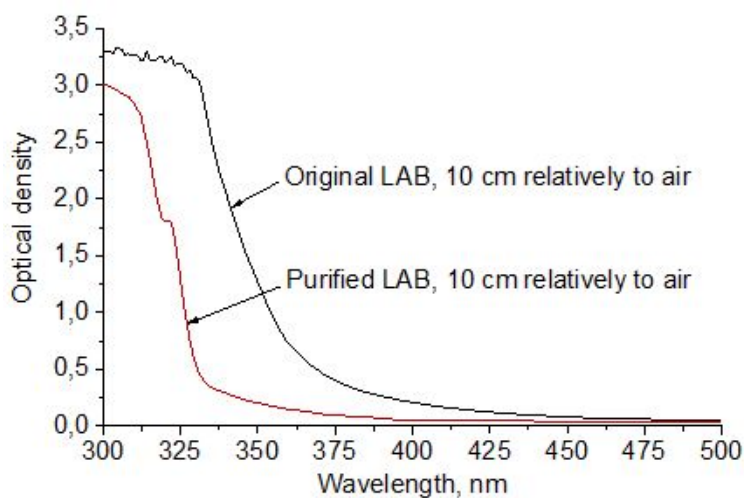


Figure 3.7.2. The absorption spectrum of the LAB samples before and after treatment by charcoal.
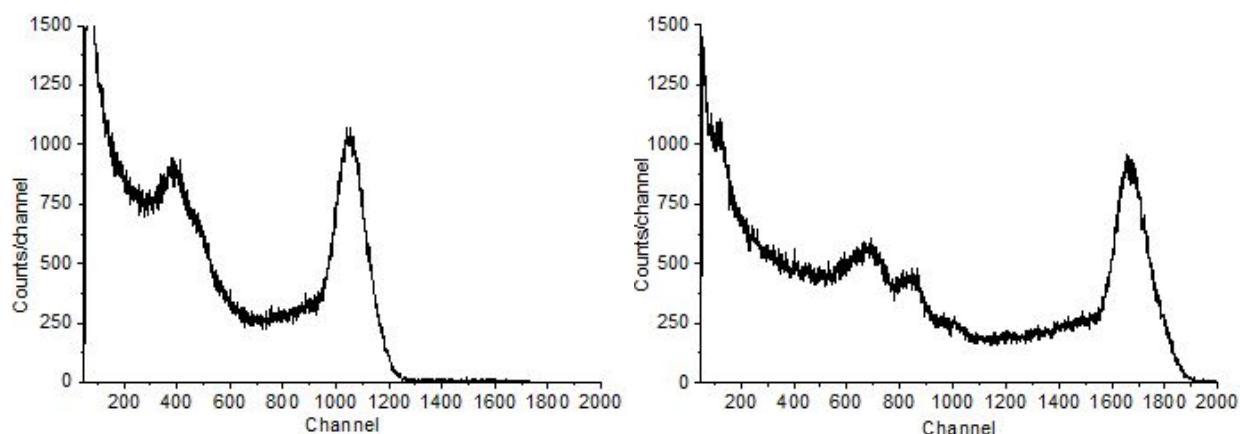


Figure 3.7.3. e + γ Spectra LS based on raw LAB (a) and purified one (b). Source – $^{207}$Bi.

## 3.7.2. 2,5-Diphenyloxazole purification.

The collaboration considers 2,5-dipxenyloxazole (PPO) as a candidate for the role of scintillation additive. The possible manufacturer – Haiso company (China). Therefore, it was very important to examine its quality.

For this aim we compared the sample of row PPO (scintillation grade) and purified one. As a purification technique we used adsorption on the "hot" column filled by alumina. This method is very effective because combines two operations (adsorption and recrystallization).

Two samples of LS based on row and purified PPO were prepared. The light output of LS containing the purified sample is slightly higher (6%) than the other sample.

# 4. Daya Bay at JINR

## 4.1. Brief summary

Within the Daya Bay Collaboration JINR team performed the following activities during the previous period.

We developed a Dubna selection algorithm which identifies candidates for antineutrino inverse beta decay (IBD) interactions with free proton.

We performed also studies estimating the background to IBD candidates. A study of optimal selection criteria minimizing the expected uncertainty of estimates of oscillation parameters was performed.

We performed an oscillation analysis of Daya Bay data based on 1230 days of collected statistics. This analysis was selected as an official analysis of Daya Bay Collaboration. The most accurate results of Daya Bay Collaboration are based on JINR team analysis. JINR team members were among the editors of a detailed Daya Bay paper.

For the first time we performed a study of wave packet impact on neutrino oscillations using the Daya Bay data. The corresponding collaboration paper was based on JINR team analysis and written by JINR team members.

The reactor antineutrino flux measurement was cross-checked by JINR team. We also participated in the review of the Daya Bay paper.

We conducted a research on measurement of reactor antineutrino energy spectra due to different isotopes. This work is not yet finalized. We also participated in a review of reactor antineutrino spectrum evolution paper by Daya Bay Collaboration.

Last but not least we conducted a search for sterile neutrino, reviewed analyses of other groups and were among the editors of Daya Bay papers.

Within the Daya Bay Collaboration we plan to continue data analyses to release the most precise determination of $\theta_{13}$ and $\Delta m^2_{32}$; more precise measurement of reactor antineutrino energy spectra and possibly its isotope decomposition; continue data taking and its calibrations.

## 4.2. IBD selection and background study

In Daya Bay experiment antineutrino IBD interactions were selected by searching for pairs of interactions separated by 1 to 200 us, with a reconstructed prompt energy, Ep, between 0.7 and 12 MeV, and a reconstructed delayed energy, Ed, between 6 and 12 MeV, with muon veto: (-2, 600) us after NHIT > 12 in outer water system (OWS) or inner water system (IWS), (0, 1.4) ms after > 3,000 p.e. for AD muon and (0, 0.4) s after > $3 \cdot 10^5$ p.e., for AD shower.

Since the Daya Bay statistic for selected IBD pairs is enough we decided to optimize IBD selection criteria cuts to get a minimal errors for final oscillation parameters. This study is done based on MC data for the 1230 days dataset. We varied three different cuts: time between prompt and delayed signal, minimum energy of prompt signal and minimum energy of delayed signal. Dependencies of errors for final oscillation parameters from selection cuts are presented in Fig. 4.2.1. We propose to set the following IBD selection cuts: time between prompt and delayed signal - 180 us, minimum energy of prompt signal - 1 MeV, minimum energy of delayed signal - 5 MeV. With the new selection criteria errors for final oscillation parameters are decreasing for $\sin^2 2\theta_{13}$ by 1.1%, for $\Delta m^2_{32}$ by 3.0%.
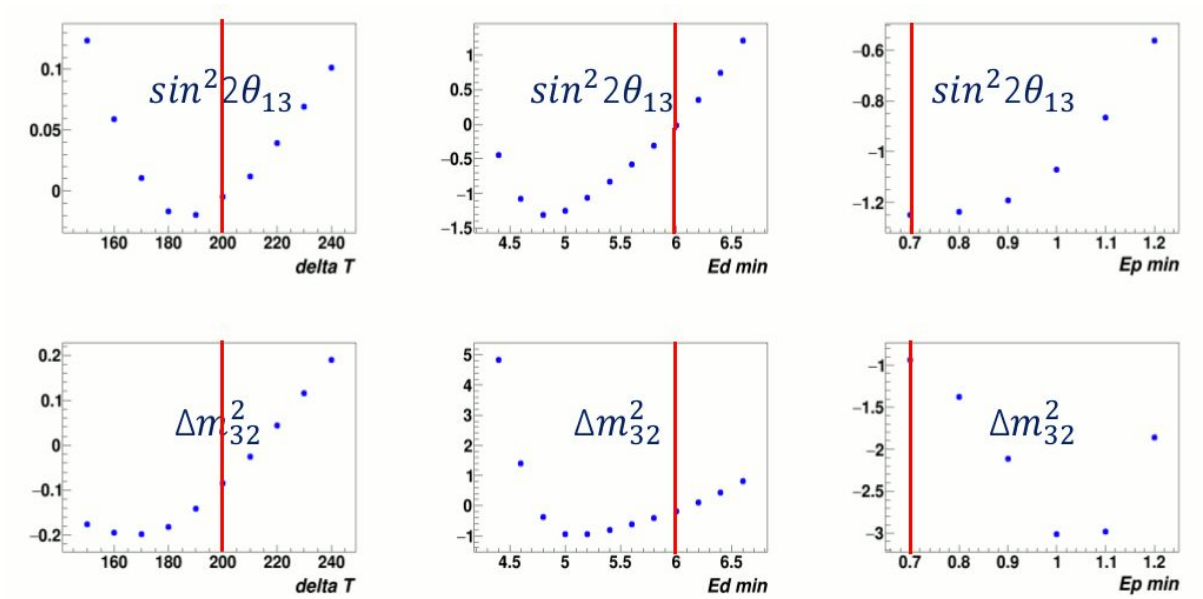
Fig. 4.2.1. Dependencies of errors for final oscillation parameters from selection cuts. Red line shows a default values for selection criteria.

Another source of the background to the IBD events is the accidental background when two mostly independent signals can mimic inverse beta events. The main source of prompt-like part of accidental events is natural radioactivity in the detector components and surrounding environment. One of the sources of delayed-like part of accidental events are $\gamma$-rays produced by the capture of neutrons from $^{241}$Am-$^{13}$C calibration sources on the AD lid. The other source of delayed-like events are particles produced from muon spallation in the detector, such as $^{12}$B and $^{12}$N. The number of delayed-like events is also increased by the produced neutrons that are captured on the Gd or H (see fig. 4.2.2). It means that we need to have a veto time window just after muon event to suppress signal from produced particles. After analysing energy spectra of single event originated from muon track we concluded that veto time window for muon tracks registered in water system should be increased from 600 us to 800 us.
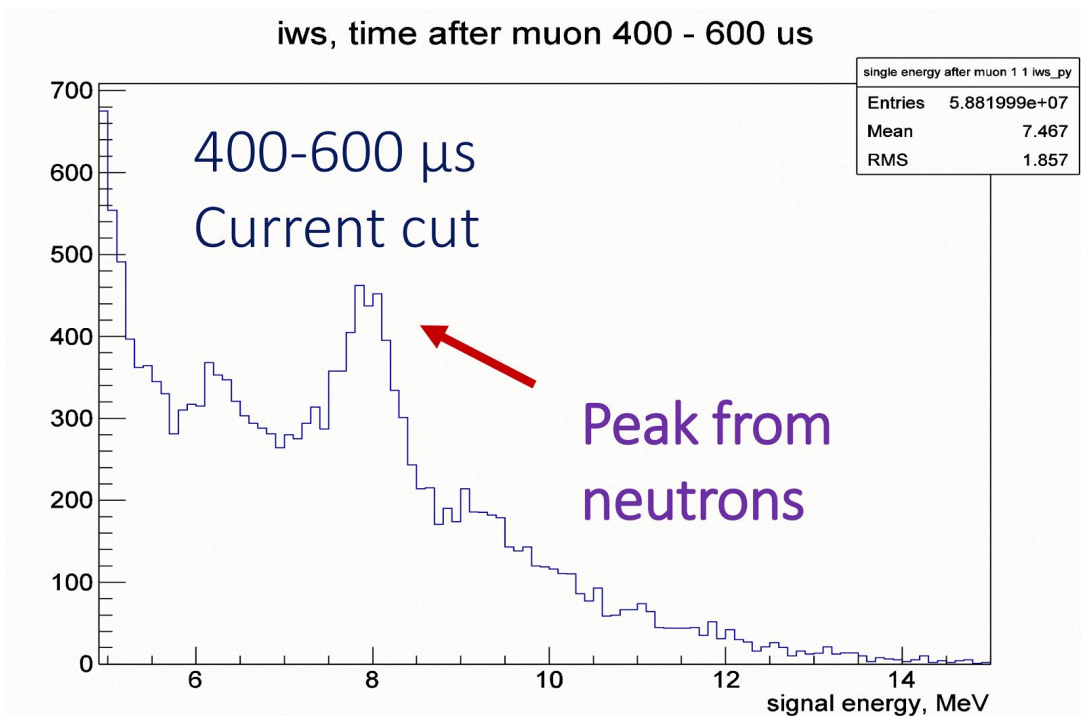


Fig. 4.2.2. Energy spectra of single events after muon track registered in inner water system.

Table 4.2.3 summarizes the antineutrino candidate data sample for all detectors with default and our selection cuts.

|  | Default selection cuts | Dubna selection cuts | Difference (%) |
|---|---|---|---|
| IBD pairs | 2528912 | 2534994 | 0.2 |
| Accidental background | 27758.9 | 22124.9 | -20.3 |
| Effective time (days) | 7725.61 | 7598.93 | -1.6 |

Table 4.2.3. Comparison of antineutrino sample for default and our IBD selection cuts.

In our analysis we also studied multiplicity cut:  when a second prompt-like signal occurred before the prompt or second delayed-like signal occurred after the delayed signal in a given time window. This cut is allow us to avoid ambiguous treatment of prompt-delayed pair and make a more clear IBD sample. After our investigation we proposed to extend our current multiplicity cut: there are no other signals before prompt and after delayed signals in a given time window.

There are few types of correlated backgrounds that are present in the IBD events sample: accidentals due to natural radioactivity, neutrons from Am-C calibration source and backgrounds produced by cosmic muons ($^9$Li/$^8$He and fast neutrons) passing through detectors and surrounding rocks.

The fast neutron background is formed by energetic neutrons produced by muons passing through the rocks surrounding detectors. Such neutrons can get into the antineutrino detectors and  by recoiling on protons and being captured on hydrogen or gadolinium produce pair of signals that pass the regular IBD criteria.

There are two methods to estimate the rate and prompt energy distribution of such events:
1. To study the distribution of IBD candidates over prompt energy above 12 MeV, all such IBD candidates are fast neutrons in fact. That distribution is fitted with a Monte-Carlo motivated phenomenological model. Extrapolation of that model into the region below 12 MeV gives the background rate and energy spectrum.
2. To construct a special set of coincidence events tagged by muons in the outer water pools (OWP) or by RPC muons. Such an events are indeed fast neutron events. Scaling the distribution of that events over prompt energy to the corresponding distribution of IBD events above 12 MeV also provide consistent estimation of background rate and spectral shape. The prompt energy spectra of fast neutron events tagged by muons in OWP above 0.7 MeV and IBD  events above 12 MeV are presented at fig 4.2.5.

The summary of current results for fast neutron rate estimation and comparison with official is given in the table 4.2.4. The slightly bigger uncertainty in our selection is due to different selection criteria. Official results were acquired with our participation and was later cross-checked by our group.

|  | Daya Bay Near Site | Ling Ao Near Site | Far Site |
|---|---|---|---|

| | | | |
|---|---|---|---|
| Dubna group's result | 0.831 ± 0.09 | 0.629 ± 0.067 | 0.052 ± 0.01 |
| Official result | 0.84 ± 0.08 | 0.64 ± 0.06 | 0.05 ± 0.01 |

Tab. 4.2.4 Fast neutron background rates (events per AD per day) by Dubna group and official result.

The Daya Bay increased statistics will allow to study fast neutron energy spectrum in more details, to better understand differences between those methods and lower systematic uncertainty related to that background. Also it will provide better understanding of correlations between fast neutron backgrounds in Double Chooz and RENO experiments and would be useful for possible joint oscillation analysis with those collaborations.
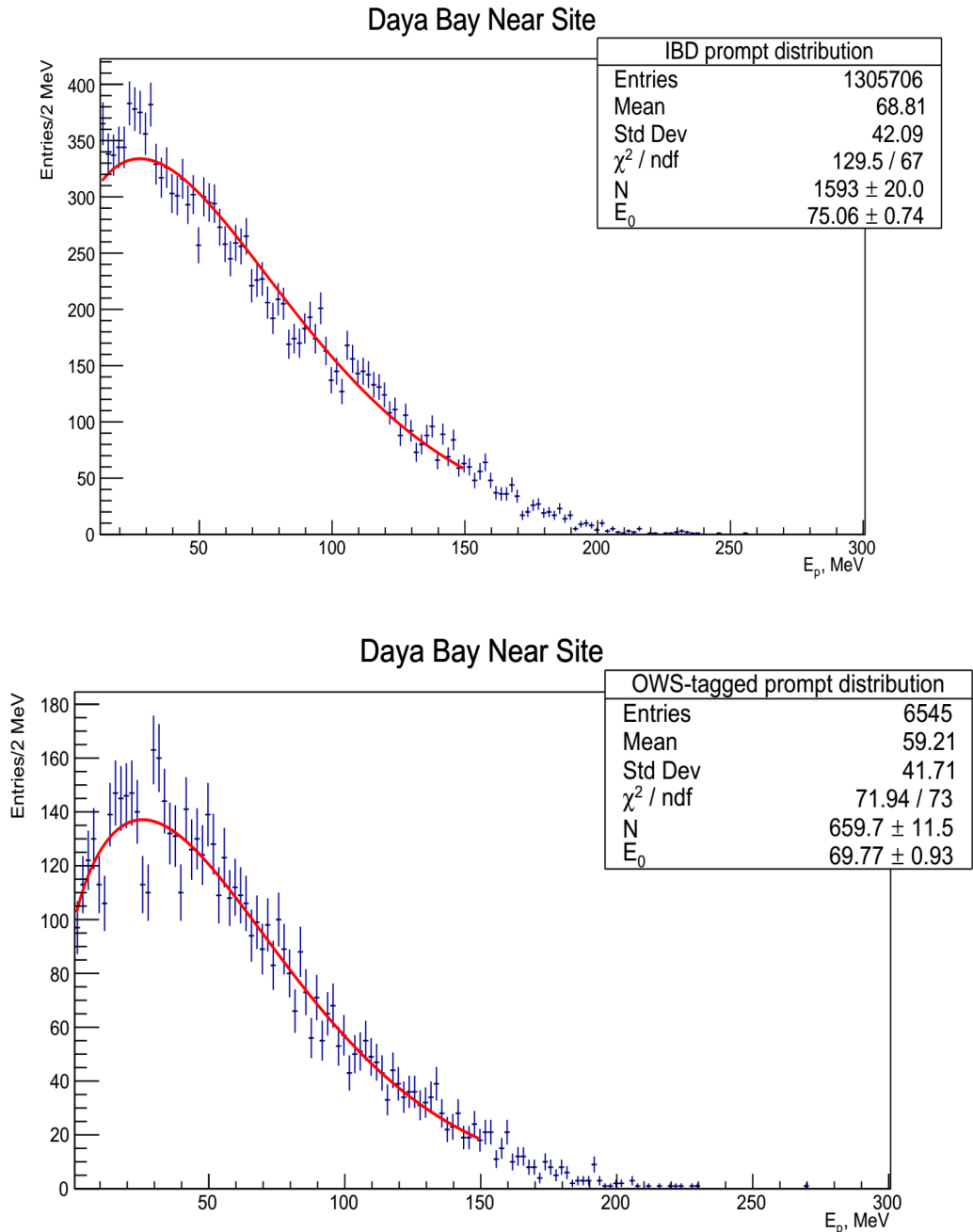


Fig. 4.2.5 The prompt energy spectra of IBD candidates above 12 MeV (upper) and prompt energy spectrum of OWS-tagged fast neutrons above 0.7 MeV (lower).

# 4.3. Neutrino oscillation analysis

Our group takes part in the Daya Bay oscillation analysis since the beginning of data taking [13]. We have developed our own fitter to analyze the Daya Bay data and are among one of the 5 groups involved in the main oscillation analysis. This year our efforts were highlighted and our analysis was chosen to be official [14].

The current dataset covers the period from 24.12.2011 to 27.09.2015 and contains 1230 calendar days of data, used for the oscillation analysis. Data for 217 days out of 1230 were acquired from 6 antineutrino detectors out of 8. The statistics contains more than 2.5M of Inverse Beta Decay (IBD) events, more than 300K of which were observed in the far site. The background contamination is around 2% with relative uncertainty below 0.2%.

When compared to our previous result [15] one can observe that we have doubled the acquired statistics. Besides that, there was a number of improvements in our understanding of the antineutrino detectors performance and systematics. One of the major improvements was the decrease of the uncorrelated detection efficiency uncertainty from 0.2% to 0.13%. The oscillation parameters estimation is affected by the uncorrelated efficiency variations, while the correlated variations are being canceled in the relative measurement with multiple detectors.

The oscillation analysis is performed by 5 independent groups. The consistency between results, estimated based on the MC is below 0.2 standard deviations. The oscillation analysis yields:

$$\sin^2 2\theta_{13} = 0.0841 \pm 0.0027 \; (stat) \pm 0.0019 \; (syst) \, ,$$

$$|\Delta m_{ee}^2| = (2.50 \pm 0.06 \; (stat) \; \pm \; 0.06 \; (syst)) \times 10^{-3} \; \text{eV}^2.$$

It is the most precise measurement of the both of the oscillation parameters. The parameter $|\Delta m_{ee}^2|$ is the flavor average between $|\Delta m_{32}^2|$ and $|\Delta m_{31}^2|$. It may be interpreted depending on neutrino mass hierarchy as:

$$\Delta m_{32}^2 = (\;\; 2.45 \pm 0.06 \; (stat) \; \pm \; 0.06 \; (syst)) \times 10^{-3} \; \text{eV}^2 \; \text{(normal hierarchy)},$$

$$\Delta m_{32}^2 = (-2.56 \pm 0.06 \; (stat) \; \pm \; 0.06 \; (syst)) \times 10^{-3} \; \text{eV}^2 \; \text{(inverted hierarchy)}.$$

Confidence regions for the $\sin^2 2\theta_{13}$ and $\Delta m_{ee}^2$ is shown in figure 4.3.1. The observed electron antineutrino survival probability as a function of $L_{eff}/E_v$ is displayed in figure 4.3.2. It indicates good agreement between observed and expected antineutrino energy spectra in each hall.

The comparison of the latest measurements of oscillation parameters $\sin^2 2\theta_{13}$ and $\Delta m_{ee}^2$ is shown on figures 4.3.3. and 4.3.4.

Our oscillation analysis does not assume any theoretical shape of the reactor antineutrino spectra. Instead, this spectrum is fitted together with two oscillation parameters as outlined in Section 4.5. Such independence of the oscillation analysis results on assumptions about the reactor antineutrino spectrum is due to multiple "near" and "far" detectors of the Daya Bay experiment.

The work by Dubna group is summarized in two dissertations. Candidate dissertation by M. Gonchar and doctor dissertation by D. Naumov will be published in April 2017. Both the defences are planned on 2017.

The Daya Bay experiment is confirmed to continue data taking till 2020. The oscillation analysis results will be updated in 2018 and in the end featuring the most precise measurement of the both oscillation parameters with uncertainty of order of 3%.
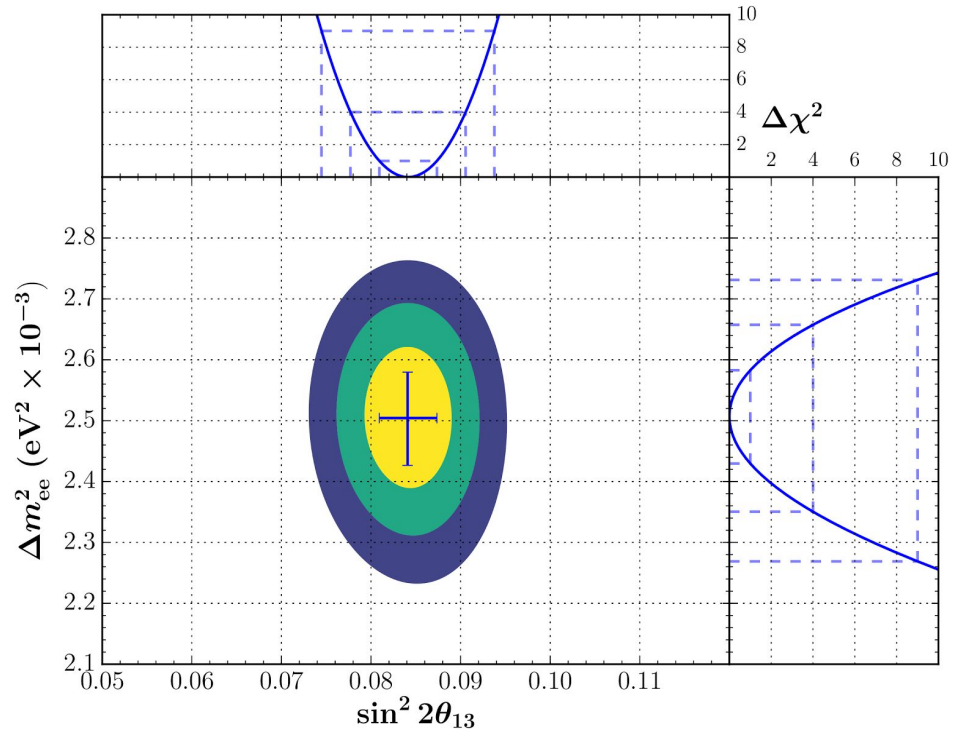
Fig. 4.3.1. Confidence regions for the neutrino oscillation parameters $\sin^2 2\theta_{13}$ and $\Delta m_{ee}^2$.
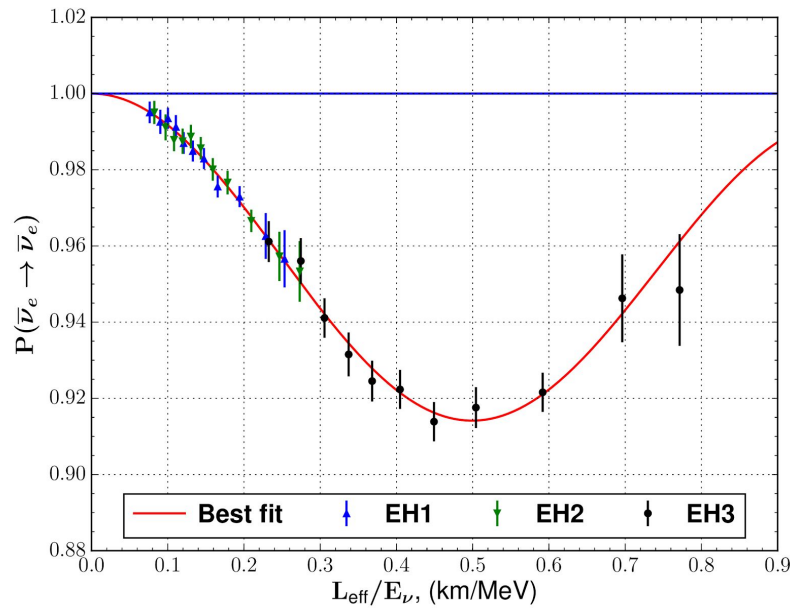


Fig. 4.3.2 Measured reactor antineutrino spectral distortion, displayed as survival probability versus $L_{eff}/E_\nu$.

55

| Experiment | | | Value |
|---|---|---|---|
| **Daya Bay** | nGd | | $0.0841 \pm 0.0033$ |
| RENO | nGd | | $0.082 \pm 0.010$ |
| **Daya Bay** | nH | | $0.071 \pm 0.011$ |
| D-CHOOZ | nGd+nH | | $0.119 \pm 0.016$ |
| RENO | nH | | $0.086 \pm 0.019$ |
| D-CHOOZ | nH | | $0.095^{+0.038}_{-0.039}$ |
| T2K | | | $0.100^{+0.041}_{-0.017}$ |
| NO$\nu$A | NH | | $0.093^{+0.079}_{-0.048}$ |
| | IH | | $0.157^{+0.106}_{-0.082}$ |
| MINOS | NH | | $0.051^{+0.038}_{-0.030}$ |
| | IH | | $0.093^{+0.054}_{-0.049}$ |
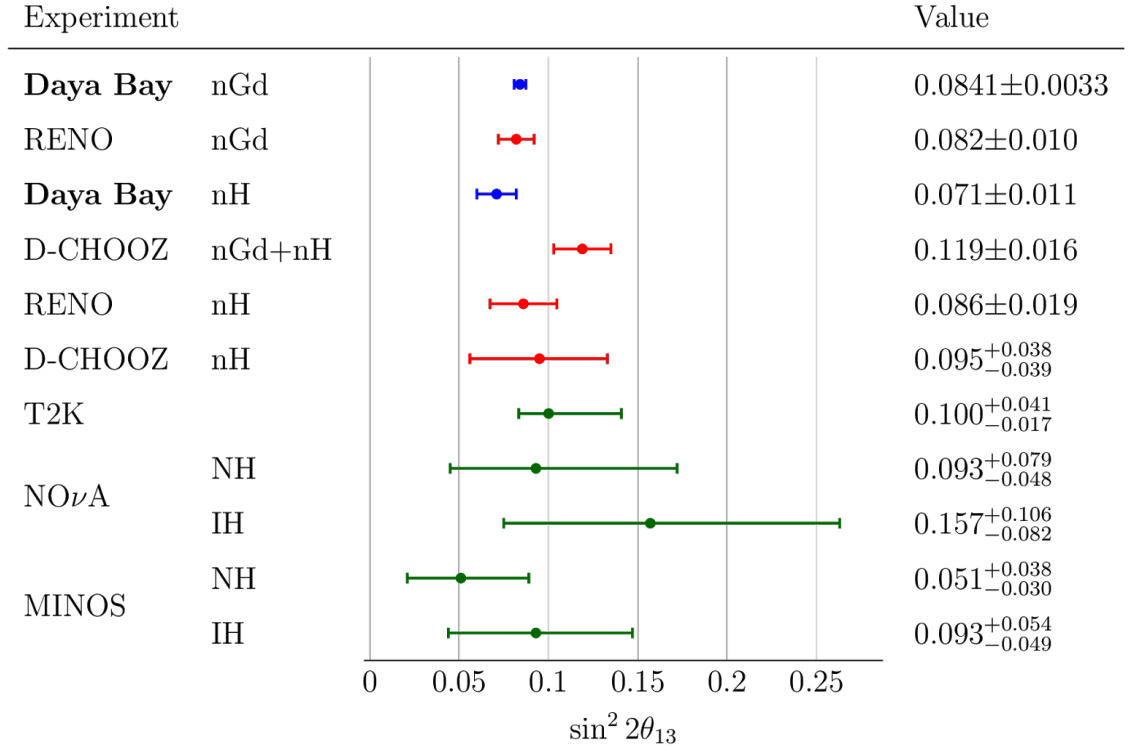
Fig. 4.3.3. Comparison of the $\sin^2 2\theta_{13}$ measurements.



| Experiment | Value $(10^{-3}\,\mathrm{eV}^2)$ |
|---|---|
| **Daya Bay** | $2.45 \pm 0.08$ |
| T2K | $2.545^{+0.081}_{-0.084}$ |
| MINOS | $2.42 \pm 0.09$ |
| NO$\nu$A | $2.67 \pm 0.12$ |
| Super-K | $2.50^{+0.13}_{-0.20}$ |
| IceCube | $2.50^{+0.18}_{-0.24}$ |
| RENO | $2.57^{+0.24}_{-0.26}$ |

Fig. 4.3.4. Comparison of the $\Delta m^2_{32}$ measurements. Normal neutrino mass hierarchy is assumed.

# 4.4. Study of wave packet impact

Plane wave approximation used in the standard neutrino oscillation theory is known to be not self-consistent and contradictory [16]. A wave packet treatment of neutrino oscillation is necessary.
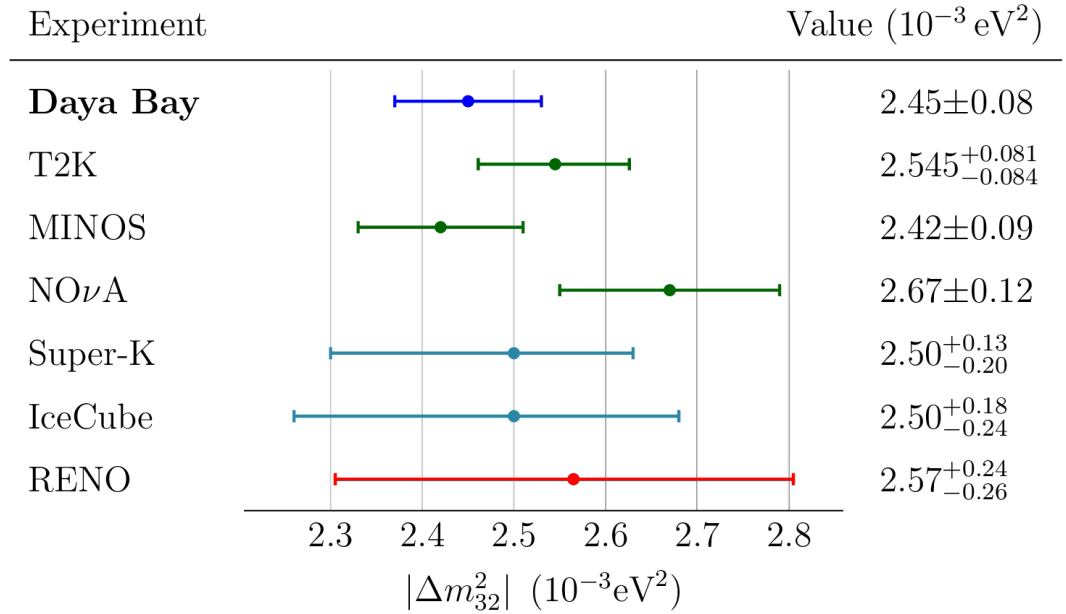
The wave packet is a coherent superposition of different waves whose momenta are distributed around the most probable value, with a certain "width" or dispersion. Therefore, a wave packet is localized in space-time as well as in energy-momentum space.

The wave packet models of neutrino oscillation were developed in roughly two varieties. The  first one relies on a relativistic quantum mechanical (QM) formalism that does not predict the dispersion  of the neutrino wave packet in  momentum space. The second one is based on calculations within quantum field theory (QFT), describing all external particles involved in neutrino production and detection  as wave packets while treating neutrinos  as virtual particles. The neutrino wave-function is  then calculated rather than postulated. The effective momentum dispersion of the neutrino wave function depends on the kinematics of neutrino production and detection and on the momentum dispersions of the external particles. Both approaches predict a number of observable effects, like a quantitative condition on the coherence of mass eigenstates in the production-detection processes, as well as a loss of  coherence.

A relativistically covariant theory of neutrino oscillations within QFT wave packet model (WP) was developed [17]. The wave packet formalism facilitates the resolution of the paradoxes of the plane wave theory, and predicts the existence of a coherence length. The latter arises due to the different group velocities of a different neutrino mass states, which causes a separation in space over time. As the wave packets separate over time they lose their coherence which suppresses the oscillations.

In comparison to the plane wave approach to the neutrino oscillations the QM wave packet approach introduces only one additional parameter — wave packet relative intrinsic momentum dispersion $\sigma_{rel}=\sigma_p/p$. For a given energy $\sigma_{rel}$ may be related to the wave packet spatial width $\sigma_x=1/2\sigma_p$.

In order to put a limit on $\sigma_{rel}$ we have suggested and performed an analysis of the Daya Bay data, acquired during period of 621 days [18]. The analysis yields the first experimental upper limit:

$$\sigma_{rel} < 0.20 \text{ at } 95\% \text{ C.L.},$$

or, equivalently, the lower limit on the WP spatial size:

$$\sigma_x > 10^{-11} \text{ at } 95\% \text{ C.L.}$$

As the wave packets are separated with time and distance long baseline experiments do have better sensitivity to the $\sigma_{rel}$. To improve the limits we implemented the model of the KamLAND experiment in our fitter. We've used published KamLAND [19,20] data for the detector description and IAEA PRIS [21] data for the reactor performance. The upper limit based on KamLAND data [22] is almost twice lower:

$$\sigma_{rel} < 0.11 \text{ at } 95\% \text{ C.L.},$$

and combination with Daya Bay result yields:

$$\sigma_{rel} < 0.10 \text{ at } 95\% \text{ C.L.}$$

The corresponding $\chi^2$ profiles are presented on figure 4.4.1. These measurements represent the first experimental constraint on the neutrino wave packet parameters. The results are included in bachelor and magister theses by M.Dolgareva [22,23].
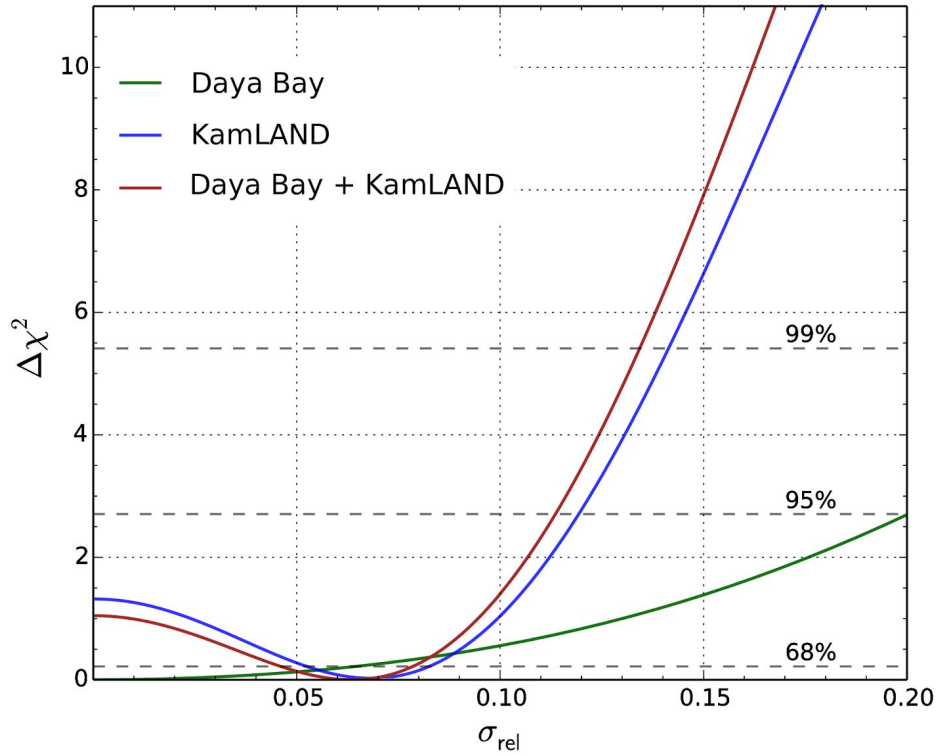
Fig. 4.4.1. $\chi^2$ profile (bottom) and allowed regions for relative neutrino energy spread $\sigma_{rel}$ versus $\Delta m^2_{ee}$ (top) and $\sin^2 2\theta_{13}$ (middle). The levels correspond to the upper limits.

# 4.5. Measurement of reactor antineutrino spectra

Nuclear reactors are intense sources of electron antineutrinos. Each Gigawatt (GW) of reactor thermal power is accompanied by about $10^{20}$ electron antineutrinos emitted isotropically every second. These antineutrino are produced inside a reactor core in fission processes of $^{235}$U nuclei. A portion of the neutrons are captured by $^{238}$U nuclei and subsequent beta decays and neutron captures lead to the production of fissile isotopes $^{239}$Pu and $^{241}$Pu. The beta-decay chains of the fission products of these four isotopes are the main source of electron antineutrinos. About six antineutrinos are produced per fission on average.

Before 2011, the prediction of antineutrino flux and spectrum was based on the beta spectra measured at ILL Grenoble for the thermal-neutron induced fission of $^{235}$U, $^{239}$Pu, and $^{241}$Pu [24], [25],[26] and the theoretical calculation of Vogel for $^{238}$U [27], which was shown to be in good agreement with available data [27,28].

In 2011, re-evaluation of the reactor antineutrino flux and spectrum [29,30] with improved theoretical treatments was carried out, and the new predicted reactor antineutrino flux was shown to be higher than the experimental data. This discrepancy is commonly referred to as the "Reactor Antineutrino Anomaly" [31].

Possible explanation of this anomaly is through oscillations into a hypothetical sterile state. This possibility lead to a number of proposals and running experiments investigating possible existence of sterile neutrino state.
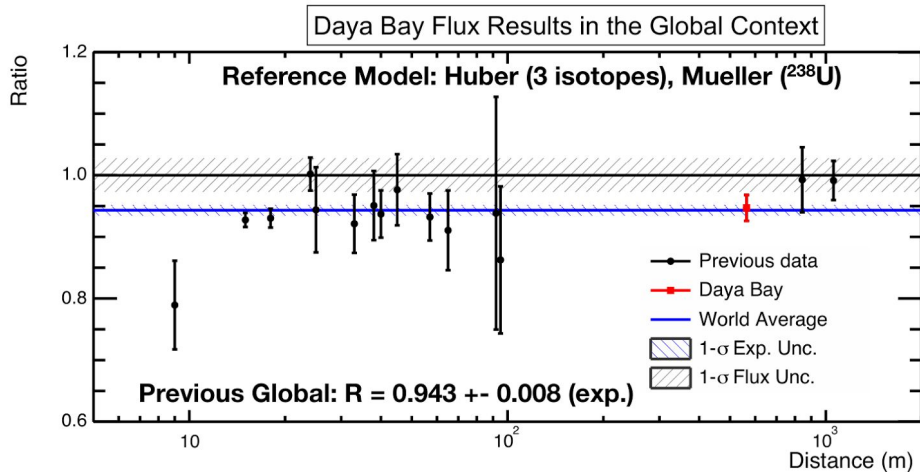
Fig.4.5.1 The measured reactor antineutrino rate as a function of the distance from the reactor, normalized to the theoretical prediction of Huber+Mueller model. The rate is corrected by 3-flavor neutrino oscillations at the distance of each experiment. The purple shaded region represents the global average and its 1 σ uncertainty. The 2.4% model uncertainty is shown as a band around unity. The measurements at the same baseline are combined together for clarity. The Daya Bay measurement is shown at the flux-weighted baseline (573 m) of the two near halls.

Fig.4.5.1 displays the measured reactor antineutrino rate as a function of the distance from the reactor, normalized to the theoretical prediction of Huber+Mueller model. This ratio is measured as: 0.946 ± 0.022 where the uncertainty is experimental. This finding agrees with results of previous reactor experiments at short baselines.

In addition to the observed deficit of IBD events with respect to model predictions, there is also an excess of observed number of events in the (4-6) MeV interval of reconstructed prompt energy. The latter is known as a 'bump'. The comparison of predicted and measured prompt energy spectra can be seen from Fig.4.5.2. These results correspond to official Daya Bay reactor spectrum analysis performed by our chinese colleagues and scrutinized by us in the reviewing process.

In Fig.4.5.3 we display the same ratio but measured by our group in an independent analysis. The energy spectrum of reactor antineutrinos is measured in our oscillation analysis in which we do fit 17 free parameters: two oscillation parameters and 15 reactor antineutrino spectrum parameters. These 15 parameters represent corrections to the average reactor antineutrino spectrum based on the Huber+Mueller model [29,32] and are shown on the figure 4.5.3. The figure features 3 reactor spectrum traits when compared to the model:

1. Overall reactor antineutrino deficit, also known as "reactor anomaly". It's seen by all the reactor antineutrino experiments [31,33];
2. Spectral shape distortion in a region 5-7 MeV, also known as "bump" or "shoulder". It's seen by precision reactor antineutrino experiments Daya Bay [34], Double CHOOZ [35] and RENO [36];
3. Spectral shape distortion around 2 MeV. This distortion, that is sometime is referred as "valley around 3-5 MeV", was noted quite recently [37].

A fair interpretation of results presented in Figs.4.5.1-4.5.3 leads us to a conclusion that data and model calculations disagree with each other. However a possible origin of this discrepancy remains yet unknown. As mentioned above, a hypothesis of an oscillation into a sterile neutrino state could be a good explanation of the observed rate and shape of reactor antineutrino.
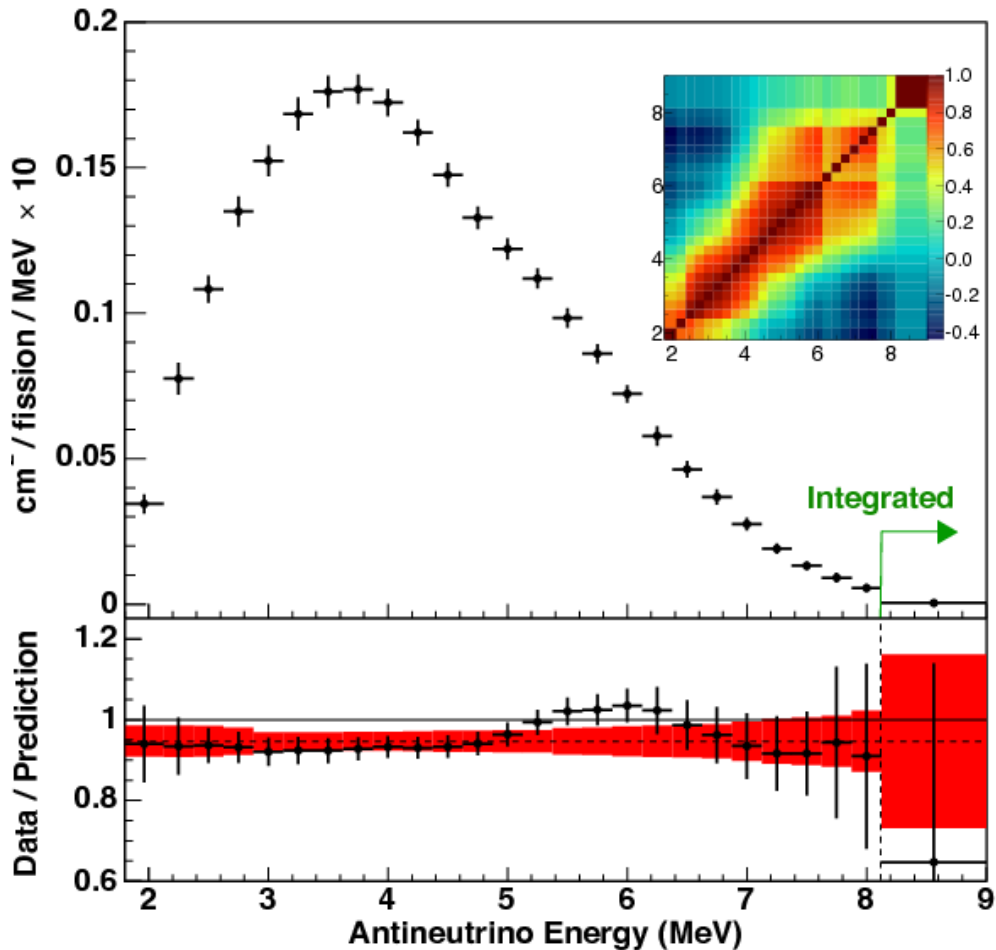
59

Fig.4.5.2 Comparison of predicted and measured prompt energy spectra. The prediction is based on the Huber+Mueller model and normalized to the number of measured events. The error bars on the data points represent the statistical uncertainty.

As we show in what follows the sterile neutrino interpretation of our data is unlikely as follows from further analyses of fuel evolution and dedicated sterile neutrino search (see Section 4.6).

Since fission yields and beta-decay branches from each fission parent isotope are not identical, antineutrino fluxes and spectra produced from the various fission isotopes differ. Thus, when a reactor experiences a change in the percent contribution to fission rates from each fissioning isotope (fission fractions), a measurable change in the reactor antineutrino flux and spectrum may also be produced. The Daya Bay experiment has observed correlations between reactor core fuel evolution and changes in the reactor antineutrino flux and energy spectrum. Fig.4.5.4 displays the IBD yield per fission, $\sigma_f$, versus effective $^{239}$Pu (lower axis) or $^{235}$U (upper axis) fission fraction. A hypothesis of $\sigma_f$ independence on fuel evolution is excluded at 10 standard deviations.

In Fig. 4.5.5 we show the combined measurement of $^{239}$Pu and $^{235}$U. Based on measured IBD yield variations, yields of $(6.17 \pm 0.17)$ and $(4.27 \pm 0.26) \times 10^{-43}$cm$^2$/fission have been determined for the two dominant fission parent isotopes $^{235}$U and $^{239}$Pu. A 7.8% discrepancy between the observed and predicted $^{235}$U yield suggests that this isotope may be the primary contributor to the reactor antineutrino anomaly.

A sterile neutrino hypothesis should yield to an equal deficit of all four isotopes. A hypothesis that all four main isotopes experience an equal deficit was explicitly tested. This hypothesis is disfavored at 2.8 standard deviations. Thus, a sterile neutrino hypothesis is unlikely to explain the observed IBD rate deficit.
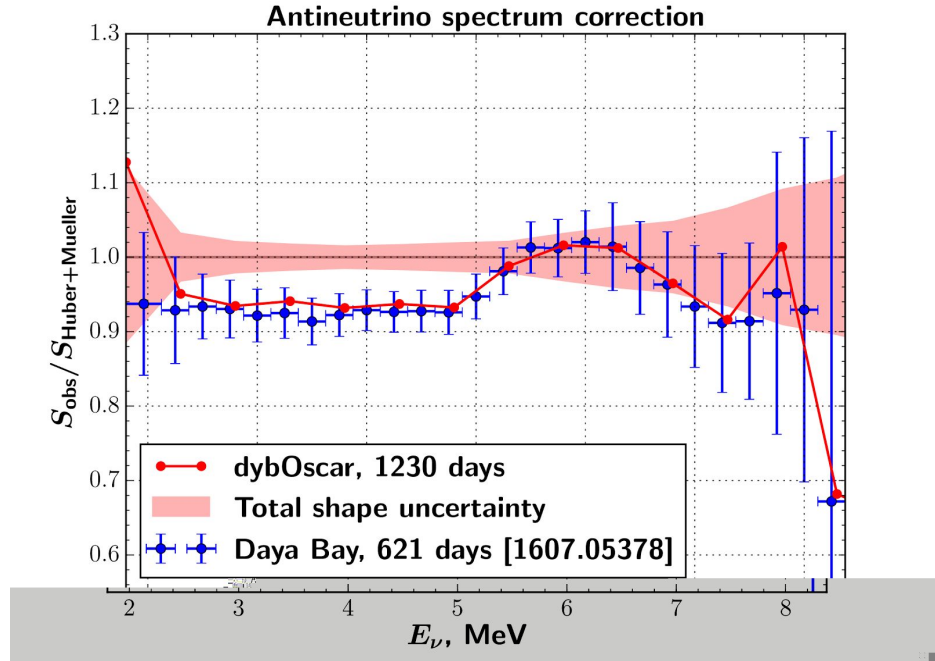
Fig. 4.5.3. Observed antineutrino energy spectrum as a ratio to the prediction of the Huber+Mueller model [29,32]. Our measurement (red line and red span) is in a good agreement with official Daya Bay reactor spectrum measurement (blue points), based on 621 days of data [34]. Blue errors correspond to the total rate+shape uncertainty while red region is for shape uncertainty only.
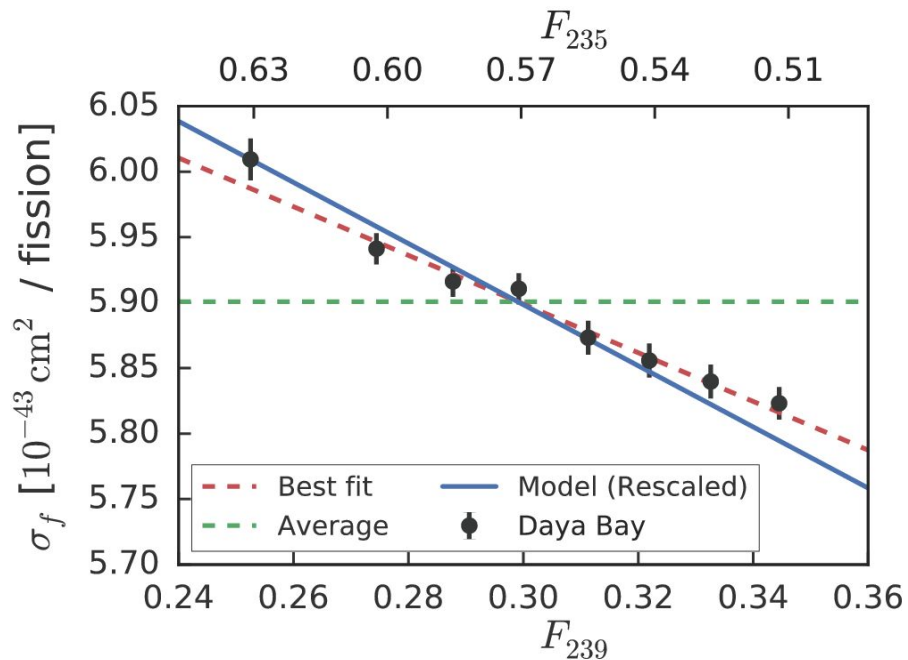


Fig.4.5.4 IBD yield per fission, $\sigma_f$, versus effective $^{239}$Pu (lower axis) or $^{235}$U (upper axis) fission fraction.

Fig.4.5.5. Combined measurement of [239]Pu and [235]U. The red triangle indicates the best fit position, while the shaded contours correspond to 1, 2,3 standard deviations confidence intervals. Prediction is shown as a black point and black 1 standard deviation allowed contour.

# 4.6. Search for sterile neutrino

An existence of sterile neutrino state would show itself as a specific modification of IBD prompt energy spectrum as can be see in Fig.4.6.1.



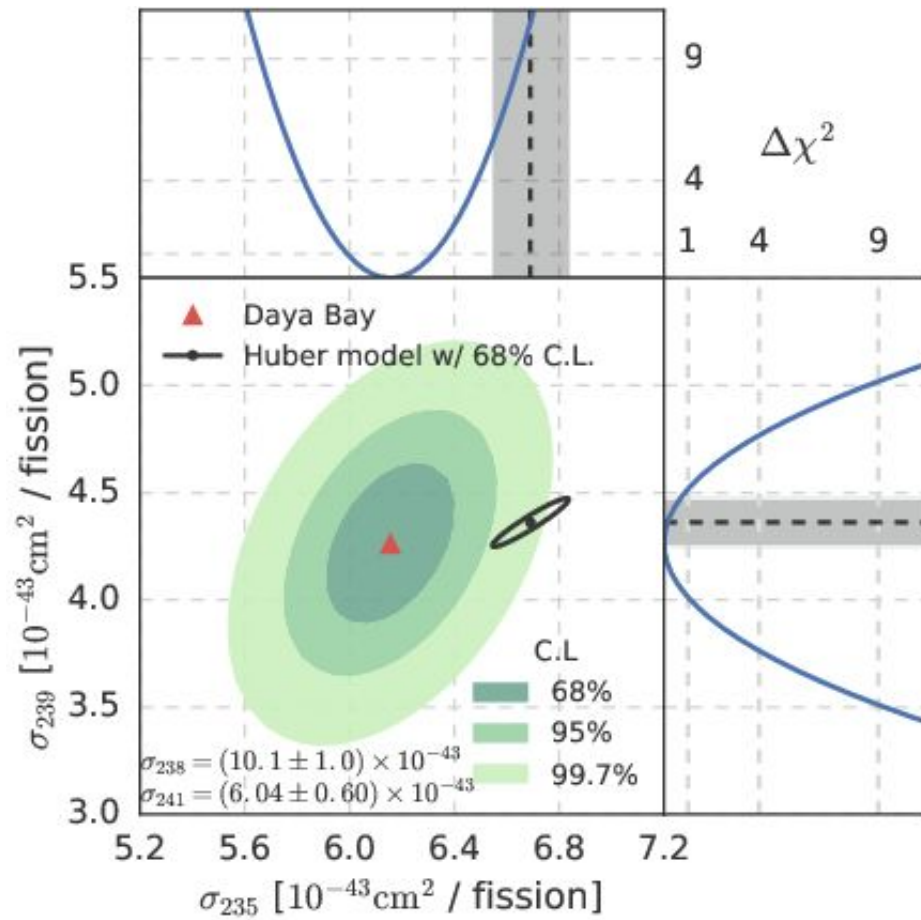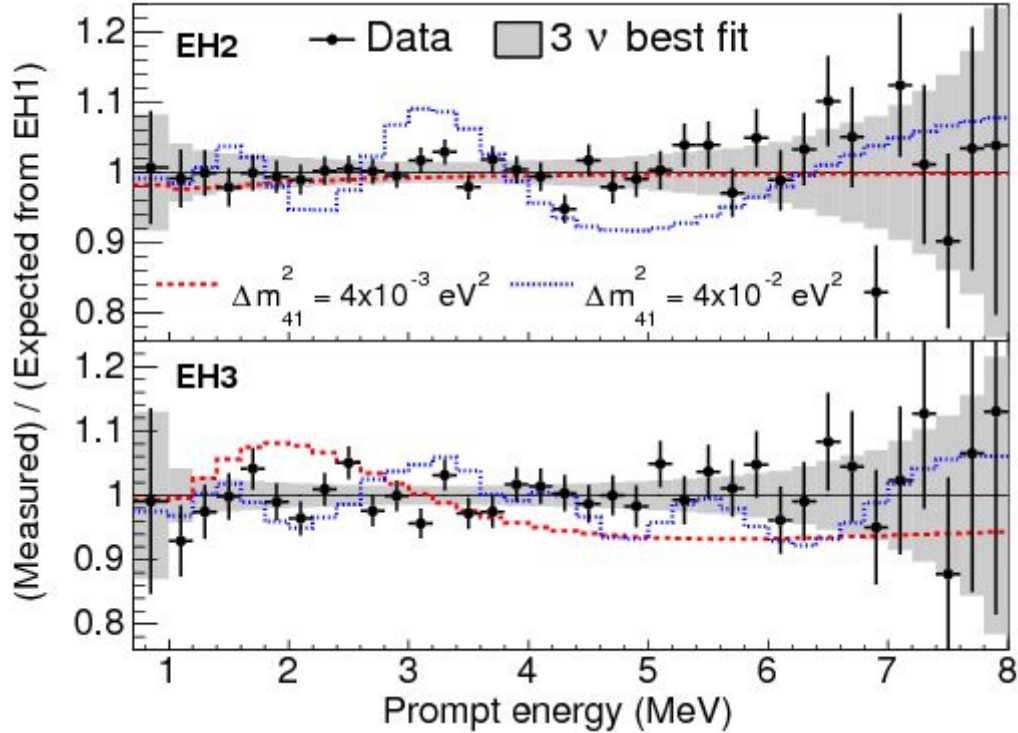Fig.4.6.1 Ratio of measured energy spectra to expectation accounting for 3 neutrino oscillations with Daya Bay best-fit parameters. Red and blue curves correspond to a case when the denominator is replaced by a 4 neutrino model with a value of $\Delta m^2_{41}$ as shown in the legend.

A comparison of measured and 4 neutrino model energy spectra performed with help of statistical analysis yields the following exclusion region in domain of $\sin^2 2\theta_{41}$ and $\Delta m^2_{41}$ as shown in Fig. 4.6.2. An analysis performed by Daya Bay collaborators of Daya Bay and Bugey-3 data excludes a significant part of the parametric space allowing to fit the reactor antineutrino anomaly.

We also performed a joint analysis together with MINOS Collaboration of $\sin^2 2\theta_{\mu e}$ and $\Delta m^2_{41}$. This analysis allows us to test the long standing LSND anomaly. Allowed (LSND, MiniBooNE) and excluded (NOMAD, KARMEN2, MINOS and DayaBay/Bugey3) at 90% confidence level regions in $\sin^2 2\theta_{\mu e}$ and $\Delta m^2_{41}$ space are displayed in Fig. 4.6.3. This result makes an interpretation of LSND (and MiniBooNE) anomalies in terms of oscillations into sterile neutrino state unlikely.

Fig. 4.6.2 Exclusion region in domain of $\sin^2 2\theta_{41}$ and $\Delta m^2_{41}$ based on Daya Bay data.

Fig. 4.6.3 Exclusion region in domain of $\sin^2 2\theta_{41}$ and $\Delta m^2_{41}$ based on Daya Bay and Bugey-3 data.



Fig. 4.6.3 Allowed (LSND, MiniBooNE) and excluded (NOMAD, KARMEN2, MINOS and DayaBay/Bugey3) at 90% confidence level regions in $\sin^2 2\theta_{\mu e}$ and $\Delta m^2_{41}$ space.
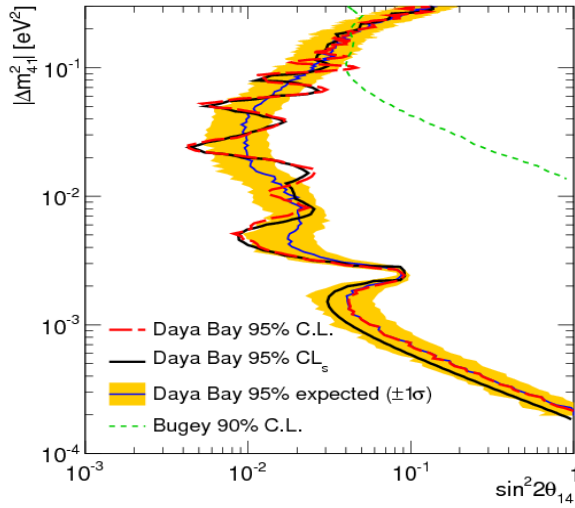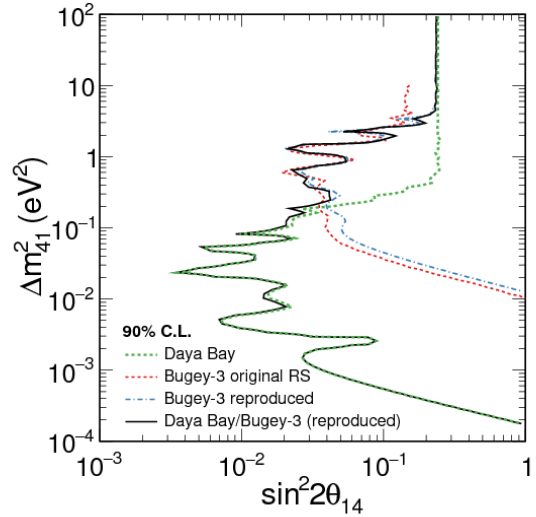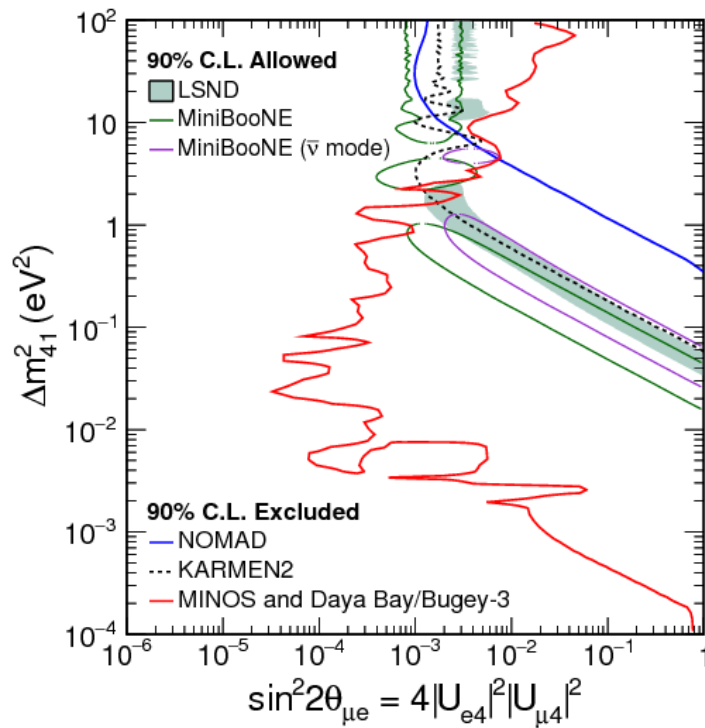
# 5. SWOT analysis

## 5.1. JUNO

| | Helpful | Harmful |
|---|---|---|
| | **STRENGTHS** | **WEAKNESSES** |
| Internal | <ul><li>Neutrino hierarchy determination</li><li>Precise oscillation parameters measurement</li><li>Geo-neutrinos measurement</li><li>Other neutrino physics (solar, atmospheric, etc.)</li></ul> | <ul><li>Failure to achieve 3% energy resolution</li><li>Insufficient PMT efficiency</li><li>Insufficient detector/structure integrity</li><li>Insufficient electronics/HV reliability</li></ul> |
| | **OPPORTUNITIES** | **THREATS** |
| External | <ul><li>Supernova burst</li><li>Diffuse Supernova background</li><li>New physics</li></ul> | <ul><li>Underground collapse and flooding</li><li>Lower than expected NPP thermal power</li></ul> |

Table 5.1. JUNO SWOT table.

The JUNO experiment is expected to be a huge step forward in scale and precision among the reactor neutrino experiments. JUNO detector will be 20 times larger than the current largest reactor antineutrino detector KamLAND. Experiment requirements include maximal PMT coverage and 3% energy resolution at 1 MeV of released energy. Therefore the detector construction has a number of technical challenges:

- Creating an acrylic sphere to hold 20 kt of liquid scintillator which is inflammable.
- Production of high efficiency PMT tubes.
- Protection of PMTs against the shock wave.
- Potting and connecting PMTs, electronics and HV system underwater on depth up to 35 meters.
- At least 20 years working time (30 years expected).

All these items indicate high reliability and safety requirements. The potential risk are and will be minimized by extensive subsystem testing and putting high reliability requirements on the detector components.

Construction of a large scale underground laboratory in Jiangmen has its own risks. Two major ones are the possibility of underground collapse or flooding. Both risks are minimized by thorough geological study and increased reliability and safety requirements.

There is a chance of delay or cancellation of two Taishan NPP cores construction. Two out of four Taishan NPP cores will produce about 25% of JUNO antineutrinos, therefore the delay in construction may require up to 25% longer data taking (7.5 years instead of 6 years) in order to achieve the required sensitivity to the neutrino mass hierarchy.

JUNO has a very rich experimental program. In case of achievement of required energy resolution JUNO will measure mass hierarchy with statistical significance of 3-4 standard deviation. This measurement does not depend on any unknown oscillation parameters (such as

CP-violating phase $\delta_{CP}$ or neutrino mixing angle $\theta_{23}$). JUNO will measure oscillation parameters $\Delta m^2_{21}$, $\Delta m^2_{32}$ and $\theta_{12}$ with sub-percent accuracy. The only input required is $\theta_{13}$ which will be measured by Daya Bay experiment with significant precision.

After KamLAND and BOREXINO, JUNO will be the third experiment to observe geoneutrinos. We expect 10 times higher statistics of geoneutrinos. Other physical topics include studies of solar and atmospheric neutrinos, search for sterile neutrinos and new physics, etc.

In case of Supernova explosion JUNO will detect several thousands of events[3] in various channels — which will be a breakthrough in this field. In addition, JUNO has a potential of detecting diffuse Supernova neutrinos.

# 5.2. Daya Bay

| | Helpful | Harmful |
|---|---|---|
| | **STRENGTHS** | **WEAKNESSES** |
| Internal | • Most precise $\sin^2 2\theta_{13}$ and $\Delta m^2_{32}$ measurement<br>• Sterile neutrino search<br>• Reactor spectra study<br>• Liquid scintillator study for JUNO | • Insufficient waterpool PMT reliability |
| | **OPPORTUNITIES** | **THREATS** |
| External | • Supernova burst | |

Table 5.1. Daya Bay SWOT table.

The Daya Bay experiment is taking data since 2011 and already proved itself as precise and reliable experiment. We expect no quantifiable threats in the ongoing period.

As the primary potential weakness we may note the insufficient waterpool PMT reliability. For the waterpool the PMT tubes from MACRO experiment are reused and currently about 10% of waterpool PMTs are out of order. These PMTs are not crucial for the analysis since the muon veto may sufficiently run in partial configuration. Also water pool PMTs may be replaced during maintenance period.

We would like to note that during detectors commissioning in 2011 new Hamamatsu PMTs were installed in the antineutrino detectors. On average we have less than one failed PMT per detector and expect no significant changes during the project period.

The major opportunity for the Daya Bay experiment would be the Supernova detection. Daya Bay will detect around 100 events in case of SN1987A-like Supernova explosion in the center of our galaxy.

The strengths of the Daya Bay experiment include:
- Precise $\sin^2 2\theta_{13}$ and $\Delta m^2_{32}$ measurement. In the 2020 the precision on both parameters will be better than 3%. This will be the ultimate $\theta_{13}$ measurement for decades.

---

[3] for SN1987A-like Supernova in the center of our galaxy

- Search for the sterile neutrinos. Daya Bay has the best sensitivity for the sterile neutrinos in the region of 0.001 eV$^2$<$\Delta m^2_{41}$<0.1 eV$^2$.
- Precision reactor antineutrino spectrum measurement.

# 6. Tasks to be addressed in 2018-2020

## 6.1. JUNO

### 6.1.1. 5.1.1. 2018
1. Commissioning and installation of additional  2 scanning stations.
2. PMT testing
   a. Naked PMT mass-testing by scanning and in the containers. Shifts on site
   b. Potted PMT mass-testing. Shifts on site
   c. Fine PMT studying with automatic scanning station
3. Start of HVU mass production and quality assurance tests
4. The Top Tracker  DAQ software development
5. Prototyping and finalization of the Top Tracker mechanical support design
6. Top Tracker modules performance monitoring with cosmic muons
7. Simulation and reconstruction
   a. Detector simulation and sensitivity estimation
   b. Study of the PMT response impact on the oscillation analysis
   c. IBD selection and background estimation methods
   d. Muon tracking algorithms in the Top Tracker

### 6.1.2. 5.1.2. 2019
1. PMT testing
   a. Naked PMT mass-testing by scanning and in the containers. Shifts on site
   b. Potted PMT mass-testing. Shifts on site
2. Finishing the HVU mass production and quality assurance tests
3. Fabrication of the Top Tracker mechanical support and shipment to JUNO
4. The Top Tracker  DAQ software development
5. Top Tracker modules performance monitoring with cosmic muons
6. Simulation and reconstruction
   a. Detector simulation and sensitivity estimation
   b. IBD selection and background estimation methods
   c. Muon tracking algorithms in the Top Tracker

### 6.1.3. 5.1.3. 2020
1. Potted PMT mass-testing. Shifts on site
2. Installation of PMTs to the JUNO detector. Shifts on site
3. Assembly and commissioning of the Top Tracker detector. Shifts  at JUNO.
4. The Top Tracker  DAQ software commissioning
5. Simulation and reconstruction
   a. Detector simulation and sensitivity estimation
   b. IBD selection and background estimation methods
   c. Muon tracking algorithms in the Top Tracker

## 6.2. Daya Bay

### 6.2.1. 5.2.1. 2018
1. Implementation of Daya Bay oscillation analysis within GNA framework
2. IBD selection of the complete dataset of Daya Bay phase I (2011-2017)
3. Background estimation
4. Oscillation analysis for the Phase I dataset
5. Detector energy response calibration
6. Remote and on-site shifts

### 6.2.2. 5.2.2. 2019
1. Implementation of combined oscillation analysis for the Daya Bay, Double CHOOZ and RENO experiments within GNA framework
2. Implementation of nH analysis of the Daya Bay data within dybOscar/GNA frameworks
3. Maintain and improve IBD selection and analysis techniques
4. Detector energy response calibration
5. Remote and on-site shifts

### 6.2.3. 5.2.3. 2020
1. IBD selection of the final dataset (2011-2020)
2. Background estimation
3. Final oscillation analysis of the complete Daya Bay data including both nGd and nH IBD selections
4. Update of the wave packet analysis based on the complete Daya Bay dataset
5. Collaborative work with Daya Bay, Double CHOOZ and RENO experiments towards combined oscillation analysis
6. Detector energy response calibration
7. Remote and on-site shifts

# 7. Conference Presentations and Seminars given by JINR team members in 2015-2017

1. D.Naumov. New Results from the Daya Bay Reactor Neutrino Experiment. Neutrino Telescopes, 13-17 March 2017, Venice, Italy (пленарный доклад);
2. D.Naumov. Latest Results from the Daya Bay Reactor Neutrino Experiment. New Trends in High-Energy Physics, 2-8 October 2016, Budva, Becici, Montenegro (пленарный доклад);
3. D.Naumov. Neutrino Physics with Nuclear Reactors. QUARKS-2016 19th International Seminar on High Energy Physics, Pushkin, Russia, 29 May - 4 June, 2016 (пленарный доклад);
4. D.Naumov. Neutrino Physics with Nuclear Reactors. Международная Сессия-конференция Секции ядерной физики ОФН РАН, 12 - 15 апреля, 2016, ОИЯИ, Дубна (пленарный доклад);
5. D.Naumov. Neutrino Oscillations in QFT with relativistic wave packets. Международная Сессия-конференция Секции ядерной физики ОФН РАН, 12 - 15 апреля, 2016, ОИЯИ, Дубна (доклад на параллельной сессии);
6. D.Naumov. Neutrino Physics program at the JINR. 4th SOUTH AFRICA - JINR SYMPOSIUM. Few to Many Body Systems: Models and Methods and Applications, September 21-25, 2015, JINR Dubna, Moscow region, Russia (пленарный доклад);
7. D.Naumov. Измерение $\theta_{13}$ , $\Delta m^2_{32}$ и ковариантная квантово-полевая теория нейтринных осцилляций, 07/02/2017 ПИЯФ, Гатчина, РФ;
8. D.Naumov. Ковариантная квантово-полевая теория нейтринных осцилляций, 09/11/2016 ИЯИ РАН, Москва, РФ;
9. D.Naumov. Измерение $\theta_{13}$ , $\Delta m^2_{32}$ и ковариантная квантово-полевая теория нейтринных осцилляций, 03/11/2016 НИИЯФ ИГУ, Москва, РФ;
10. D.Naumov. Измерение $\theta_{13}$ , $\Delta m^2_{32}$ и ковариантная квантово-полевая теория нейтринных осцилляций, 20/10/2016 ЛТФ ОИЯИ, Дубна, РФ;
11. A.Olshevskiy. Accelerator Neutrino Physics. Международная Сессия-конференция Секции ядерной физики ОФН РАН, 12 - 15 апреля, 2016, ОИЯИ, Дубна (пленарный доклад);
12. A.Olshevskiy. The Scientific Heritage of Bruno Pontecorvo, The Triumph of Neutrino Oscillations. Seminar at Pisa, 13 October 2015.
13. N.Anfimov. Testing methods for 20-inches PMTs of the JUNO experiment. INSTR-2017, Novosibirsk, Russia, 27 Feb - 3 Mar 2017.
14. O.Smirnov. Geoneutrino studies with JUNO detector, International Workshop: Neutrino Research and Thermal Evolution of the Earth, October 25 – 27, 2016, Sendai, Japan
15. T.Antoshkina. Optical simulation of PMT. The 2016 European School of High-Energy Physics (poster report), Norway, 15-28 June 2016.
16. T.Antoshkina. Optical simulation of PMT. 45th meeting of the PAC for Particle Physics in JINR (poster report), Dubna, 16-17 January 2017
17. T.Antoshkina. JUNO experiment. 44th meeting of the PAC for Particle Physics in JINR (poster report), Dubna, 14-15 December 2015
18. T.Antoshkina. Optical simulation of PMT. JUNO electronics & PMT workshop, Dubna, 16-19 April 2016
19. T.Antoshkina. Studying of zonal characteristics of PMT. AYSS-2016, Dubna (секционный доклад), 14-18 March 2016.

20. Yu.Gornushkin. Status of the JUNO experiment. Международная Сессия-конференция Секции ядерной физики ОФН РАН, 12 - 15 апреля, 2016, ОИЯИ, Дубна ( доклад на параллельной сессии);
21. Yu.Gornushkin Background suppression in the JUNO experiment. 38th International Conference on High Energy Physics 3-10 August 2016, Chicago, USA (poster report);
22. K.Treskov. The usage of wave packet approach to neutrino oscillations in analysis of reactor and solar experiments, 44th meeting of the PAC for Particle Physics in JINR (poster report), Dubna, 14-15 December 2015
23. K.Treskov. Fast neutron background in the Daya Bay experiment. AYSS-2016, Dubna(section report, winner of section), 14-18 March 2016.
24. K.Treskov. Inverse beta-decay event selection and fast neutron background in the Daya Bay experiment. The 2016 European School of High-Energy Physics (poster report), Norway, 15-28 June 2016
25. K.Treskov. Inverse beta-decay event selection and fast neutron background in the Daya Bay experiment, 45th meeting of the PAC for Particle Physics in JINR (poster report), Dubna, 16-17 January 2017.
26. K.Treskov. Preliminary results on fast neutron background. Daya Bay Collaboration Meeting, Beijing, IHEP, 17-20 March 2016.
27. K.Treskov. Global analysis toolkit overview. Daya Bay Collaboration Meeting, Taipei, 7-11 December 2016.
28. M.Gonchar, "Oscillation analysis in Daya Bay experiment". XIX International Scientific Conference of Young Scientists and Specialists. Dubna, 16-20 February, 2015.
29. M.Gonchar, „Измерение параметров смешивания нейтрино амплитуды осцилляций $\sin^2 2\theta_{13}$ и расщепления масс $\Delta m^2_{32}$ в эксперименте Daya Bay". DLNP seminar. Dubna, October, 2015
30. M.Gonchar, "Neutrino mass hierarchy measurement in JUNO", seminar for students, Dubna, 11 February 2016.
31. M.Gonchar, "Recent results from Daya Bay experiment". International session-conference of the section of nuclear physics of PSD RAS. Dubna, 12-15 April, 2016.
32. M.Gonchar, poster, "Oscillation analysis in Daya Bay experiment". Neutrino 2016. London 4-9 July, 2016.
33. M.Gonchar, "New results from the Daya Bay experiment". DLNP seminar. Dubna. 10 November 2016.
34. M.Gonchar, "JINR neutrino programme. Daya Bay and JUNO: precision measurements with reactor neutrinos". 46th meeting of the PAC for Particle Physics. Dubna, 16-17 January, 2017.
35. M.Gonchar, poster, "Oscillation analysis in Daya Bay experiment". 46th meeting of the PAC for Particle Physics. Dubna, 16-17 January, 2017.
36. M.Dolgareva, "Study of the neutrino decoherence effects in Daya Bay experiment". XIX International Scientific Conference of Young Scientists and Specialists. Dubna, 16-20 February, 2015.
37. M.Dolgareva, "A study of the wave packets approach to the neutrino oscillations based on Daya Bay and KamLAND data". XIX scientific conference of young scientists and specialists. Dubna, 14-18 March, 2016.
38. M.Dolgareva, poster, "Study of decoherence effects in neutrino oscillations at Daya Bay". ICHEP 2016. Chicago, 3-10 August 2016.
39. M.Dolgareva, poster, "Study of decoherence effects in neutrino oscillations at Daya Bay". 46th meeting of the PAC for Particle Physics. Dubna, 16-17 January, 2017.

# 8. Theses prepared within 2015-2017

1. Diploma theses
    a. K.Treskov, specialist's thesis, "Нейтринные осцилляции в веществе и возможность экспериментального исследования декогеренции в солнечных экспериментах" [38]. 2015.
    b. M.Dolgareva, master thesis, "Исследование эффектов декогерентности волновых пакетов в нейтринных осцилляциях на основе данных экспериментов KamLAND и Daya Bay" [22]. 2016.
    c. V.Sharov, bachelor thesis, "Измерение характеристик крупногабаритных фотоэлектронных умножителей для эксперимента JUNO". Moscow State University. 2016.
2. Candidate of Science theses
    a. M.Gonchar, "Измерение угла смешивания $\theta_{13}$ и расщепления масс нейтрино $\Delta m^2_{32}$ в эксперименте Daya Bay". 2017.
3. Doctor of Science theses
    a. D.Naumov, "Измерение $\theta_{13}$, $\Delta m_{32}^2$ и ковариантная квантово-полевая теория нейтринных осцилляций". 2017.

# 9. Published papers within 2015-2017

1. Bednyakov V. A., Naumov D. V., Smirnov O. Y. Neutrino physics and JINR // Phys. Usp. — 2016. — T. 59, No 3. — C. 225—253.
2. Measurement of electron antineutrino oscillation based on 1230 days of operation of the Daya Bay experiment / F. P. An [et al.]. — 2016. — arXiv: 1610.04802 [hep-ex]. Accepted to Phys. Rev. D.
3. New measurement of $\theta_{13}$ via neutron capture on hydrogen at Daya Bay / F. P. An [et al.] // Phys. Rev. — 2016. — T. D93. — C. 072011. — arXiv: 1603.03549 [hep-ex].
4. Study of wave packet treatment of neutrino oscillations at Daya Bay / M. Dolgareva [et al.] // PoS. — 2016. — T. ICHEP2016.
5. Improved Measurement of the Reactor Antineutrino Flux and Spectrum at Daya Bay / F. P. An [et al.] // Chin. Phys. — 2016. — T. C2017. — C. 41. — arXiv:1607.05378 [hep-ex].
6. Improved Search for a Light Sterile Neutrino with the Full Configuration of the Daya Bay Experiment / F. P. An [et al.] // Phys. Rev. Lett. — 2016. — Vol. 117, no. 15. — P. 151802. — arXiv: 1607.01174 [hep-ex].
7. Improved Measurement of the Reactor Antineutrino Flux and Spectrum at Daya Bay / F. P. An [et al.] // Chin. Phys. — 2017. — Vol. C41, no. 1. — P. 013002. — arXiv:1607.05378 [hep-ex].
8. Measurement of the Reactor Antineutrino Flux and Spectrum at Daya Bay / F. P.An [et al.] // Phys. Rev. Lett. — 2016. — T. 116, No 6. — C. 061801. — arXiv:1508.04233 [hep-ex].
9. New Measurement of Antineutrino Oscillation with the Full Detector Configuration at Daya Bay / F. P. An [et al.] // Phys. Rev. Lett. — 2015. —T. 115, No 11. — C. 111802. — arXiv: 1505.03456 [hep-ex].
10. The Detector System of The Daya Bay Reactor Neutrino Experiment / F. P. An [et al.] // Nucl. Instrum. Meth. — 2016. — T. A811. — C. 133—161. — arXiv:1508.03943 [physics.ins-det].
11. Neutrino Physics with JUNO / F. An [et al.] // J. Phys. — 2016. — T. G43. — C. 030401. — arXiv: 1507.05613 [physics.ins-det].
12. The muon system of the Daya Bay Reactor antineutrino experiment / F. P. An [et al.] // Nucl. Instrum. Meth. — 2015. — T. A773. — C. 8—20. — arXiv:1407.0275 [physics.ins-det].

# 10. Number of publications of the team members

| Personal Info | Total number of publications | Hirsch index<br>Total number of citations |
|---|---|---|
| Naumov D.V. | 90 | 31<br>5,792 |
| Olchevski A.G. | 707 | 126<br>81,853 |
| Smirnov O.Y. | 139 | 35<br>4,919 |
| Anfimov N.V. | 28 | 8<br>964 |
| Gonchar M.O. | 25 | 16<br>3,092 |
| Chukanov A.V. | 56 | 27<br>2,994 |
| Treskov K.A. | 7 | 5<br>71 |
| Selyunin A. | 18 | 6<br>159 |
| Gornushkin Y.A. | 100 | 38<br>10,478 |
| Dmitrievsky S.G. | 33 | 17<br>1,724 |
| Antoshkina T.A. | 0 | 0<br>0 |
| Biktemerova S.V. | 11 | 4<br>191 |
| Butorov I.V. | 7 | 7<br>541 |
| Gromov V.O. | 2 | 1<br>44 |
| Naumova E.E. | 15 | 12<br>664 |

| | | |
|---|---|---|
| Morozov N. | 27 | 4<br>758 |
| Nemchenok I. | 48 | 23<br>4,860 |
| Rybnikov A. | 14 | 3<br>66 |
| Sadovski A. | 125 | 24<br>7988 |
| Fedoseev D. | 2 | 2<br>52 |
| Fomenko N.V. | 1 | 0<br>0 |
| Sotnikov A. | 129 | 33<br>3997 |
| Biare D. | 3 | 2<br>181 |
| Gorchakov O. | 77 | 19<br>1045 |
| Kolganov N. | 0 | 0<br>0 |
| Korablev D. | 50 | 20<br>1639 |
| Krasnoperov A. | 83 | 31<br>3092 |
| Rezinko T. | 6 | 3<br>63 |
| Fomenko K. | 140 | 40<br>6,069 |
| Formozov A. | 2 | 1<br>44 |
| Sokolov S. | 0 | 0<br>0 |
| Strizh M. | 0 | 0<br>0 |
| Chuvashova A | 0 | 0<br>0 |

# 11. People and Tasks

| № | Name | Info | 2018 DB | J. | Tot. | 2019 DB | J. | Tot. | 2020 DB | J. | Tot. | Tasks |
|---|------|------|---------|-----|------|---------|-----|------|---------|-----|------|-------|
| 1 | N. Anfimov | staff | 0 | 0.5 | **0.5** | 0 | 0.5 | **0.5** | 0 | 0.5 | **0.5** | PMT testing group leader |
| 2 | T. Antoshkina | PhD student | 0 | 1 | **1** | 0 | 1 | **1** | 0 | 1 | **1** | PMT optics response simulation. Formulation of requirements for PMT testing quality |
| 3 | D. Biaré | engineer | 0 | 1 | **1** | 0 | 1 | **1** | 0 | 1 | **1** | scanning station, TT DAQ |
| 4 | S. Biktemerova | PhD student | 0 | 0.5 | **0.5** | 0 | 1 | **1** | 0 | 1 | **1** | sensitivity estimation, detector simulation, data analysis |
| 4 | I. Butorov | engineer | 0 | 0.5 | **0.5** | 0 | 0.5 | **0.5** | 0 | 0.5 | **0.5** | Designing and technical work |
| 6 | A. Chukanov | candidate | 0.5 | 0.5 | **1** | 0.4 | 0.6 | **1** | 0.3 | 0.7 | **1** | Software development for reconstruction, data analysis |
| 7 | A. Chuvashova | student | 0 | 0.3 | **0.3** | 0 | 0.3 | **0.3** | 0 | 0.3 | **0.3** | TT muon tracking |
| 8 | S. Dmitrievsky | candidate | 0 | 0.5 | **0.5** | 0 | 0.5 | **0.5** | 0 | 0.5 | **0.5** | Simulation and software development for TT |
| 9 | D. Fedoseev | engineer | 0 | 0.5 | **0.5** | 0 | 0.5 | **0.5** | 0 | 0.5 | **0.5** | Designing and technical work |
| 10 | K. Fomenko | candidate | 0 | 0.5 | **0.5** | 0 | 0.5 | **0.5** | 0 | 0.5 | **0.5** | PMTs magnetic shielding |
| 11 | A. Formozov | PhD student | 0 | 0.8 | **0.8** | 0 | 1 | **1** | 0 | 1 | **1** | study of the LS intrinsic resolution, MC |
| 12 | M. Gonchar | PhD student | 0.7 | 0.3 | **1** | 0.5 | 0.5 | **1** | 0.5 | 0.5 | **1** | sensitivity estimation, detector simulation, data analysis |
| 13 | O. Gorchakov | candidate | 0 | 0.5 | **0.5** | 0 | 0.5 | **0.5** | 0 | 0.5 | **0.5** | PMT response study, detector simulation, energy resolution estimation |
| 14 | Yu. Gornushkin | candidate | 0 | 0.5 | **0.5** | 0 | 0.5 | **0.5** | 0 | 0.5 | **0.5** | The TT project coordination |
| 15 | V. Gromov | engineer | 0 | 1 | **1** | 0 | 1 | **1** | 0 | 1 | **1** | Software development for TT JUNO. |
| 16 | N. Kolganov | student | 0 | 0.1 | **0.1** | 0 | 0.3 | **0.3** | 0 | 0.9 | **0.9** | Software development for reconstruction, data analysis |
| 14 | D. Korablyev | staff | 0 | 0.5 | **0.5** | 0 | 0.5 | **0.5** | 0 | 0.5 | **0.5** | software development for PMT testing, PMT testing |

| № | Name | Info | 2018 | | | 2019 | | | 2020 | | | Tasks |
|---|------|------|----|----|------|----|----|------|----|----|------|-------|
| | | | DB | J. | **Tot.** | DB | J. | **Tot.** | DB | J. | **Tot.** | |
| 18 | A. Krasnoperov | candidate | 0 | 0.3 | **0.3** | 0 | 0.3 | **0.3** | 0 | 0.3 | **0.3** | Software development for TT JUNO. |
| 19 | N. Morozov | candidate | 0 | 0.2 | **0.2** | 0 | 0.2 | **0.2** | 0 | 0.2 | **0.2** | calculation of magnetic shielding |
| 20 | D. Naumov | candidate | 0.5 | 0.5 | **1** | 0.4 | 0.6 | **1** | 0.3 | 0.7 | **1** | project management. Reactor spectrum measurement. Oscillation analyses. Global analysis |
| 21 | E. Naumova | PhD student | 1 | 0 | **1** | 0.8 | 0.2 | **1** | 0.7 | 0.3 | **1** | Reactor spectrum measurement. |
| 22 | I. Nemchenok | candidate | 0.1 | 0.5 | **0.6** | 0.1 | 0.5 | **0.6** | 0.1 | 0.5 | **0.6** | Investigation of properties and stability of liquid scintillator |
| 23 | A. Olshevskiy | doctor | 0.1 | 0.3 | **0.4** | 0.1 | 0.3 | **0.4** | 0.1 | 0.3 | **0.4** | analysis preparation, HV and other JINR hardware activities coordination |
| 21 | T. Rezinko | staff | 0 | 0.5 | **0.5** | 0 | 0.5 | **0.5** | 0 | 0.5 | **0.5** | PMT testing |
| 25 | A. Rybnikov | engineer | 0 | 0.5 | **0.5** | 0 | 0.5 | **0.5** | 0 | 0.5 | **0.5** | PMT testing |
| 26 | A. Sadovsky | candidate | 0 | 0.5 | **0.5** | 0 | 0.5 | **0.5** | 0 | 0.5 | **0.5** | PMT HV R&D |
| 27 | A. Selyunin | engineer | 0 | 0.5 | **0.5** | 0 | 0.5 | **0.5** | 0 | 0.5 | **0.5** | PMT testing |
| 28 | O. Smirnov | candidate | 0 | 0.5 | **0.5** | 0 | 0.5 | **0.6** | 0 | 0.8 | **0.8** | PMTs magnetic shielding, energy resolution studies |
| 24 | S. Sokolov | engineer | 0 | 1 | **1** | 0 | 1 | **1** | 0 | 1 | **1** | Designing and technical work, PMT testing |
| 30 | A. Sotnikov | engineer | 0 | 0.3 | **0.3** | 0 | 0.3 | **0.3** | 0 | 0.3 | **0.3** | PMTs magnetic shielding, PMT tests |
| 31 | M. Strizh | student | 0.3 | 0 | **0.3** | 0.3 | 0 | **0.3** | 0.3 | 0 | **0.3** | reconstruction of neutrino directionality |
| 32 | K. Treskov | PhD student | 0.6 | 0.4 | **1** | 0.5 | 0.5 | **1** | 0.3 | 0.7 | **1** | sensitivity estimation, software development, data analysis, participation in detector calibration |
| | **Total FTE** | | 3.8 | 15.5 | **19.3** | 3.1 | 17.1 | **20.3** | 2.6 | 18.5 | **21.1** | |
| | **People** | | 8 | 30 | **32** | 8 | 31 | **32** | 8 | 31 | **32** | |
| | **FTE/person** | | 0.48 | 0.52 | **0.6** | 0.39 | 0.55 | **0.63** | 0.33 | 0.6 | **0.66** | |

Fig. 11.1. FTE distribution for Daya Bay and JUNO experiments and tasks overview.

**The average age of the JINR JUNO/Daya Bay team is ~40 years. There are 3**

bachelor and master students, 6 young scientists preparing PhD, 8 engineers, 11 staff members with PhD degree and 1 professor. More detailed information may be found on charts in figures 11.1. and 11.2.
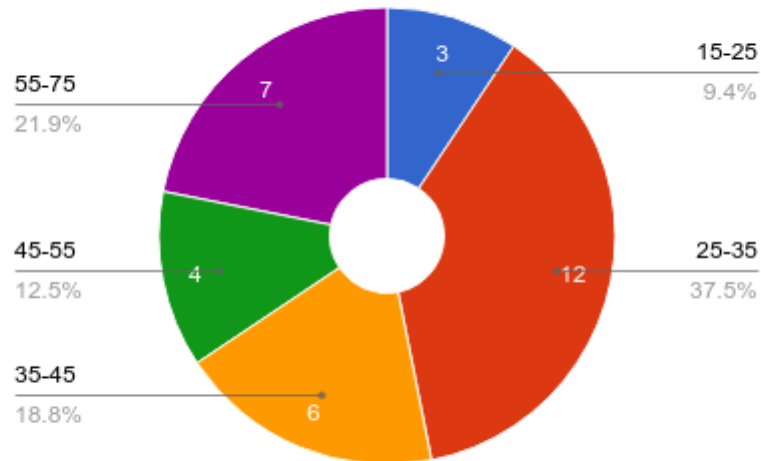


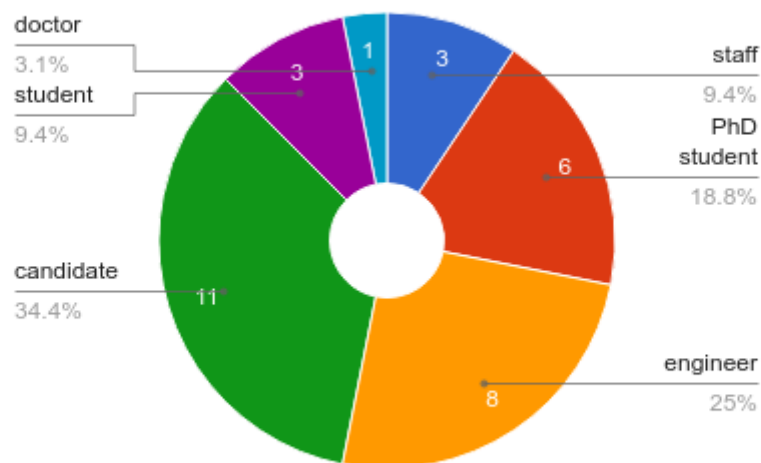**Fig. 11.1. The age distribution.**



**Fig. 11.2. The status distribution.**

# 12. Requested Resources

For the proposed extension of the JUNO/Daya Bay project at JINR the resources that are requested from the JINR budget for the period of 2018-2020 are presented in the table 12.1. The breakdown on the visits cost is presented in the table 12.2.

The total request to the JINR budget for the years 2018-2020 amounts to 2990K$.

| | | |
|---|---|---|
| **High Voltage** | 20K units × 100 $ | **2000** K$ |
| Components and PCB production | | 1000 |
| PCB and Unit assembly, sealing | | 500 |
| Testing | | 400 |
| Supply | | 100 |
| **Top Tracker** | | **180** K$ |
| Materials | 140 tons × 0.68K$ | 95.0 |
| Production costs | 140 tons × 0.48K$ | 67.5 |
| Transportation | 7 containers x 2.5K$ | 17.5 |
| **PMT testing** | | **100** K$ |
| Materials | | 10 |
| Equipment | | 10 |
| Storage disks | 100Tb × 2(replicaiton) × 3(servers) | 25 |
| 3 Data servers | on-site, IHEP, JINR | 45 |
| 2 Scanning Stations production + electronics | year 2018 | 10 |
| **EMF shielding** | | **30** K$ |
| Materials | | 9 |
| Equipment | | 9 |
| Production costs | | 12 |
| **Daya Bay common fund contribution** | | **180** K$ |
| **Travels** | | **500** K$ |
| **Total** | | **2 990** K$ |

Table 12.1. Requested resources.

| Travels per year | Total | 2018 | 2019 | 2020 |
|---|---|---|---|---|
| **JUNO** | | | | |
| General Collaboration Meetings<br>2 meetings × 8 persons × 1week (1.5K$/week) | 72 | 24 | 24 | 24 |
| Experts during PMT and electronics tests<br>14 man × months. (4K$/month) | 168 | 56 | 56 | 56 |
| HV work<br>2 times × 2man × 1week (1.5K$/week) | 18 | 6 | 6 | 6 |
| EMF work<br>2 times × 2 man × 1week (1.5K$/week) | 18 | 6 | 6 | 6 |
| TT monitoring<br>2 times × 2 man × 2 weeks(2K$/week) | 24 | 8 | 8 | 8 |
| TT installation:<br>15 man × months (3K$/month) | 45 | - | - | 45 |
| Software work<br>2 times × 4man × 2 weeks (2K$/week) | 48 | 16 | 16 | 16 |
| **Daya Bay** | | | | |
| General Collaboration Meetings (China)<br>2 times × 3 men × 1 week (1.7K$/week) | 31 | 11 | 10 | 10 |
| Shifts (8 weeks, 1.3K$/week) | 31 | 11 | 10 | 10 |
| **JUNO+Daya Bay** | | | | |
| Conferences, schools<br>6 man × visits (2.5K$/visit) | 45 | 15 | 15 | 15 |
| Total | 500 | 153 | 151 | 196 |

Table 12.2. Breakdown of the money requested for visits.

# 13. Bibliography

1. Akiri T., et al. The 2010 Interim Report of the Long-Baseline Neutrino Experiment Collaboration Physics Working Groups // arXiv [hep-ex]. 2011.
2. An F.P. et al. Observation of electron-antineutrino disappearance at Daya Bay // Phys. Rev. Lett. 2012. Vol. 108, № 17. P. 171803.
3. Li Y.-F. et al. Unambiguous determination of the neutrino mass hierarchy using reactor neutrinos // Phys. Rev. D Part. Fields. 2013. Vol. 88, № 1.
4. Kim S.-B. New results from RENO and prospects with RENO-50 // Nucl. Part. Phys. Proc. 2015. Vol. 265-266. P. 93–98.
5. Ayres D.S., et al. NOvA: Proposal to build a 30 kiloton off-axis detector to study nu(mu) ---> nu(e) oscillations in the NuMI beamline // arXiv [hep-ex]. 2004.
6. Aartsen M.G., et al. Letter of Intent: The Precision IceCube Next Generation Upgrade (PINGU) // arXiv [physics.ins-det]. 2014.
7. Ribordy M., Smirnov A.Y. Improving the neutrino mass hierarchy identification with inelasticity measurement in PINGU and ORCA // Phys. Rev. 2013. Vol. D87, № 11. P. 113007.
8. Abe K., et al. A Long Baseline Neutrino Oscillation Experiment Using J-PARC Neutrino Beam and Hyper-Kamiokande // arXiv [physics.ins-det]. 2014.
9. Indumathi D. India-based Neutrino Observatory (INO) // Pramana. 2004. Vol. 63. P. 1283–1293.
10. Bednyakov V.A., Naumov D.V., Yu Smirnov O. Neutrino physics and JINR // Phys. Usp. 2016. Vol. 59, № 3. P. 225–253.
11. Billen J.H. L.M. Young. POISSON SUPERFISH. 1996.
12. Armstrong A.G.A.M., Riley C.P., Simkin J. Tosca User Guide: three-dimensional static electromagnetic/electrostatic analysis package: version 3.1 may 1982. 1982.
13. An F.P., et al. Observation of electron-antineutrino disappearance at Daya Bay // Phys. Rev. Lett. 2012. Vol. 108. P. 171803.
14. An F.P., et al. Measurement of electron antineutrino oscillation based on 1230 days of operation of the Daya Bay experiment // arXiv [hep-ex]. 2016.
15. An F.P., et al. A new measurement of antineutrino oscillation with the full detector configuration at Daya Bay // Phys. Rev. Lett. 2015. Vol. 115, № 11. P. 111802.
16. Akhmedov E.K., Kh. Akhmedov E., Yu. Smirnov A. Paradoxes of neutrino oscillations // Phys. At. Nucl. 2009. Vol. 72, № 8. P. 1363–1381.
17. Naumov D.V., Naumov V.A. A diagrammatic treatment of neutrino oscillations // J. Phys. G Nucl. Part. Phys. 2010. Vol. 37, № 10. P. 105014.
18. An F.P., et al. Study of the wave packet treatment of neutrino oscillation at Daya Bay // Submitted to: Phys. Lett. B. 2016.
19. Gando A., et al. Reactor On-Off Antineutrino Measurement with KamLAND // Phys. Rev. 2013. Vol. D88, № 3. P. 033001.
20. O'Donnell T.M. Precision Measurement of Neutrino Oscillation Parameters with KamLAND. UC, Berkeley, 2011.
21. International Atomic Energy Agency. Power Reactor Information System [Electronic resource]. URL: https://www.iaea.org/pris/.
22. Долгарева М.А. Исследование эффектов декогерентности волновых пакетов в нейтринных осцилляциях на основе данных экспериментов KamLAND и Daya Bay. Дубна: МФТИ, 2016.
23. Долгарева М.А. Исследование эффекта декогерентности в нейтринных осцилляциях. Дубна: МФТИ, 2014.
24. Schreckenbach K. et al. Determination of the antineutrino spectrum from 235U

thermal neutron fission products up to 9.5 MeV // Phys. Lett. B. 1985. Vol. 160, № 4-5. P. 325–330.

25. von Feilitzsch F., Hahn A.A., Schreckenbach K. Experimental beta-spectra from 239Pu and 235U thermal neutron fission products and their correlated antineutrino spectra // Phys. Lett. B. 1982. Vol. 118, № 1-3. P. 162–166.

26. Hahn A.A. et al. Antineutrino spectra from 241Pu and 239Pu thermal neutron fission products // Phys. Lett. B. 1989. Vol. 218, № 3. P. 365–368.

27. Vogel P. et al. Reactor antineutrino spectra and their application to antineutrino-induced reactions. II // Phys. Rev. C Nucl. Phys. 1981. Vol. 24, № 4. P. 1543–1553.

28. Bemporad C., Gratta G., Vogel P. Reactor-based neutrino oscillation experiments // Rev. Mod. Phys. 2002. Vol. 74, № 2. P. 297–328.

29. Mueller T.A. et al. Improved Predictions of Reactor Antineutrino Spectra // Phys. Rev. 2011. Vol. C83. P. 054615.

30. Huber P. Determination of antineutrino spectra from nuclear reactors // Phys. Rev. C Nucl. Phys. 2011. Vol. 84, № 2.

31. Mention G. et al. The Reactor Antineutrino Anomaly // Phys. Rev. 2011. Vol. D83. P. 073006.

32. Huber P. On the determination of anti-neutrino spectra from nuclear reactors // Phys. Rev. 2011. Vol. C84. P. 024617.

33. Giunti C. Which reactor antineutrino flux may be responsible for the anomaly? // arXiv [hep-ph]. 2016.

34. An F.P., et al. Improved Measurement of the Reactor Antineutrino Flux and Spectrum at Daya Bay // arXiv [hep-ex]. 2016.

35. Abrahao T., et al. Measurement of $\theta_13$ in Double Chooz using neutron captures on hydrogen with novel background rejection techniques // arXiv [hep-ex]. 2015.

36. Seo S.-H. New Results from RENO and The 5 MeV Excess // arXiv [hep-ex]. 2014.

37. Ko Y.J., et al. A sterile neutrino search at NEOS Experiment // arXiv [hep-ex]. 2016.

38. Тресков К.А. Нейтринные осцилляции в веществе и возможность экспериментального исследования декогеренции в солнечных экспериментах. Иркутск: ИГУ, 2015.